Mechanical Deformation of Neutrophil into Pulmonary Capillaries Induces Cytoskeletal Remodeling, Pseudopod Projection and Changes in Biomechanical Properties

by

Belinda Yap

B.Eng., M.Eng. Mechanical Engineering
National University of Singapore, 1999

SUBMITTED TO THE HARVARD-MIT DIVISION OF HEALTH SCIENCES & TECHNOLOGY IN PARTIAL FULFILLMENT OF THE REQUIREMENTS FOR THE DEGREE OF

DOCTOR OF PHILOSOPHY IN MECHANICAL AND MEDICAL ENGINEERING
AT THE
MASSACHUSETTS INSTITUTE OF TECHNOLOGY

JUNE 2005

Signature of Author: _____
Harvard-MIT Division of Health Sciences & Technology
April 29, 2005

Certified by: _____
Roger D. Kamm, Ph.D.
Professor of Mechanical and Biological Engineering
Thesis Supervisor

Accepted by: _____
Martha L. Gray, Ph.D.
Edward Hood Taplin Professor of Medical and Electrical Engineering
Director, Harvard-MIT Division of Health Sciences and Technology

Mechanical Deformation of Neutrophil into Pulmonary Capillaries Induces Cytoskeletal Remodeling, Pseudopod Projection and Changes in Biomechanical Properties

by

Belinda Yap

Submitted To The Harvard-MIT Division Of Health Sciences & Technology
on 29 April, 2005 in Partial Fulfillment of the
Requirements for the Degree Of Doctor Of Philosophy in
Mechanical and Medical Engineering

ABSTRACT

Neutrophils traversing the pulmonary microcirculation are subjected to mechanical stimulation during their deformation into narrow capillaries. To better understand the time-dependant changes caused by this mechanical stimulus, in the first part of the thesis, neutrophils were caused to flow into a microchannel, which allowed simultaneous visualization of cell morphology, and passive rheological measurement by tracking the Brownian motion of endogenous granules. Above a threshold stimulus, mechanical deformation resulted in neutrophil activation with pseudopod projection. The activation time was inversely correlated to the rate of mechanical deformation experienced by the neutrophils. A reduction in shear moduli was observed within seconds after the onset of the mechanical stimulus, suggesting a sudden disruption of the neutrophil cytoskeleton when subjected to mechanical deformation. However, the magnitude of the reduction in moduli was independent of the degree of deformation. Recovery to nearly the initial values of viscoelastic moduli occurred within one minute. These observations confirm that mechanical deformation of neutrophils, similar to conditions encountered in the pulmonary capillaries is not a passive event; rather, it is capable of activating the neutrophils and enhancing their migratory tendencies.

The second part of the thesis seeks to understand the changes in the cytoskeletal structure and the extent of biological activation as a result of this deformation process. Neutrophils were passed through narrow polycarbonate filter pores under physiological driving pressures, fixed and stained downstream in order to visualize the F-actin content and distribution. Below a threshold capillary size, the cell remodeled its cytoskeleton through initial F-actin depolymerization, followed by recovery and increase in F-actin content associated with formation of pseudopods. This rapid depolymerization and subsequent recovery of F-actin was consistent with our previous observation of an immediate reduction in moduli with eventual recovery when the cells were subjected to deformation. Results also show that neutrophils must be retained in their elongated shape for an extended period of time for pseudopod formation, suggesting that a combination of low driving pressures and small capillary diameters promotes cellular activation. These observations show that mechanical deformation of neutrophils into narrow pulmonary capillaries have the ability to influence cytoskeletal structure, the degree of cellular activation and migrational capabilities of the cells.

Thesis Supervisor: Roger D. Kamm, Ph.D.
Title: Professor of Mechanical and Biological Engineering

TABLE OF CONTENTS

CITATIONS TO PREVIOUSLY PUBLISHED WORKS

This dissertation is based on the following papers:

I. **Yap, B. & Kamm, RD.** Mechanical Deformation of Neutrophils into Narrow Channels Induces Pseudopod Projection and Changes in Biomechanical Properties. *J. Appl Physiol*, 98:1930-1939, 2005.

II. **Kaazempur-Mofrad, MR., Abdul-Rahim, NA., Karcher, H., Mack, PJ., Yap, B., Kamm, RD.** Exploring the Molecular Basis for Mechanosensation, Signal Transduction and Cytoskeletal Remodeling. *Acta Biomaterialia* 2005 in press.

III. **Yap, B. & Kamm, RD.** Cytoskeletal Remodeling and Cellular Activation during Deformation of Neutrophils into Narrow Channels, submitted for publication in *J. Appl Physiol* 2005.

ACKNOWLEDGEMENTS

I have been very fortunate in my graduate school career here to have the opportunity to work with and learn from very intelligent, interesting, and enthusiastic individuals.

First and foremost, I would like to thank my mentor and primary advisor, Professor Roger D. Kamm, for his constant guidance, encouragement, and patience during the tenure of this work. He has created a highly collaborative working environment with opportunity to work with people from various expertises. I thank him for his inspiration, wisdom, humility, advice and always being there whenever I needed any help. I would also like to thank my other committee members, Professors Frank B. Gertler, Richard T. Lee and Peter TC. So, for their continued assistance throughout this study.

In addition, I would like to thank those who have helped me with various aspects of my experiments, in particular, Jorge Ferrer, Hayden Huang, Maxine Jonas, Jan Lammerding, Hang Lu, Thierry Savin, and Alisha Sieminski and members of the Yaffe lab. Thanks are also due to all members of the Kamm lab for their support, companionship and for providing an enjoyable yet intellectually stimulating working atmosphere.

I gratefully acknowledge financial support by grants from the National University of Singapore and the Whitaker Foundation Graduate Student Fellowship.

I would also like to thank my friends for their understanding and support, for keeping my spirits high, and for making my journey and stay here in Boston such a wonderful experience.

Finally, I would like to express my thanks and gratitude to my parents, brother, sister-in-law, and my nephew for their unconditional love and support and for always believing in me.

DEDICATION

This thesis is dedicated to my parents

Yap Teck Fook & Lim Kwi Shiong

for their love and support, and without whom I would have never achieved what I have.

Chapter 1

Introduction

1.1 The Neutrophils

Neutrophils (33; 44), also known as, polymorphonuclear leukocytes (PMN), are the most abundant type of white blood cell, comprising 50-70% of the circulating white cell population in humans. They are a major player in the innate immune response, in particular, the phagocytosis and killing of pathogens that penetrate the body's physical barriers. Neutrophils are also responsible for ridding the body of dead or necrotic cells.

Neutrophils are terminally differentiated cells with short life spans. They are found in the bone marrow, blood and tissues (although normally, neutrophils are absent from healthy tissues). Upon release from the bone marrow into the circulation, they typically survive in blood for 6-7 hours, after which they migrate into surrounding tissue sites and survive for another 1-4 days. A normal healthy adult produces approximately 10^{11} neutrophils per day resulting in mean concentration of leukocyte in blood of roughly 4.4×10^{6} cells/ml.

1.2 Ultrastructure, Morphology and Composition of Neutrophils

Neutrophils have multilobed nuclei (2 – 5 lobes) connected by strands of chromatin (Fig. 1a). The chromatin strands can be difficult to distinguish; hence, neutrophils might appear as having multiple nuclei. The multilobed nuclei of mature neutrophils allow the cells to squeeze through tight endothelial cell junctions during transmigration towards infected sites. Immature neutrophils are incompletely segmented and characterized by a 'C-shaped' nucleus (Fig. 1b).

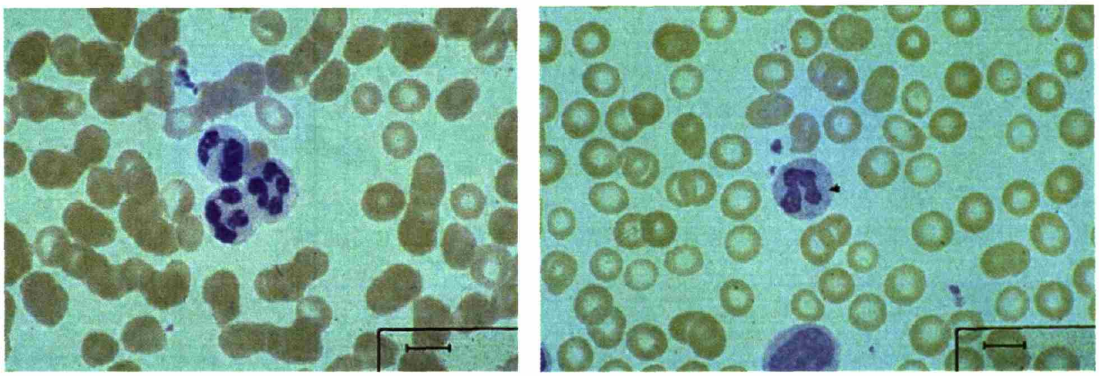

Fig. 1 Left panel (a) shows multilobed nuclei of a mature neutrophil. Right panel (b) shows an immature neutrophil with an incompletely segmented nucleus.(2)

Neutrophils also contain distinctive cytoplasmic granules ranging from 0.1 to 0.8 μm (70; 71) in diameter, and can be divided into 2 main types, azurophil (primary) and specific (secondary). The individual granule population can be distinguished either morphologically (Fig. 2) (azurophil granules are larger, denser and more homogeneous while specific granules are spherical or rod-shaped) or using Wright's stain (azurophil will be violet while specific granules stain light pink i.e. neutral).

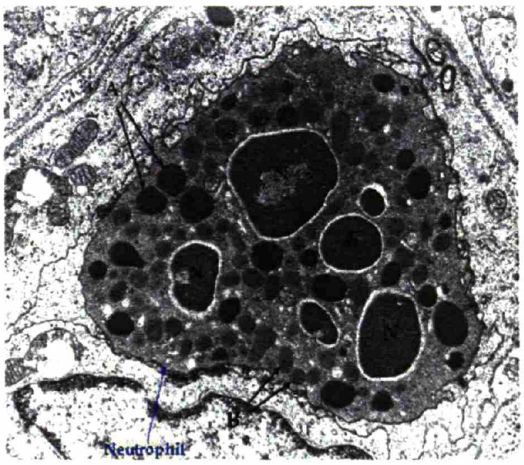

Fig. 2 TEM of neutrophil. A = azurophil granules; B = specific granules; N = mulitilobed nucleus (2)

In order to begin understanding the dynamics of neutrophils and build quantitative models that describe their behavior, studies have been performed to determine the morphology of these cells (32; 75;

78; 89). In the passive or resting state, neutrophils are spherical in shape with mean diameters of 7.03 μm in isotonic medium. The cell membrane of a neutrophil exists in multiple folds (Fig. 3); this excess surface area is above that required to envelope the cell. However, the cell membrane area stays constant; hence, it serves to limit the extent of swelling and deformation. This point to the importance of cell membrane area in governing the dynamics of the neutrophil during various host defense functions. The volume and membrane surface areas of neutrophil obtained from various studies are shown in Table 1. The results vary depending on the chemical fixation methods and imaging modalities.

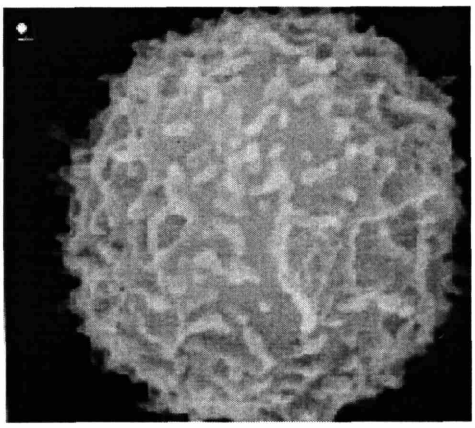

Fig. 3 Scanning electron micrograph of a passive neutrophil showing its membraneous folds (1)

Table 1. Neutrophil morphometry

Fixation Treatment and Imaging Technique	G and TEM (75; 78)	GO and TEM (32)	DCF and TEM (32)	Live cell and LM (89)
Average cell volume, μm^3	182	236	325	299
Average projected cell membrane area, μm^2	155	185	229	214
Average membrane surface area, μm^2	295	n.a.	n.a.	546

G = glutaryldehyde
GO = glutaryldehyde-osmium tetroxide
DCF = dimethyl sulfoxide-cyrofixation-freeze-substitution
LM = light microscopy
TEM = transmission electron microscopy
n.a. = parameter not measured in study

The composition of the neutrophil has also been quantified from TEM images (Table 2). Compared with data for average cell volume, there is less discrepancy in the results obtained for neutrophil composition from different fixation techniques. Similar to cell membrane, the multi-lobed nucleus of a neutrophil has an excess membrane area, about twice that is required to enclose the volume of the nucleus (78).

Table 2. Neutrophil constituent volume distribution

Fixation Treatment and Imaging Technique	G and TEM (75; 78)	GO and TEM (32)	DCF and TEM (32)
Nucleus, %	21.3	26.33	24.71
Mitochondria, %	0.6	0.19	0.99
Cytoplasm, %	78.1 (15.4% taken up by granules)	73.48	74.3

G = glutaryldehyde

GO = glutaryldehyde-osmium tetroxide

DCF = dimethyl sulfoxide-cyrofixation-freeze-substitution

TEM = transmission electron microscopy

1.3 Mechanical Properties of Neutrophils – Active and Passive States

The mechanical properties of neutrophils play a critical role in governing their function in the circulation. These properties have direct implications in key processes such as their motion and deformation in blood vessels, transmigration between capillary wall endothelial cells into the interstitium, rolling of neutrophils on venous endothelium, deformation of neutrophils during release from the bone marrow and deformation during phagocytosis. Hence, it is useful to develop an accurate rheological model of neutrophils that would allow us to quantitatively describe and understand these dynamic events in normal and pathological conditions.

Rheological modeling of neutrophils has traditionally been divided into passive and active models. Neutrophils in the passive state undergo deformation only when they are subjected to an

externally applied force. Passive behavior of neutrophils is observed when they are traversing the microcirculation; the cells deform as they encounter narrow constrictions but recover their spherical shape once they pass through the capillaries into larger vessels. In vitro experiments of passive neutrophils are carried out by suspending the cells in solutions that remove calcium, such as anticoagulants EDTA or citrate, or by introducing chemicals such as cytochalasin B which inhibits actin polymerization.

In contrast, neutrophils are defined to be in an active state if they deform spontaneously without being subjected to any externally applied force. The energy required for the deformation comes from the cells themselves. Neutrophils in this state form local cytoplasmic projections called pseudopodia, which are regions high in actin content due to active actin polymerization, but devoid of organelles (Fig. 4). Neutrophils exhibit this active state when they are undergoing transmigration through the endothelial monolayer or during phagocytosis. Activated neutrophils in-vitro can be observed when the cells are suspended in plasma or Ringer's solution or when the neutrophils are stimulated with chemoattractants such as fMLP or complement fragments.

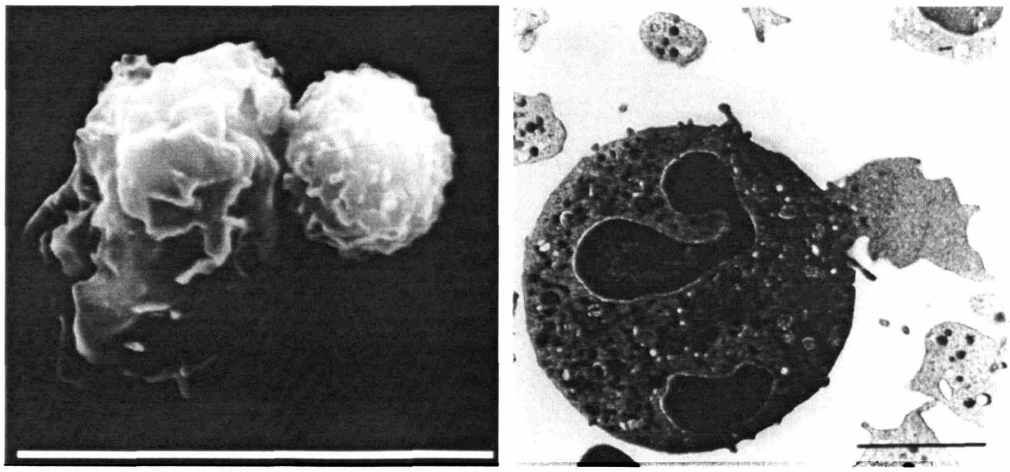

Fig. 4 Scanning electron micrograph (left panel) and transmission election micrograph (right panel) of activated neutrophils with pseudopods (76)

1.4 Rheological Modeling of Passive Neutrophils

Most of the present models of the rheological behavior of passive neutrophils have been derived from micropipette aspiration studies (Fig. 5).

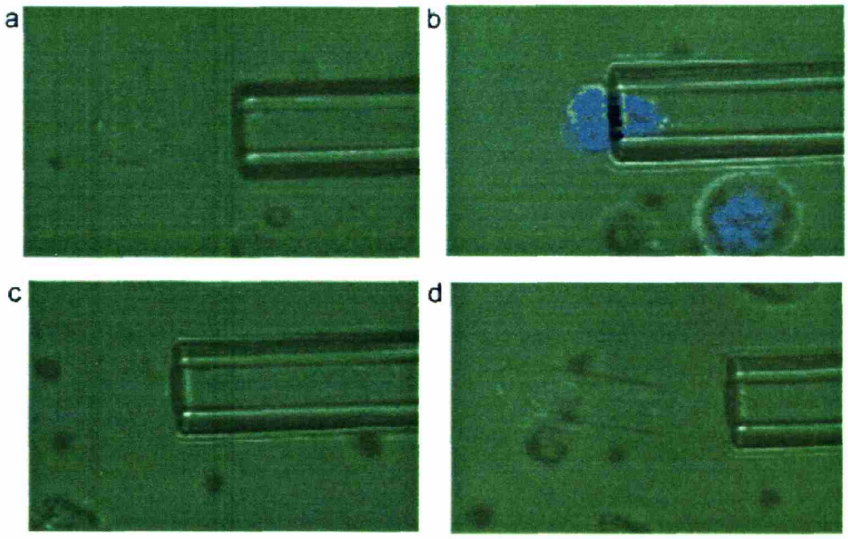

Fig. 5 Micrographs showing micropipette aspiration of a neutrophil. Neutrophil flows into the micropipette when pressure in the pipette is lowered (panels a-c). When the pressure gradient is reversed, the neutrophil is ejected out from micropipette (panel d) and eventually recovers back its spherical shape. [Adapted from (49)]

Schmid-Schonbein et al.(79) first modeled the passive properties of neutrophils as a homogeneous sphere comprised of a standard viscoelastic solid. This model described the small deformation experienced by a neutrophil at the initial stages of the aspiration. However, the model was not able to adequately predict the relaxation properties of neutrophils after ejection from a large micropipette. Hence, the parameters of the standard viscoelastic model were altered by Sung et al.(85) to fit both the instantaneous short elastic deformation as well as the long-time recovery characteristics of the neutrophils.

Aside from the standard solid model, another early model developed for passive neutrophils was the Newtonian liquid interior with a constant cortical tension shell surrounding the liquid core (25; 26; 36; 68; 111). This model applied to the large, continuous, liquid-like deformation of neutrophils into micropipettes for suction pressures in excess of a threshold and to the recovery behaviour of cells after release from the micropipettes. However, this model failed to describe the instantaneous elastic deformation observed when cells were subjected to suction pressures.

A new model that comprised an improvement of the two earlier models described above, was proposed (18; 19). The model consisted of a pre-stressed constant-tension shell surrounding a Maxwell fluid sphere. The shell represented the actin-rich cortical layer of a neutrophil while the Maxwell fluid modeled the average properties of all the intracellular components of the cell. This model was found to describe both the short-time, small deformation and the long-time recovery behavior of neutrophils after large deformation. Although this model was able to capture both the rapid and slow deformation regimes, it did so by continuously varying the viscoelastic coefficients depending on the extent and rate of deformation. These variations were attributed to the heterogeneity of the internal structure of neutrophil, with different cellular components participating in different stages of deformation. The heterogeneity of the internal structure was recognized by demonstrating that the nucleus of a lymphocyte (which was assumed to be similar in properties to that of neutrophils) was much stiffer than the cytoplasm. Despite arriving at a less than satisfactory model, this work first highlighted the need to account for the cellular contents of the neutrophil in order to arrive at the 'true', rather than the apparent properties of the cell.

The inhomogeneous nature of the neutrophil internal structure suggested that the cytoplasm exhibited a non-Newtonian behavior (94). This shear-rate dependence behavior was first studied by Tsai et al.(94) who proposed a power-law fluid model to explain the shear thinning behavior observed during micropipette experiments. In spite of this more refined model, the rapid recoil region still could not be adequately captured. An attempt was made by Drury and Dembo (23) to improve the shear thinning model by incorporating the effects of cortical dissipation. Comparing finite element results of the model to micropipette aspiration experiments showed that the proposed model was able to explain the

dependence of time scale of aspiration to pipet pressure and size. The model was also able to account for the rapid acceleration of the neutrophil during the final stage of aspiration and predict the geometry of the cell during the course of aspiration. However, the model still has a major shortcoming in that it could not explain the 'jump' of neutrophil into the micropipette during the initial pressure ramp. Hence, a constitutive equation that could describe all the possible types of deformation and recovery behaviors of the neutrophil still eluded us.

Failure of the "lumped" approach to explain the complex behavior of neutrophils had prompted several groups to propose the compound drop model (37; 50; 51; 92). It was put forward in an effort to represent more accurately the morphology and physical properties of the major cellular components, and to reconcile the diverse values (two orders of magnitude difference) of cytoplasmic viscosity that had been published. The model comprised three layers - a cortical shell with a constant surface tension, the cytoplasm, and a nucleus. The results showed that the rheological behavior of the nucleus must be explicitly accounted for, if any of the Newtonian or non-Newtonian models were to succeed in describing the dynamics of the neutrophils. However, experiments were performed on lymphocytes, rather than on neutrophils, with the assumption that both have similar mechanical properties. Thus, the applicability of this model to neutrophils is somewhat questionable since morphology of neutrophils is different compared to lymphocytes (for e.g. neutrophils possess multi-lobed nuclei in contrast to lymphocytes, which have a symmetrical single lobed nuclei), and there is no direct evidence to establish that neutrophils and lymphocytes have comparable mechanical properties.

1.5 Rheological Modeling of Activated Neutrophils

The rheological properties of activated neutrophils is less well known compared to that of passive neutrophils. This is attributed to the wide diversity of the response of neutrophils following stimulation. In numerous published works, the rheological model for an activated neutrophil is simplified by assuming that it is similar to the passive neutrophil model, but with modified model parameters values to account

for changes in mechanical properties exhibited by the cells at different levels of activation. Activated neutrophils were reported to exhibit an increase in cell stiffness.

An experimental study by Worthern et al.(104) employed a cell poking technique, (Fig. 6) using a glass microneedle as an indenter to probe single neutrophils induced by fMLP.

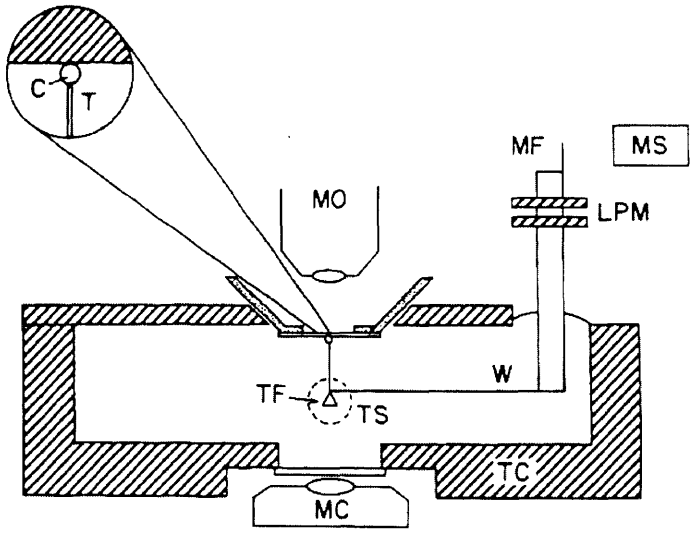

Fig. 6 Schematic of cell poking setup. The cell (C) is subjected to indentation by the glass microneedle (T)

Neutrophils were indented at a constant rate and the time course of the resultant force on the probe was recorded. Zahalak et.al. (112) performed a finite element simulation of the experimental results, treating the neutrophils as purely elastic. Bathe et al. (8) also obtained the results of Worthern et al. and simulated the indentation experiments to quantify the effects of fMLP stimulation on the mechanical properties of the neutrophils. The model chosen for the fMLP-stimulated cells, similar to that for the non-stimulated neutrophils, was a viscoelastic Maxwell substance bounded by a layer with constant cortical tension. From the simulation, the appropriate Maxwell model parameter values were determined for two levels of fMLP-activation.

Mechanical properties of activated neutrophils were also evaluated using magnetic twisting cytometry (Fig. 7) to determine its increase in apparent stiffness when the cells were subjected to

inflammatory stimuli such as complement protein 5 (C5) fragments or formylmethionyl-leucyphenylalanine (fMLP).

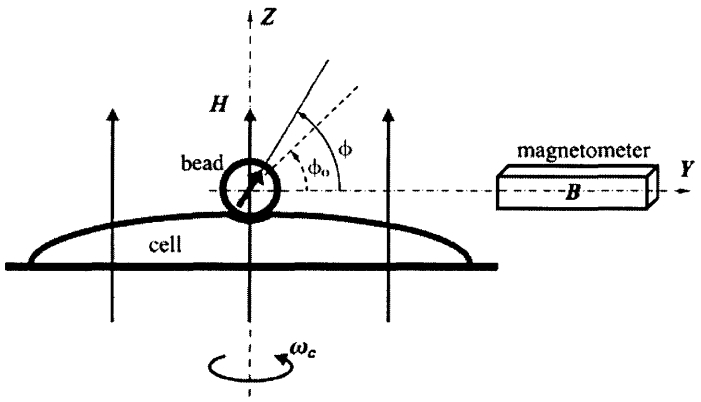

Fig. 7 Schematic diagram of the magnetic twisting cytometry measurements. Ferromagnetic microbeads attached to the cell membrane are twisted by a magnetic field and the angular rotation of the beads are recorded with a magnetometer (72)

The stiffness was inferred by measuring the angular rotation of ferromagnetic beads bound to neutrophils via antibody ligation on application of a specific magnetic torque (27; 102). In this study, the stiffening of neutrophils occured within 2 minutes after treatment with C5 fragments or fMLP and persisted beyond 15 minutes thereafter.

1.6 Physiological Relevance of Rheological Studies

As mentioned in the previous section, rheological modeling of neutrophils enables us to describe quantitatively the behavior of these cells under physiological conditions. An accurate model would have the additional benefit of allowing us to predict the behavior of neutrophils when sub- or supra-physiological conditions are imposed, situations that could be encountered, for example, as part of therapeutic measures. In the present study, we choose to focus on the motion and deformation of neutrophils through narrow capillaries and their recruitment in healthy and diseased lungs.

Neutrophils encounter narrow capillary segments mainly during their transit across the pulmonary microvasculature. Studies done to compare neutrophil and pulmonary capillary diameters (17) had shown that neutrophil diameters range from 6 to 8 μm while pulmonary capillaries have diameters of 2 to 15 μm . Hence, for neutrophils to traverse the pathway from arteriole to venule across the pulmonary capillary bed, which comprise of 50 to 100 such capillary segments (38; 39), the cells would almost certainly have to deform to pass through the capillary bed. Measurements of neutrophil shape factor showed that neutrophils in capillaries were elongated while those in arterioles were nearly spherical, thus confirming the view that neutrophils deform when they encounter narrow capillary segments (17; 31). Other evidence of neutrophil deformation comes from videomicroscopy, where neutrophils were observed to move through the capillary bed in hops as the cells stop to deform when they encounter narrower capillaries (61).

The necessity for cell deformation through narrow capillaries results in an extended neutrophil capillary transit time and formation of a marginated pool of neutrophils in healthy lungs. This increased concentration of neutrophils improves the likelihood of the cells detecting any inflammation present in the lung parenchyma. Adhesion molecules have been shown not to play any significant role in neutrophil transit through the noninflamed pulmonary microvasculature (16). Hence, mechanical properties of neutrophils and capillary geometry are the key parameters governing the behavior of neutrophils in healthy lungs.

The transit time of the neutrophils through individual noninflamed pulmonary capillary segments was first modeled computationally by Huang et al.(42) using rheological results from previously published micropipette aspiration studies. Since micropipettes have blunt-ended entrance geometries, the model was further refined by Bathe et al.(8) to include the effects of capillary entrance geometry (by varying the minimum capillary radius and radius of curvature of constriction). As mentioned before, Bathe et al. modeled the neutrophil as a homogeneous viscoelastic Maxwell substance with a constant cortical tension.

In the event of an acute inflammatory response such as occurs in the case of adult respiratory distress syndrome or bacteria pneumonia, circulating neutrophils sequester in the microvasculature and emigrate into the lungs (16). The initial sequestration of neutrophils occurs through changes in mechanical properties of the neutrophils rather than mediated by adhesion molecules (16). Inflammatory mediators bind to receptors on neutrophil membranes and activate the cells. As a result, neutrophils change their shape and are also induced to stiffen, reducing the deformability of the cells as they pass through the narrow capillaries. Capillary transit time is significantly prolonged, facilitating subsequent adhesion of neutrophils to endothelium and emigration out of the capillaries.

The effect of different levels of fMLP stimulation had also been modeled computationally by Bathe et al.(8) in their effort to obtain a general mathematical expression of neutrophil transit time through pulmonary capillaries.

1.7 Mechanical Deformation of Neutrophils – An Active or Passive Process?

As mentioned in the previous section, neutrophils traversing both healthy and inflammed pulmonary microvasculature must change their shape in order to pass through narrow capillaries they encounter. In the literature, this deformation process has been regarded and modeled as a passive process (23), i.e., the neutrophils do not experience any functional changes when they negotiate through the microcirculation. The mechanical properties (of either passive or activated neutrophils) are assumed to remain unchanged prior to, during or after passing through the narrower capillaries; the only change occurs in cell shape.

A paper by Kitagawa et al. (55) questioned this view and showed that the mechanical deformation of neutrophils in the pulmonary capillaries induced functional changes that could influence their passage through these narrow constrictions. An in-vitro filtration system was used to mimic the mechanical deformation process. They found that deformation promotes cross-linking of the actin network, thus stabilizing the cytoskeleton. Mechanical deformation also results in signal transduction with elevated

concentrations of cytoplasmic free Ca^{2+} and upregulation of adhesion molecule, CD11b/CD18. Priming the neutrophils with chemoattractants such as fMLP was seen to augment the biological effect of the deformation.

These results clearly demonstrate that mechanical deformation of neutrophils cannot simply be treated as a passive process; instead, this mechanical force is an important stimulant to the neutrophils, akin to the effect of chemoattractants.

1.8 Microrheology - Moving Forward from Continuum Models

The concept of microrheology has emerged in recent years in part from realization that homogeneous, continuum models fail to explain fully the mechanical behavior of the cells. This is because homogeneous models do not account for the detailed microstructure of the cells and neglect their capability for biological remodeling. Microrheology with its associated techniques can be used to study inhomogeneities inside cells by measuring local mechanical properties on a scale of microns or less (63; 67). The viscoelastic parameters are determined from observing the motion of micron- or submicron-sized particles (either embedded or endogeneous probes).

Microrheological techniques can be broadly classified into two categories; active manipulation and passive observation of the thermal fluctuation of probe particles. Both categories have a host of methods, each proved to be useful for their intended application. These techniques are reviewed in detail in a paper by MacKintosh and Schmidt (63). However, present purposes, because we want to avoid any external manipulation of the cell that constitutes a mechanical force, we focus on the second category, namely, determination of rheological properties of cells by tracking the thermal fluctuations of microscopic inclusions. In particular, we will pay special attention to a new technique called multiple-particle tracking microrheology (MPTM), which is described in detail in the following references (29; 30; 98) .

1.9 The Cytoskeletal Structure of Neutrophils

The cytoskeletal network of neutrophils provides structural integrity as well as dictates for the most part, the mechanical and dynamic behavior of the cells. The cytoskeleton has three major components, the actin, microtubules (MTs) and intermediate filaments (IFs). The neutrophil cytoskeletal content, like most other cells, is predominantly composed of actin filaments, with MTs and IFs, existing in relatively low numbers (5).

In order to understand the function of cytoskeletal components in governing the behavior of neutrophils, various experimental techniques had been employed. One common method is to observe the distribution of fluorescently-stained cytoskeletal components under a fluorescence microscope. Neutrophils were fixed and stained with phalloidin to determine the F-actin content and distribution (73) (Fig. 9).

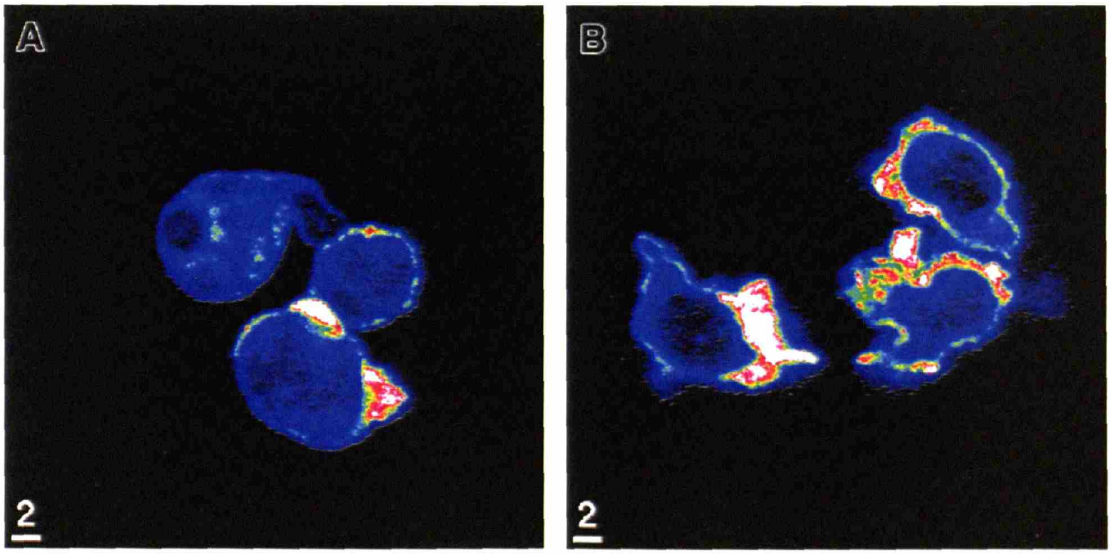

Fig. 9 Confocal microscopy images of F-actin stain for (A) passive neutrophils and (B) neutrophils after stimulation with fMLP

It was found that passive circulating neutrophils were primarily spherical and contained F-actin that was distributed in the central region or periphery of the cell. There was occasional cell activation evidenced

by actin-rich pseudopods. Stimulation with fMLP results in distinct shape distortion, with abundant pseudopods being formed and irregularities present on the plasma membrane. The F-actin content was increased and concentrated as a discontinuous rim on the submembrane region and in the pseudopods; no F-actin was seen to localize to the central regions.

In double-staining experiments (87) to study the association of F-actin and myosin, myosin was found to aggregate together with F-actin in the submembrane region in resting neutrophils. Motile neutrophils alter their distribution of actin and myosin from the resting state. As a result of activation, there is a high concentration of myosin in lamellipodia, perinuclear and granular region of cytoplasm while the F-actin localized in lamellipodia and perinuclear portion.

The role of cytoskeletal components can also be studied by treating the cells with reagents that manipulate the cytoskeleton. Colchicine, for example, is a widely used microtubule-depolymerising agent. It binds to tubulin and inhibits microtubule polymerization, and at high enough colchicine concentration, can cause microtubule networks to depolymerise (5). Cytochalasin D (88; 100) has the ability to disrupt F-actin polymerization.

While actin microfilaments have been acknowledged to play a key role in governing the mechanical properties of the neutrophils (90; 94; 95), conflicting results have been reported on the function of microtubules. An early study by Chien and Sung (11) indicated that treatment of neutrophils with colchicine reduced the rigidity of the cells. However, subsequent work by Tsai et al. (96) reported that microtubules have negligible contribution to the rheological behavior of passive neutrophils. In yet another study by Saito et al. (73), microtubular reassembly was found to be important in the normal sequestration and passage of neutrophils through the pulmonary capillaries and transmigration from microvasculature into the tissue. However, the stiffening and margination response induced by C5a or fMLP did not require participation of microtubules. In contrast, F-actin polymerization was essential in inducing the stiffening response observed on neutrophils exposed to inflammatory stimuli.

IFs in neutrophils are formed mainly from vimentin. Although IFs are not directly responsible for generating movements, they have important effects on the shape and mechanical properties of many cells,

including neutrophils, and can constrain and modify their movements. A major function of IFs is to stabilize cellular architecture against external mechanical forces (62; 94).

1.10 Biological Remodeling within Cells

The ability to visualize and/or quantify cytoskeletal redistribution is fundamental to our understanding of the behavior of cells and the mechanical properties that they exhibit. This section reviews various techniques that have been developed for this purpose.

One of the earliest studies to describe the deformation field in cells was carried out by Simon and Schmid-Schönbein (82; 83). The experiments were performed on motile neutrophils that had ingested latex microspheres. Imaging was provided by light microscopy and the movements of the microsphere markers were recorded over time. Since the microscope can only provide a single plane of focus, the deformation of the cell cytoplasm was quantified with planar instead of three-dimensional strain.

In a study done by Caille et al.(10), the internal deformation of endothelial cells subjected to uniaxial stretch of the substrate was measured. Information of strain field was gathered from fluorescent beads embedded in the cytoskeleton as intracellular markers and change in nucleus shape revealed by live nucleic acid staining. The shape of the cell as a whole was delineated using a long-term fluorescent cell tracer. Three-dimensional images of cell deformation were acquired using confocal microscopy. However, similar to Simon and Schmid-Schönbein (82), Caille et al. only performed a two-dimensional strain analysis because of limited resolution of bead position perpendicular to the plane of the substrate.

A complete three-dimensional characterization of the strain field inside cells was accomplished by Huang et al.(40) with a two-photon magnetic manipulator workstation. Human aortic smooth muscle cells that had endocytosed fluorescent beads, were subjected to focal stresses imposed by a magnetic trap. The trap exerted force on the cells via magnetic particles that were attached to the cell surface. Local displacements and ultimately, the three-dimensional deformation map were quantified from a cross correlation program. However, image acquisition was relatively slow with each data block requiring

approximately 20 minutes to complete. This precludes the use of the workstation to map strain field of cells in motion unless a faster imaging capability is integrated.

Aside from tracking endocytosed particles, the spatiotemporal distribution of cytoskeletal movement had also been elucidated through direct visualization of fluorescent-labeled cytoskeletal components. One recent study (34; 35) involved using GFP-vimentin fusion protein expressed in endothelial cells to evaluate changes in position of intermediate filaments (IF) in response to onset of shear stress. Images were collected from a confocal microscope and based on three-dimensional image deconvolution, the pattern of IF movement was mapped throughout the endothelial cell. The time scale of image acquisition was comparable to that of Huang et al. (about 20-30 min per data block).

1.11 Microfabrication in the Study of Blood Rheology

In the last decade, as application of microfabrication in biology became more widespread, microfabricated devices have been used with increasing frequency in the analysis of blood cell rheology, due to its ability to resolve cellular flow behavior and mimic flow in the microcirculation.

One of the earliest attempts to microfabricate a system for blood rheological studies was carried out by Cokelet et al.(12) This work involved developing a transparent microvascular network with circular or elliptical cross-sections. The microchannels were etched on flat glass surfaces using photoetching process.

A parallel array of microchannels fabricated on the surface of silicon substrate had been used to examine the behavior of erythrocytes and interactions of leukocytes and platelets exposed to fMLP and ADP in microcirculation (53; 54). A similar setup was used to evaluate PMN deformability by comparing the transit times before and after the cells were treated with rolipram, a suppressant of leukocyte activation (74).

Tracey et al (91) and Sutton et al. (86; 91) developed a silicon micromachined haemocytometer, comprising 22 channel array of 100 μm long channels, 3.0 to 4.0 μm width, to study the deformability

of erythrocytes flowing through channels of dimensions similar to blood capillaries. The microdevice was coupled to a macrofluidics system that was capable of imposing physiological pressure differentials across the microchannels, an advantage over classical rheometry techniques such as micropipette aspiration and filtration technique, which are performed at supraphysiological driving pressures.

Tsukada et al. (99) built microchannels on a crystal glass wafer to ensure optical clarity for visualization of erythrocyte motion. Their study involved detecting the decrease in erythrocyte deformability in patients with diabetes mellitus.

Recently, Shevkoplyas et.al. (81) has utilized microfabrication technology to design a network of microchannels that resemble the mammalian microvascular network in dimension and distribution. They showed that this in-vitro model was able to capture many of the flow behavior of red blood cells in vivo.

In our study of neutrophil rheology, we exploited the proven benefits of using microfabricated channels and combine this with the flexibility and robustness of soft lithography with PDMS.

1.13 Soft Lithography for Micro- and Nano-Fabrication

The ability to create devices with spatial dimensions comparable to those of biological processes has a huge impact on research and application in biology and medicine (101). Microfabrication, for example, can be used to control the geometry of devices precisely down to $1\,\mu m$, thus, enabling manipulation and analysis of cells at the single cell level. Besides giving us the ability to study cellular mechanics and dynamics of individual cells, experiments on multiple single cells to attain statistically significant data can be performed more efficiently compared to conventional techniques with lower cell throughput such as micropipette aspiration. Poor reproducibility in the fabrication of micropipettes and operator dependency factors during experiments also limit its effectiveness in extensive rheological studies of cells. Employing the highly reproducible microfabrication techniques with the possibility of automation can easily circumvent these problems. Nanofabricated devices (105), defined as systems with

characteristic lengths between 1 and 100 nm, is a useful technique to study biological activities at the submicron level, for example, cell transmigration through the endothelium.

Soft lithography (103; 106) is a new technique for micro- and nano-fabrication based on self-assembly and replica molding of soft, organic materials. It is an inexpensive, non-photolithographic fabrication strategy, which uses an elastomer (most popular being PDMS) as the final casts (65), or as stamps and molds to generate patterns and structures (113). However, this technique still relies on lithography in its initial step for the printing of masters. Conventional photolithography is usually employed with photomasks to produce positive relief of photoresist on silicon wafer. Feature sizes down to 1 μm on the photomasks can be replicated successfully, however, effects of diffraction preclude this approach for patterns with nanometer resolution. To achieve higher resolution, advanced lithographic methods such deep UV photolithography, e-beam writing or X-ray lithography can be used to form features on photoresist down to resolution of ~10 nm. The master produced with lithography will subsequently be used for casting of PDMS.

PDMS is the material of choice in the fabrication of biological devices because it has several distinct advantages. It is optically transparent for wavelengths from 230 – 700 nm; rendering PDMS suitable for most imaging techniques including fluorescent microscopy. PDMS is relatively inexpensive, and the micro-molding process employed is simple and rapid compared to traditional etching and bonding processes of silicon and glass. Replica molding thus permits a high yield of disposable microchannels, diminishing any potential problems such as sterilization and clogging of the channels. PDMS also bonds easily to itself and other materials such as glass to obtain a liquid-tight seal.

Chapter 2

Mechanical Deformation of Neutrophils into Narrow Channels: Effect on Pseudopod Projection and Changes in Biomechanical Properties

2.1 Introduction

Neutrophils play a vital role in our host defense against an extensive number of potentially harmful pathogens that are present in our environment. To comprehend the behavior of the neutrophils in our circulation and tissues requires understanding of the cells' mechanical properties and how mechanical and chemical stimuli alter these properties. It is also essential to appreciate the contribution of cell cytoskeleton in governing the mechanics of neutrophils, and consequently the function of these cells in health and disease.

Neutrophils often encounter narrow capillary segments during their transit through the pulmonary and systemic microcirculations. Since neutrophil diameters (6-8 μm) often exceed the diameter of a pulmonary capillary (2-15 μm) (17), neutrophils would almost certainly have to deform in passing from arteriole to venule, particularly in the pulmonary capillary bed, where it has been estimated that a typical flow pathway encompasses 50 to 100 such capillary segments (38; 39). Measurements of neutrophil shape showed that neutrophils in capillaries are elongated while those in arterioles are nearly spherical, thus confirming the view that neutrophils deform when they encounter narrow capillary segments (17; 31).

Mechanical forces have been recognized to play an important role in modulating the behavior and function of cardiovascular cells in health and disease (41; 43). Although the effects of mechanical stimuli

on cells have been a topic of extensive research, much of the focus has been on endothelial cells in the context of atherosclerotic disease. Neutrophil, and leukocyte activity in general, is assumed to be mediated in large part by biochemical factors, with effects from mechanical stimulation often ignored. However, recent studies have shown that leukocytes are sensitive to fluid shear stress, which can influence their degree of substrate adhesion and the formation of pseudopods, and reduce their cytoskeletal stiffness (13; 56; 66). Similarly, the mechanical deformation of neutrophils into narrow pulmonary capillaries, initially considered to be a passive process, is now recognized to enhance adhesiveness to ICAM-1 through upregulation of CD11b/CD18, reorganizing and stabilizing the cytoskeleton and increasing free $[Ca^{2+}]_i$ (55). Consequently, neutrophils likely have the capability of sensing mechanical force or deformation and altering their rheological properties in response. Despite the importance of these effects in the microcirculation, no rheological studies have yet been conducted subjecting neutrophils to the deformations they experience while traversing the pulmonary circulation. Interestingly, one of the established techniques for measuring the viscoelastic properties of neutrophils, the micropipette aspiration method, involves deformation of the cell under a fixed suction pressure into a narrow micropipette (26; 68; 93; 94). This technique mimics the flow condition that the cell experiences while deforming into a pulmonary capillary. The rheological properties deduced from this technique, however, assume that the neutrophil remains passive during deformation, and hence, that its rheology is unchanged when drawn into the pipette. Indeed, some of these micropipette experiments showed some indications of neutrophil activation attributed to mechanical deformation of the cell (25).

In such cases for which mechanical deformation by external forces give rise to a change in rheological properties, it is advantageous to seek methods of measurement that avoid cell manipulation. Multiple-particle-tracking microrheology (57; 58; 98) offers a solution as this method is able to non-invasively measure the local viscoelasticity by monitoring the Brownian motion of endogeneous granules present in the cytoplasm of the cell. A similar technique has been applied to locomoting neutrophils, with active manipulation of a granule using an optical trap (108; 109) . This thesis examines the effects of mechanical deformation on the behavior and rheological properties of the neutrophils in the pulmonary

capillaries, using microfabrication techniques (65; 103) to construct an in-vitro poly-dimethyl-siloxane (PDMS) system with dimensions comparable to the pulmonary capillaries. PDMS being optically transparent enabled direct observation of the neutrophil morphology, and simultaneously allowed us to employ the technique of multiple-particle-tracking microrheology to directly measure the viscoelastic properties of the cell.

2.2 Materials and Methods

2.2.1 Neutrophil Isolation

Human venous blood (~ 30 mls) was drawn from healthy volunteers by venipuncture into syringes containing 3 mls of sodium citrate (0.1 M) as an anticoagulant. The isolation was in accordance with a protocol approved by the M.I.T. Committee on Use of Humans as Experimental Subjects. The blood was diluted with HBSS without Ca^{2+} or Mg^{2+} (Invitrogen Corp., Carlsbad, CA) to make up 50 mls. 25 mls of the diluted blood was carefully layered over two tubes, each containing 10 mls of Histopaque – 1077 (Sigma-Aldrich, St. Louis, MO). Neutrophils were isolated from mononuclear cells by density gradient centrifugation on the Histopaque –1077 at 175 g for 30 min at room temperature. After centrifugation, the distinct layers obtained are as shown schematically in Fig. 10. The supernatant plasma layer was collected for later use in the experiment. The mononuclear layer was carefully removed with a Pasteur pipette, and the remaining neutrophil and red blood cell (RBC) layer were resuspended in first, an equal volume of HBSS without Ca^{2+} or Mg^{2+}, and then a 1:1 dilution of dextran (average molecular weight 500,000, 2% final concentration, Pharmacia Corp., Peapack, NJ). The RBCs were allowed to sediment for 30 min at room temperature, after which, the neutrophil-rich supernatant was collected and pooled from both tubes, rinsed with HBSS, and centrifuged at 175 g for 5 min at room temperature. Residual RBCs were removed by hypotonic lysis with 3 mls of deionized water for ~ 30 s. Isotonicity was restored by the addition of 45 mls of HBSS without Ca^{2+} or Mg^{2+}, and the sample was then centrifuged at 175 g for 5 min at room temperature. The isolated neutrophils were resuspended in either HBSS without

Ca^{2+} or Mg^{2+} only, or in medium (HBSS without Ca^{2+} or Mg^{2+} + 2% autologous plasma). After counting with a haematocytometer, the neutrophil concentration was adjusted depending on experimental requirements to 1.0×10^6 cells/ml, and kept either at room temperature or incubated in a $37°C$ water bath. The resulting cell suspensions contain > 95% neutrophils.

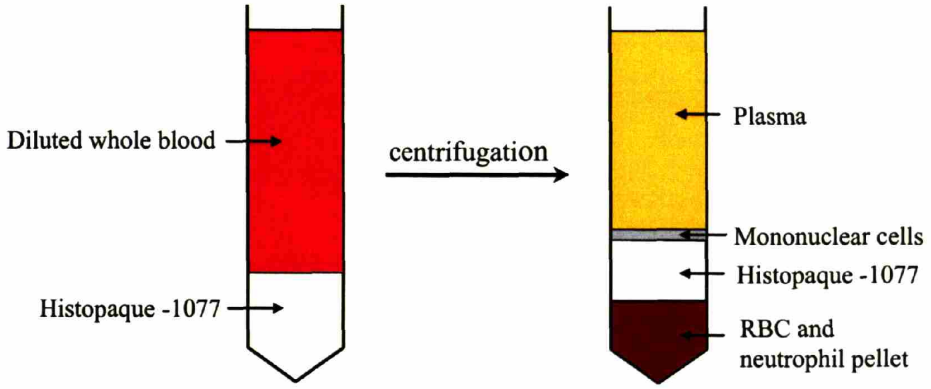

Fig. 10 Distinct layers resulting from density gradient centrifugation of whole blood during neutrophil isolation protocol.

2.2.2 Design and Fabrication of Microfluidic Device

The design of the microchannel used to mimic a pulmonary capillary and the connecting reservoirs is shown in Fig. 11. The channel width is set at 5 μm, narrow enough that the neutrophils will need to deform to fit through.

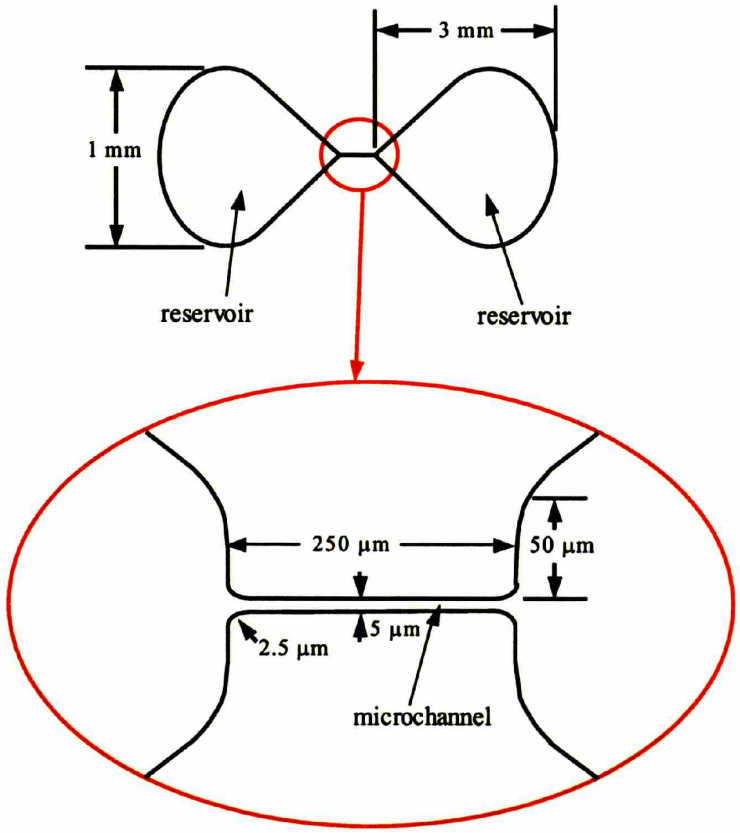

Fig. 11 Schematic showing design of the microchannel and its connecting reservoirs. The microchannel section is enlarged to highlight the channel geometry. The important channel dimensions are: length 250 μm, width 5 μm and inlet radius of curvature 2.5 μm. Diagrams are not drawn to scale.

The design was drawn in AutoCAD (Autodesk Inc., San Rafael, CA) for fabrication on chromium masks (Photronics Inc., Brookfield, CT). The fabrication of the master utilized the technique of two-level photolithography (7; 48) (Fig. 12).

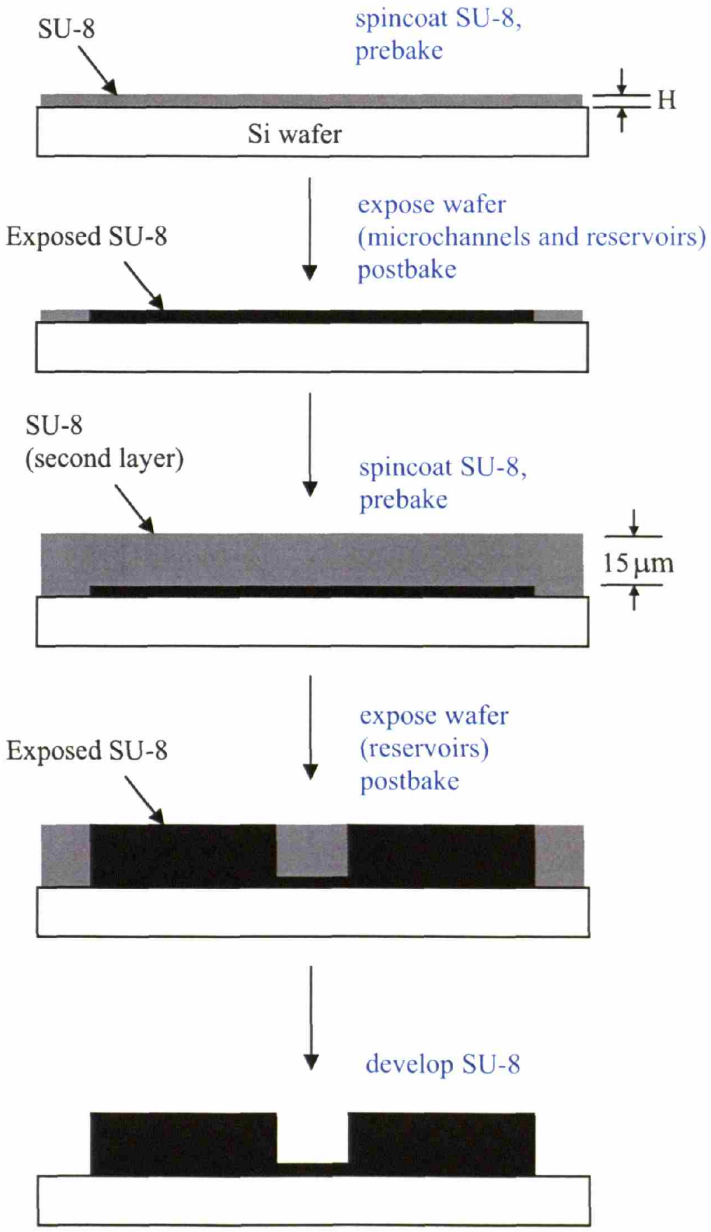

Fig. 12 Steps involved in microfabrication of master on silicon wafer by two-level photolithography. H has height of either 1.5 or 2.5 μm (adapted and modified from (48)).

Silicon wafers (100mm, 425-525 μm, 1-10 Ω – cm, [1-0-0]; Transition Tech. Int., Sunnyvale, CA) were spin-coated with the first layer of SU-8 2002 photoresist (Microchem Corp., Newton, MA) to a thickness

of either 1.5 or 2.5 μm, and prebaked at 95°C for 2 min. The resist was then exposed to UV light with an intensity of 10 $mWcm^{-2}$ for 11.5 s through the first chromium mask with features of the microchannel and the reservoirs (Fig. 13a). The resist was post-baked at 95°C for 2 min, which crosslinked the regions exposed to UV light. Next, a second layer of SU-8 2010 photoresist was spin-coated to a thickness of 15 μm on top of the first layer, followed by pre-baking at 95°C for 4 min. The second chromium mask with features of the reservoirs (Fig. 13b) only was aligned, and the photoresist was exposed for 20 s. After post-baking again at 95°C for 3 min, SU-8 developer (Microchem Corp., Newton, MA) was used for 5 min to develop the features in both resist layers. Finally, the height of the microchannel was checked with a profilometer (Dektak 2, Veeco Instruments, Woodbury, NY). An image of the master is shown in Fig. 14.

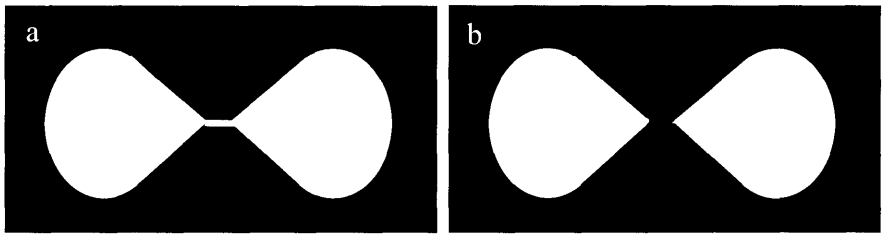

Fig. 13 Schematic of features in (a) first chromium mask which comprise microchannel and reservoirs and (b) second chromium mask with reservoirs only.

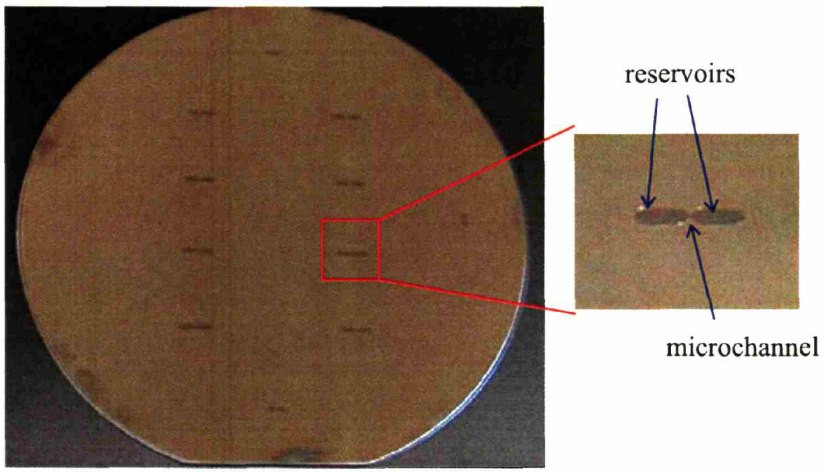

Fig. 14 Photograph of SU-8 master fabricated on a silicon wafer, with an enlarged view of one unit of the microfluidic system highlighting the reservoirs and the microchannel connecting them. As many as twelve such identical units could be fabricated on a single silicon wafer.

When the master was successfully fabricated, the device was formed in PDMS by replica molding (46) (Fig. 15).

The master of photoresist was first treated with trimethylchlorosilane (Sigma-Aldrich, St. Louis, MO) to prevent adhesion of PDMS to the master after curing. A curing agent and PDMS prepolymer (SYLGARD 184 Silicone Elastomer Kit, Dow Corning, Midland, MI) were mixed together in a 1:10 weight ratio and degassed for 5 min to remove air bubbles. The mixture was then poured onto the master and cured in an oven at 80°C for 3 hr. When cured, the PDMS was removed by peeling off the master. Inlet and outlet reservoir ports were formed by punching the PDMS with a 16-gauge adapter needle. Through these bored tunnels, inlet and outlet tubes would later be inserted, which allowed connection of the microfluidic device to the external macrofluidic system described below.

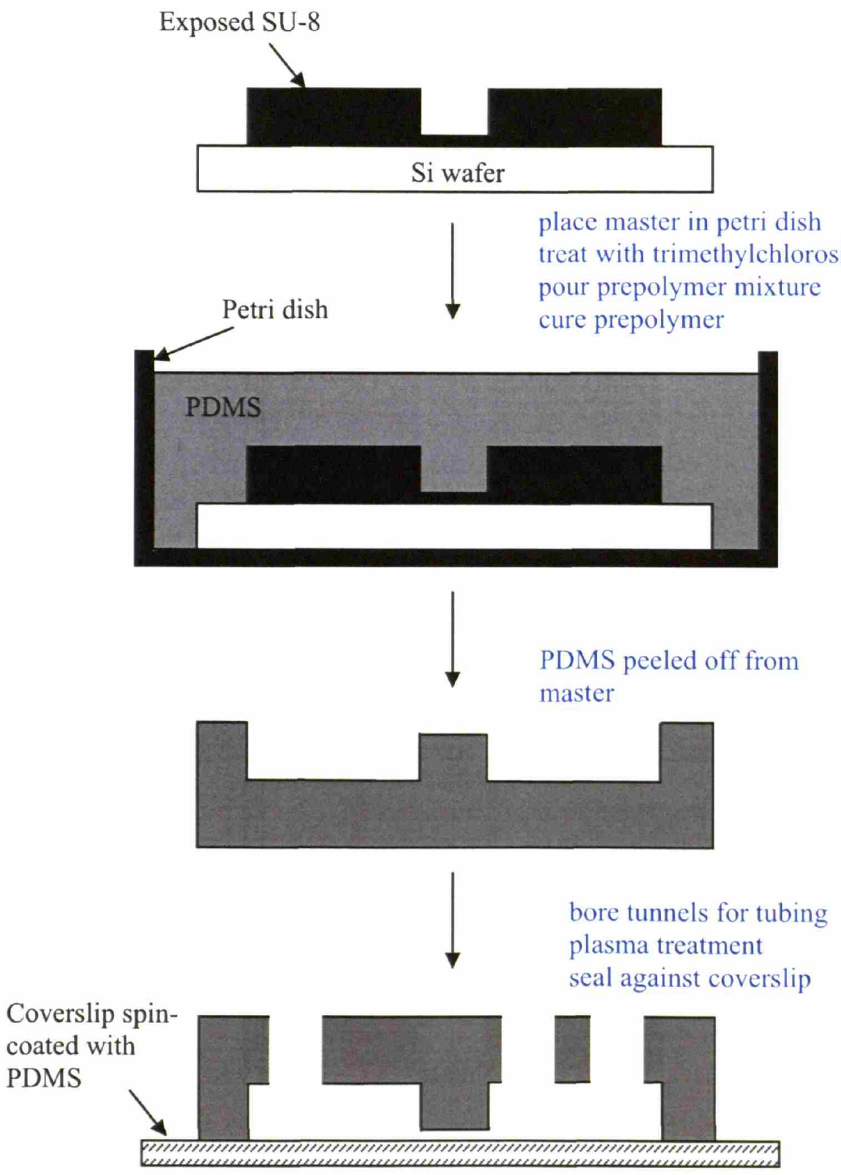

Fig. 15 Steps involved in replica molding of master with PDMS. (adapted and modified from (46)).

The final step involved sealing the PDMS to a glass coverslip. The coverslip was also spin-coated with a thin layer of the same PDMS elastomer and cured in the oven. Both the microdevice and the coverslip were subjected to plasma oxidation for 30 s (Plasma Cleaner, Harrick Scientific Corporation, Ossining, NY), after which the surfaces were brought together to form an irreversible seal and produce the finished device (Fig. 16).

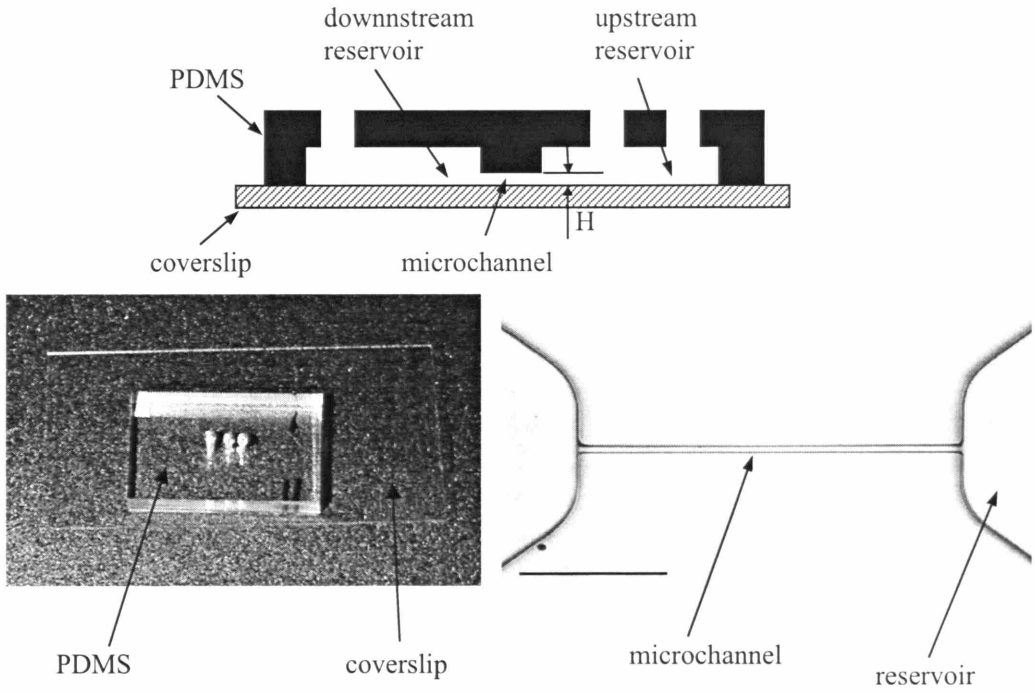

Fig. 16 (Top) Schematic diagram of the finished PDMS microfluidic device with two inlet and one outlet reservoir ports. The device is sealed on a glass coverslip. H represents the microchannel height, which is either 1.5 or 2.5 μm. Diagram is not drawn to scale. (Bottom left) Photograph of a finished microfluidic device. The holes seen on the PDMS are the reservoir ports. (Bottom right) Image of microchannel molded from PDMS as seen under a light microscope. Scale bar, 100 μm.

2.2.3 Macrofluidic System Setup

The microfluidic device was connected to a macrofluidics system that is capable of imposing physiological pressure differentials across the microchannels. The reservoir ports of the microfluidic device were connected to the macrofluidic system (Fig. 17) via plastic tubing (I.D. 0.5mm). The macrofluidic system has its own set of macro-reservoirs (to distinguish them from the microfluidic reservoirs). Pressure differential was imposed across the microchannel by varying the difference in height of water between the upstream and downstream macro-reservoirs. The upstream high-pressure macro-reservoir was positioned approximately 60 cm H_2O above the water level of the downstream

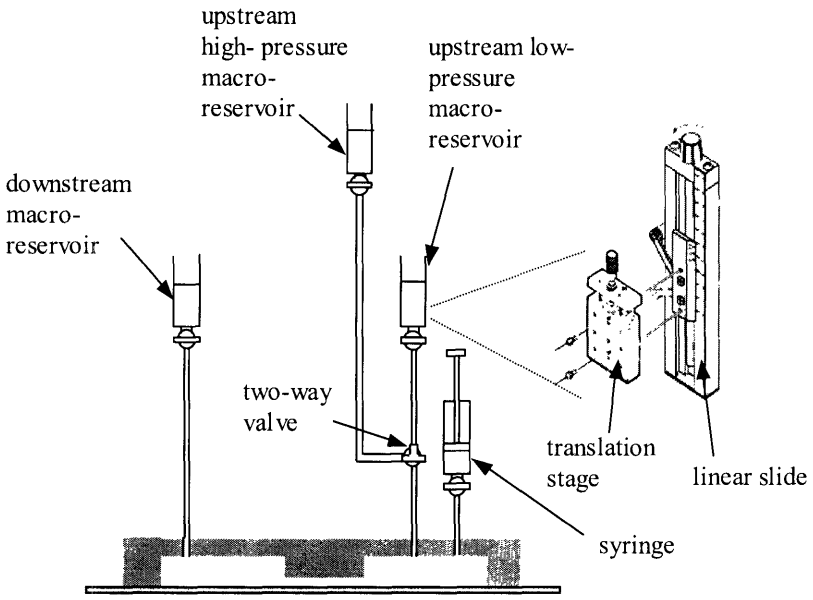

Fig. 17 Schematic showing the macrofluidic system setup and its connections to the microfluidic device.

macro-reservoir, producing a high flow rate of fluid used for purposes such as purging or cleaning the microfluidic system. The upstream low-pressure macro-reservoir was attached to a linear translation stage (Edmund Optics, Barrington, NJ), which, in turn was mounted on a linear slide (Rapid Advance Unislides, Velmex, Inc., Bloomfield, N.Y.). The linear translation stage was capable of fine-scale adjustment in (0.01 mm steps) between 0 and 25 mm, while the linear slide permitted coarse-scale adjustment (1 mm steps) between 0 and 28 cm. The upstream high and low-pressure macro-reservoirs were coupled via a two-way valve. With the use of wide macro-reservoirs (to ensure that the level of water in the reservoir remained practically unchanged during an experiment), the macrofluidic system enabled the precise determination of pressure differential applied across the microchannel. A syringe attached to the second port of the upstream microfluidic reservoir allowed the introduction of fluid or cells into the device.

2.2.4 Optical Microscopy

Neutrophils were observed using a differential interference contrast (DIC) microscope (Eclipse TE2000, Nikon Inc., Melville, NY) equipped with an oil immersion condenser lens (N.A. 1.4) and a 100×/1.4N.A. Plan Apochromat objective lens. Images were acquired with a video camera (CCD-100, Dage-MTI Inc., Michigan City, IN), and recorded onto a SVHS tape at 30 frames/s with a cassette recorder (SVO-9500MD, Sony Corporation, New York, NY). The movies were then converted into digital form with a computer equipped with a frame grabber card (Scion LG-3, Frederick, MD) (Fig. 18).

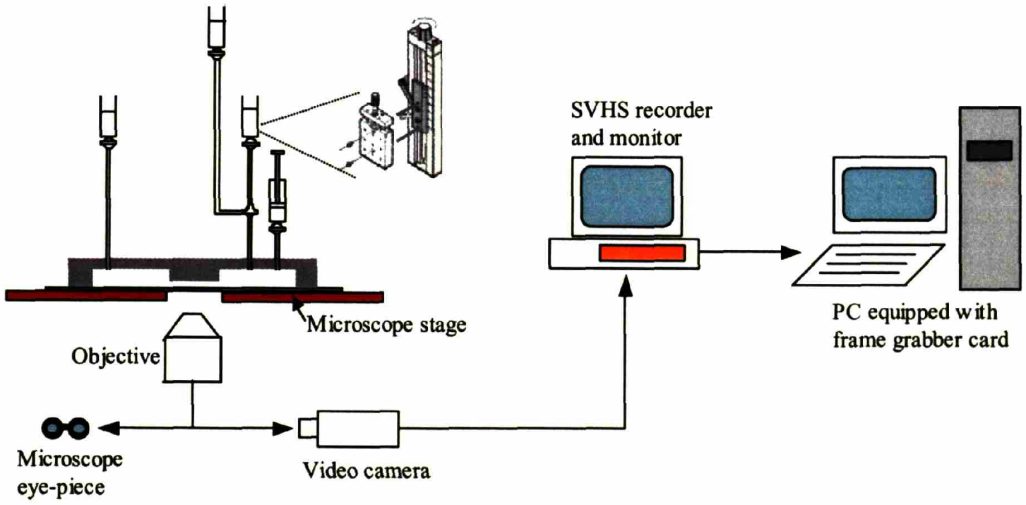

Fig. 18 Schematic showing the complete system setup

2.2.5 Deformation and Trapping of Neutrophils inside Microchannel

The microfluidic device was first incubated with 1% Pluronic F108 solution ($PEO_{129}/PPO_{56}/PEO_{129}$ triblock copolymers, BASF Corp, Mount Olive, NJ) in water for 2 hrs. This served to passivate the PDMS surface and deter cell adhesion. The PPO domain adsorbs to hydrophobic surfaces, creating a surface coating of hydrophilic PEO domain (Fig. 19). Consequently, the modified surface would prevent cell adhesion by resisting protein adsorption to surfaces, and the mechanism of resistance is thought to be attributed to its hydrophilicity, flexibility, chain mobility and high steric exclusion volume of the polymer in water (47).

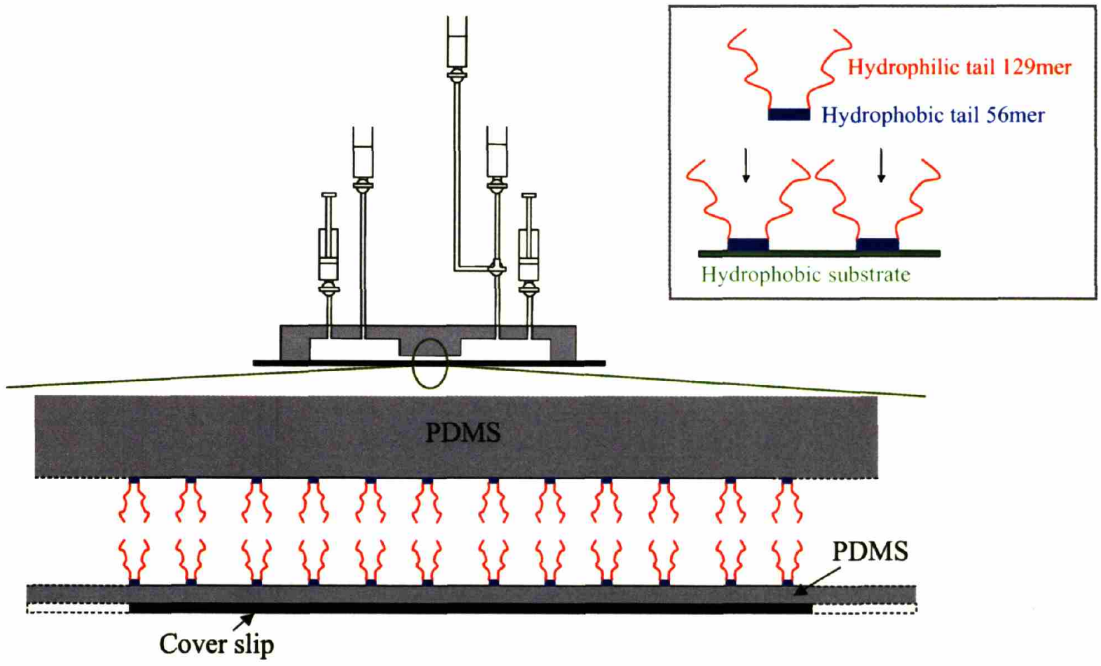

Fig. 19 Schematic showing the effect of incubating the microfluidic device with Pluronic F108. The microchannel section is enlarged to highlight the surface coating of the hydrophobic PDMS surfaces. (Inset) Diagram shows how the hydrophobic portion of the polymer (PPO domain) adsorbs to hydrophobic surfaces, leaving a surface coating of the hydrophilic portions (PEO domains)

The device was then flushed with medium (HBSS without Ca^{2+} or Mg^{2+} + 2% autologous plasma) for 15 min. An objective heater (Bioptech Inc., Butler, PA) set to 37°C, was used for experiments at body temperature.

To calibrate the pressure of the system, yellow-green fluorescent 0.1 μm microspheres (carboxylate-modified polystyrene fluospheres, Molecular Probes, Eugene, OR), diluted in HBSS (w/o Ca^{2+} or Mg^{2+}) at a concentration of 5×10^{8} beads/ml, were introduced into the upstream microfluidic reservoir. The fluorescent beads were observed through the microscope, which was also equipped for epifluorescence. The beads, which moved freely through the microchannel, were used to establish the

zero pressure difference, zero flow condition: with the two-way valve connected to the upstream low pressure macro-reservoir, the height of this reservoir was adjusted until the beads in the microchannel remained stationary. The details of the pressure calibration process is shown schematically in Fig. 20.

Neutrophils suspended in medium were then introduced into the upstream microfluidic reservoir. By setting the upstream two-way valve to open to the upstream high pressure macro-reservoir, the cells flowed quickly towards the microchannel entrance zone. Finally, the low-pressure macro-reservoir was raised to impose the desired pressure differential across the channel, initiating a flow of neutrophils into the microchannel (Fig. 17). Once a neutrophil had entered the microchannel, the low-pressure macro-reservoir was returned to its initial height, immediately stopping its flow through the channel.

2.2.6 Entrance Time and Time to Pseudopod Projection

Neutrophil behavior was recorded from the start of its deformation into the channel up to the formation of the first pseudopod projection either at the leading or trailing edge of the cell. The playback of the video recording allowed precise determination of neutrophil entrance time and the first observation of pseudopod projection. The entrance time was taken to be the interval between when the neutrophil leading edge touched the channel entrance (first contact) and when the trailing edge cleared the channel mouth after deformation. The time to pseudopod formation was defined as the time from first contact to the first appearance of the pseudopod projection.

2.2.7 Viscoelastic Properties of the Neutrophil Evaluated Using Multiple-Particle-Tracking Microrheology

Brownian motion of endogeneous granules inside the neutrophils was monitored using particle-tracking algorithms (14) written in the IDL software (Research Systems, Boulder, CO) from the instant the neutrophil was trapped in the microchannel until the observation of pseudopod projection. The focal plane for particle tracking was selected near the center of the microchannel in order to minimize wall effects. From the video images, the cytoplasm of the neutrophil was divided into two zones (Fig. 21);

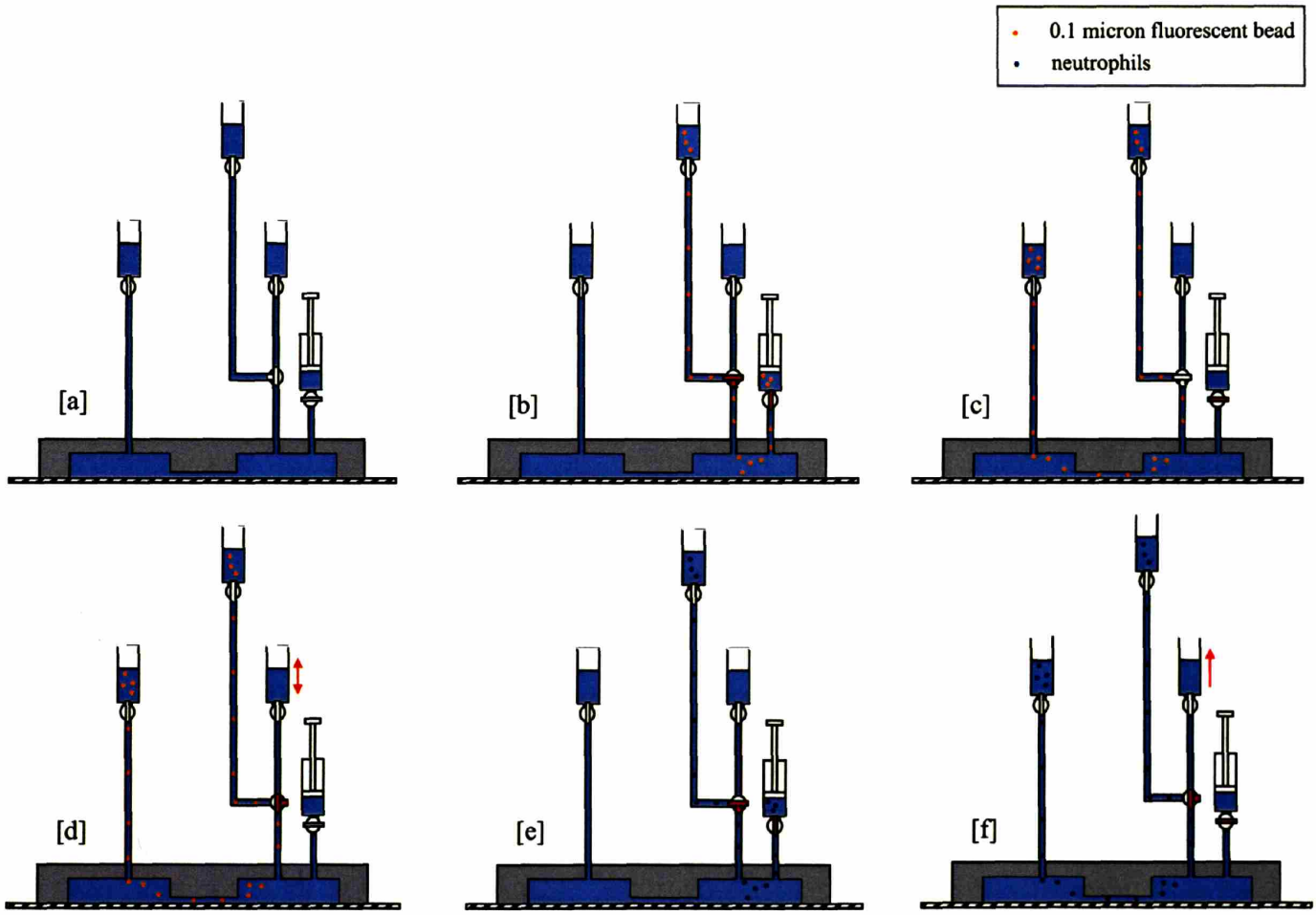

(a)	Initial position of all valves.
(b)	Introduction of 0.1 μm yellow-green fluorescent beads into the upstream microfluidic reservoir and upstream high-pressure macro-reservoir.
(c)	Fluorescent beads were allowed to flow through the microchannel into the downstream microfluidic and macro-reservoir
(d)	Two-way valve was adjusted so that the microfluidic reservoir was connected to the upstream low-pressure macro-reservoir. The height of this macro-reservoir was adjusted to attain zero-pressure, zero flow condition (beads in the reservoir remained stationary).
(e)	By switching back the two-way valve, neutrophils were introduced into the upstream microfluidic reservoir and upstream high-pressure macro-reservoir, so as not to disturb the calibrated fluid level in the low-pressure macro-reservoir.
(f)	The two-way valve was switched back once again to the upstream low-pressure macro-reservoir. This macro-reservoir was raised to a height which imposed the desired pressure differential as neutrophils flowed into the microchannel.

Fig. 20 Schematic showing sequence of steps involved in calibrating the pressure of the experimental setup, and subsequently the introduction of neutrophils into the system.

zone 1, just proximal to the nucleus, and zone 2, the remainder of the cytoplasm up to the cell tip. Granules in zone 1, as well as granules exhibiting obvious directed active movements in both zones were excluded from particle tracking.

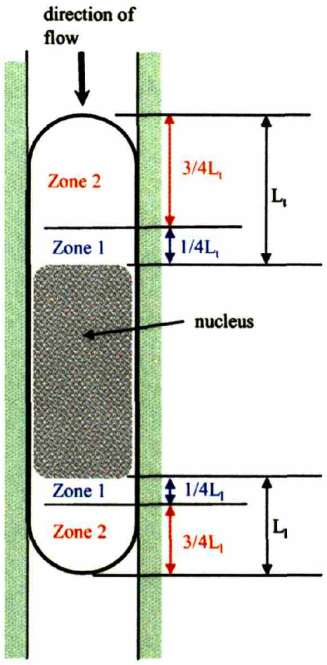

Fig. 21 Schematic diagram illustrating the division of the neutrophil cytoplasm into two regions; zone 1, proximal to the nucleus and zone 2, distal from nucleus up to the cell leading or trailing edge. Only granules dispersed in zone 2 were selected for particle tracking. L_l = length from nuclear boundary to the leading edge; L_t = length from nuclear boundary to the trailing edge.

In addition, only granules that appeared circular were selected for tracking, achieved by setting the computer algorithms to track particles with eccentricity of 0.3 or less (major and minor axis difference of less than 5%). Only particles that remained in focus for at least 30 frames were analyzed. Because of the high density of granules present in the neutrophil cytoplasm, all the tracks performed by the computer algorithms were visually checked with the original video images. This ensured that the same particle was followed throughout a particular track, and was not mistaken for neighboring particles that could have crossed its path. From these particle trajectories, mean-square displacements (MSD) and the frequency-

dependent elastic modulus, $G'(\omega)$, and loss modulus, $G''(\omega)$, were computed according to the methods of Mason et al. (64). The shortest time lag of 1/30s was chosen for these viscoelastic calculations as it gave the best statistical accuracy. The radius of a typical neutrophil granule was taken to be 300 nm (108) in these computations. Temporal changes in G' and G'' were examined by performing independent analysis on 5 s time intervals.

As control, the multiple-particle tracking technique was also performed on round passive neutrophils (Fig. 22A). This was carried out in a simple chamber assembled from a glass slide and a coverslip, using double-sided scotch tape as "spacer" between them. Neutrophils suspended in medium were introduced into the chamber with a pipette, and the edges of the chamber were subsequently sealed to prevent evaporation. Again, granules close to the nucleus were excluded from the particle track.

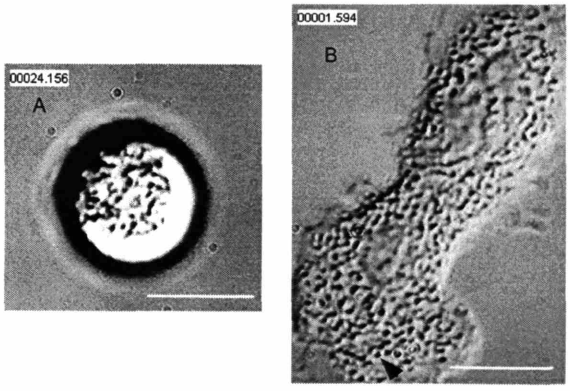

Fig. 22 (A) Image of a round, passive neutrophil. Clearly seen are the endogeneous granules in the cytoplasm of the cell. Scale bar, 5 μm . (B) Image of a neutrophil that had spread out on a coverslip showing many endogeneous granules dispersed throughout the cytoplasm. Only granules located at least 2 μm away from the nucleus (an example is shown with an arrow) were tracked while granules situated proximal to the nucleus were ignored in the tracking. Scale bar, 5 μm .

To confirm the validity and accuracy of the particle tracking system, the technique was repeated with adherent and spread neutrophils (Fig. 22B) on a glass coverslip. Neutrophils suspended in HBSS without Ca^{2+} or Mg^{2+}, were introduced into a glass slide and coverslip chamber as before. The absence of plasma in the suspension resulted in adhesion and spreading of the neutrophils on the coverslip. Only granules in the cytoplasm which were located at least 2 μm away from the nucleus of the cell were tracked. Values obtained for G' and viscosity, η, at 1 Hz were compared with published results of non-invasive intracellular measurement of neutrophils (108). Because the measurements were performed at a higher frequency to allow comparison with the published data, particles chosen for tracking were in focus for at least 100 frames.

The IDL programming code and commands used in the particle tracking can be found in Appendix 1.

2.2.8 Statistical Analysis

All results are expressed as the means ± SE. Comparisons of data were carried out using the paired, two-tailed student t-test, and findings that showed either $p<0.05$ or $p<0.01$ were considered significant.

2.3 Results

Neutrophils were introduced into microchannels comprising two different cross-sectional dimensions; a larger cross-sectional area with dimensions of 5 μm in width (W) and 2.5 μm in height (H), and a second smaller area with channel width of 5 μm and height of 1.5 μm. The effective diameter, D_{eff}, of the microchannels was calculated using the relationship $D_{eff} = \sqrt{4WH/\pi}$, hence, giving us effective diameters of 4.0 μm and 3.1 μm, denoted by D_L and D_S, respectively. Most experiments were carried out at 37°C, but some were also conducted at 23°C in order to examine the temperature-dependent behavior

of the cell. We found experimentally that the threshold pressure for the cell to successfully deform into the microchannels was ~ 0.4 mm H_2O for D_L, and ~ 2 mm H_2O for D_S. Therefore, different pressure ranges were used for the two channels: ΔP = 1, 10 and 50 mm H_2O for D_L, and ΔP = 10 and 50 mm H_2O for D_S. These values of ΔP chosen were above the threshold pressure for the respective channel diameters, but within physiological limits experienced by neutrophils in pulmonary capillaries (42).

Typical trajectories of the granules, individual MSD and average MSD plots for neutrophils before and after mechanical deformation are shown in Fig. 23A, 23B and 23C.

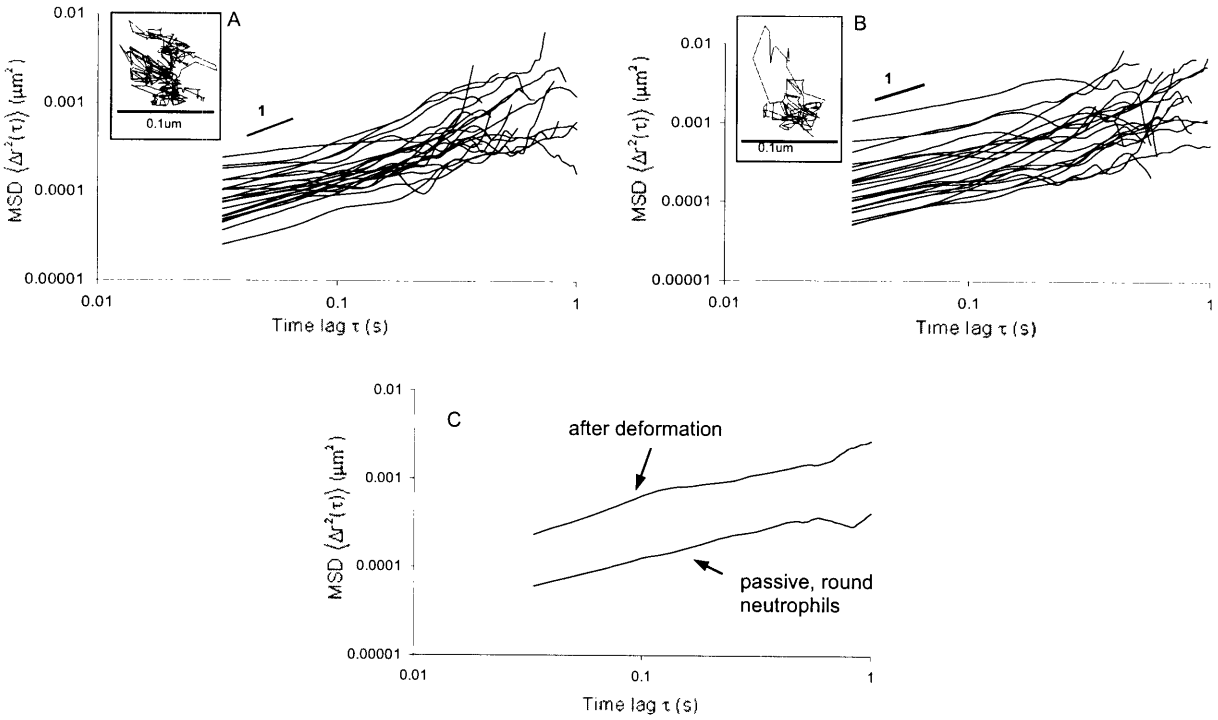

Fig. 23 (A) Individual MSD traces of randomly selected endogeneous granules for passive, round neutrophils (Inset) Typical trajectory of the centroid of a granule used to calculate the MSD. (B) Individual MSD traces of randomly selected endogeneous granules for neutrophils that have undergone deformation into a microchannel (Inset) Typical trajectory of the centroid of a granule used to calculate the MSD. (C) Typical plot of average mean-squared-displacement (MSD) curves for neutrophils before and after exposure to mechanical stimulation.

A representative sequence of events during neutrophil deformation, followed by trapping and, ultimately, pseudopod formation is depicted in Fig. 24. The location of pseudopod projection occurred randomly (either at the leading or trailing edge of the cell but never at both sites). Following pseudopod formation, the cell would begin to crawl along the microchannel in the direction of the pseudopod protrusion.

An increase in ΔP resulted in a decrease in entrance time (Fig. 25) as evidenced for example by comparing the data for D_L, 1 mm H_2O, 37°C and D_L, 10 mm H_2O, 37°C. Increasing the cross sectional area of the microchannel produced a similar effect (D_S, 10 mm H_2O, 37°C vs. D_L, 10 mm H_2O, 37°C), as was the case when the temperature was raised from 23°C to 37°C (e.g. D_L, 1 mm H_2O, 23°C vs. D_L, 1 mm H_2O, 37°C).

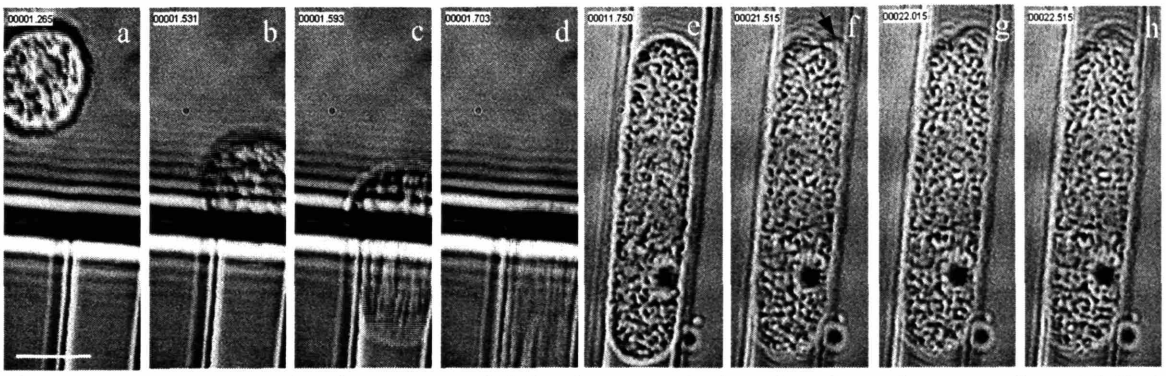

Fig. 24. Image sequence showing a neutrophil flowing towards the microchannel entrance [panel (a)], the leading edge of the cell just crossing the channel inlet [panel (b)], the cell undergoing deformation [panel (c)], the trailing edge of fully deformed cell just clearing the channel mouth [panel (d)] and subsequently, the neutrophil was trapped in the channel [panel (e)]. After some time, the cell can be seen to form pseudopod projection [panels (f) to (h)]. Arrow in panel (f) points to the location at the trailing edge of the cell where pseudopod protrusion was first seen. Here, the neutrophil was flowing into D_L under pressure difference of 50 mm H_2O at 37°C. Scale bar, 5 μm.

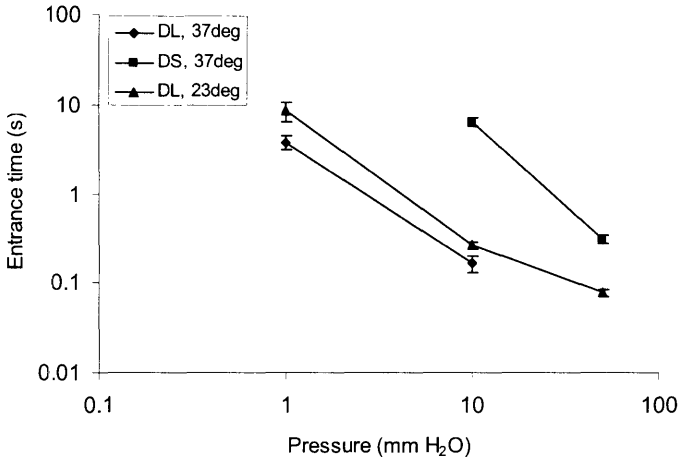

Fig. 25 Entrance time for different experimental conditions. Data are expressed as means ± SE. The number of observations, n, for the corresponding experimental conditions are as follows: D_L, 1 mm H_2O, 37deg (n=8); D_L, 10 mm H_2O, 37deg (n=8); D_S, 10 mm H_2O, 37deg (n=4); D_S, 50 mm H_2O, 37deg (n=4); D_L, 1 mm H_2O, 23deg (n=5); D_L, 10 mm H_2O, 23deg (n=8); D_L, 50 mm H_2O, 23deg (n=6)

The time to pseudopod formation is shown in Fig. 26 for different experimental conditions. Pseudopods were observed for D_L, 1 mm H_2O and D_L, 10 mm H_2O at 37°C, but not for similar conditions at 23°C. Only when ΔP was raised to 50 mm H_2O for the case of D_L, 23°C, was pseudopod projection observed, and then, only after ~100s from the time of cell entry into the channel. For D_L, 1 mm H_2O, 23°C and D_L, 10 mm H_2O, 23°C, no pseudopod projection was observed even though the cells were monitored for >10 min.

Since the time to pseudopod activation varied with temperature, we focused on the conditions at 37°C to examine the effect of entrance time. Comparison of experiments carried out at 37°C (Fig. 27) showed a clear inverse correlation between deformation rate (computed as the inverse of entrance time) and the time of pseudopod formation. These results suggest that neutrophil activation as reflected by pseudopod formation will occur more rapidly when neutrophils are subjected to a higher rate of deformation.

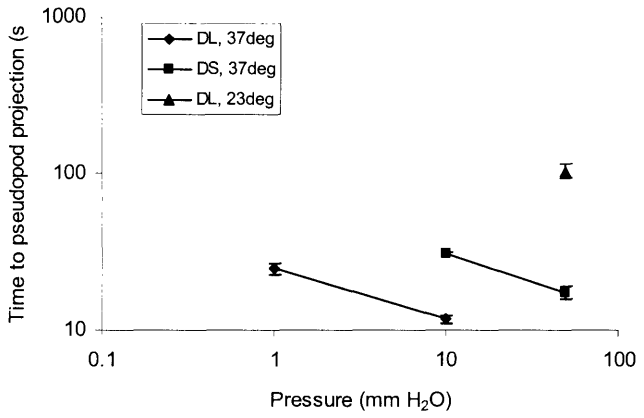

Fig. 26 Time to pseudopod projection for different experimental conditions. Data are expressed as means ± SE. The number of observations, n, for the corresponding experimental conditions are as follows: D_L, 1 mm H_2O, 37deg (n=5); D_L, 10 mm H_2O, 37deg (n=8); D_S, 10 mm H_2O, 37deg (n=4); D_S, 50 mm H_2O, 37deg (n=4); D_L, 50 mm H_2O, 23deg (n=5). Not shown in the figure are data for D_L, 1 mm H_2O, 23 deg (n=5) and D_L, 10 mm H_2O, 23 deg (n=6), in which, no pseudopod projection was observed even though the cells were monitored for at least 10 min.

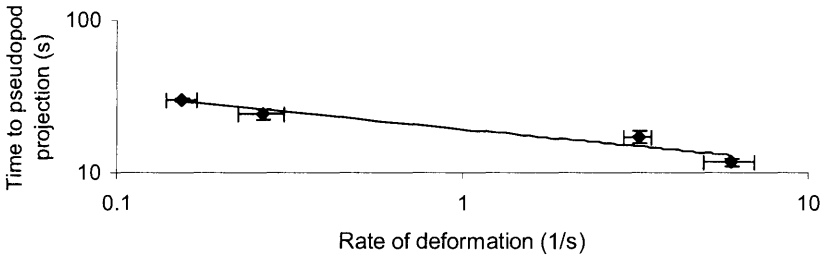

Fig. 27 Effect of rate of deformation on time to pseudopod projection for neutrophils at 37°C .

To investigate the effects of mechanical deformation on the viscoelastic properties of neutrophils, we used the multiple-particle-tracking method. The technique was first applied to adherent and spread neutrophils (Fig. 22B). Measurements at 1 Hz (see Table 3) revealed an elastic modulus, G', of 43.8 ± 5.0 dyn/cm^2, and viscous modulus, η, of 2.2 ± 0.3 dyn-s/cm^2. Round, passive neutrophils introduced into the

glass slide-coverslip chamber and allowed to settle on the coverslip were also studied. Due to the presence of plasma in their surrounding medium, the majority of the neutrophils (~98%) remained round (Fig. 22A) and free of pseudopod projection. Some of these adhered non-specifically to the coverslip whereas the rest floated loosely at the bottom of the chamber. Because the round, adherent cells remained stationary, they were chosen for particle tracking. The viscoelastic values of neutrophils were G'= 242 ± 21 dyn/cm^2 and G"= 470 ± 40 dyn/cm^2 at 37°C, as summarized in Table 3. These values were significantly lower ($p<0.05$) than the viscoelastic moduli at 23°C (G'= 303 ± 19 dyn/cm^2 and G"= 649 ± 55 dyn/cm^2), highlighting the effect of temperature on the mechanical properties of the cell.

	G' (dyn/cm^2)	G'' (dyn/cm^2)	G''/G'
Adherent, spreading neutrophil, 37 deg (n=4;N=70)	44	14	0.32
Passive, round neutrophil, 37 deg (n=4;N=51)	242	470	1.9
Passive, round neutrophil, 23 deg (n=4;N=71)	303	649	2.1

Table 3 Elastic modulus (G'), loss modulus (G") and the ratio (G"/G'), each evaluated at a lag time of 0.03s, of adherent, spread neutrophils at 37°C and passive, round neutrophils at 37°C and 23°C. n = number of cells; N = number of granules.

In order to study the effect of mechanical deformation on the viscoelastic properties of neutrophils, particle tracking was performed once the cells had entered the microchannel. The experiments were carried out at 37°C. The motion of neutrophil granules was monitored as soon as the cell was immobilized and the image focused. Tracking continued until the first observation of pseudopod projection, beyond which the cell began to crawl and granular motion became erratic, complicating the analysis. The temporal changes in G' and G" for the different flow conditions are shown in Figs. 28 and 29, respectively.

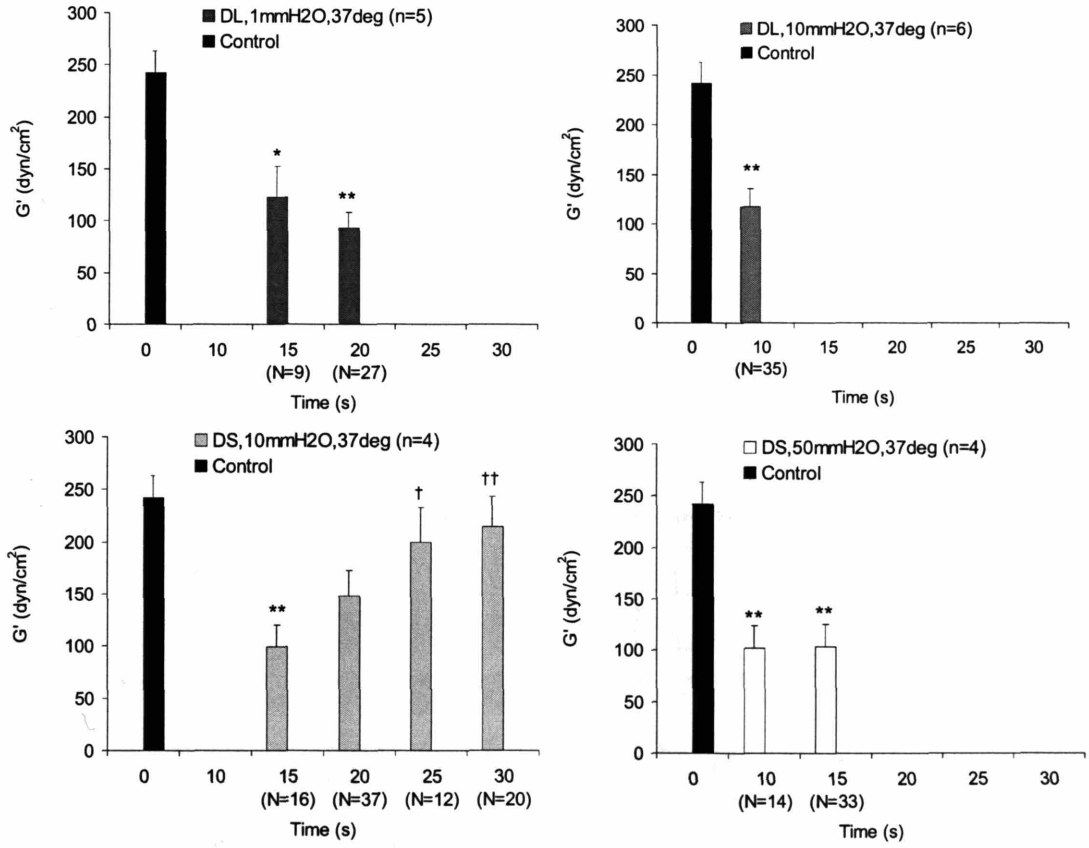

Fig. 28. Temporal change in elastic modulus, G', of neutrophil after mechanical deformation into a microchannel, at a lag time of 0.03s. Graphs show changes in G' under different flow conditions at 37°C. Time = 0 s represents the instance when leading edge of cell had just crossed the channel inlet. The time at which G' could first be recorded varied due to dissimilar entrance time for the different flow conditions. Value of G' for passive, round neutrophils at 37°C (Table 3) serves as control. Data are expressed as means ± SE. n = number of cells; N = number of granules; *P<0.05 and **P<0.01 when compared to control; †P<0.05 and ††P<0.01 when compared to data at t = 15s.

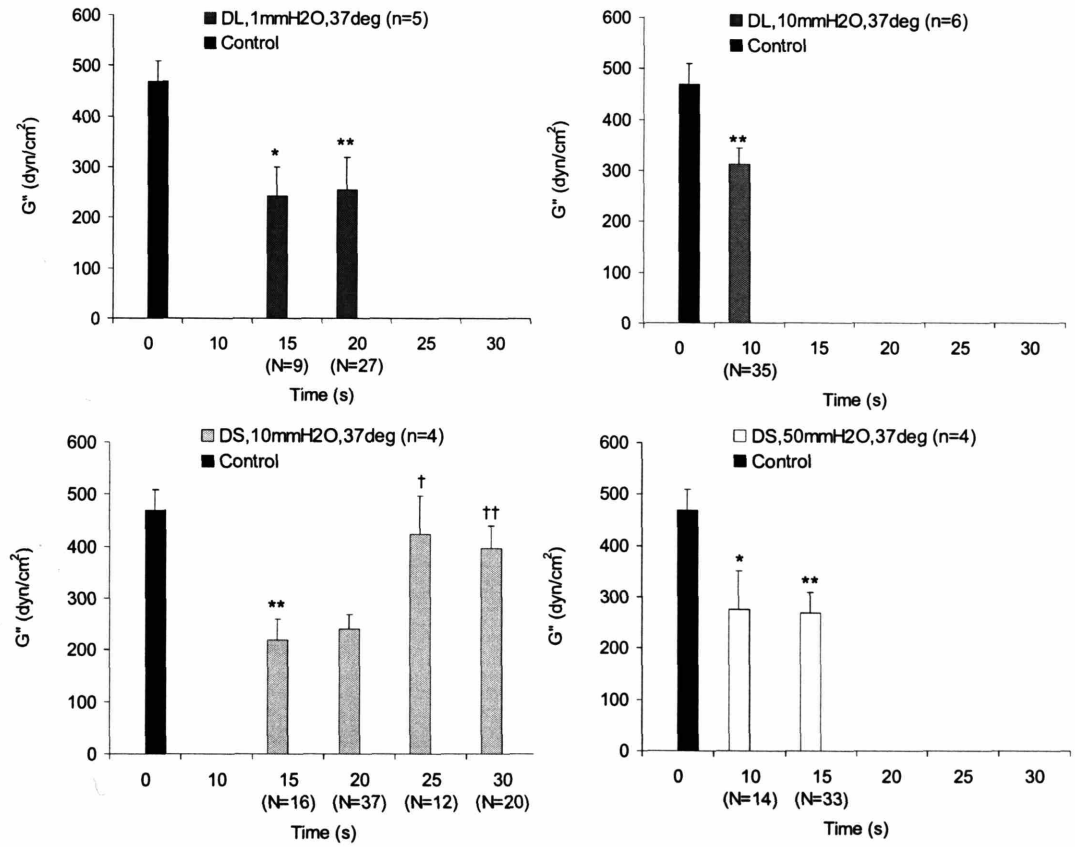

Fig. 29 Temporal change in loss modulus, G", of neutrophil after mechanical deformation into a microchannel, at a lag time of 0.03s. Graphs show changes in G" under different flow conditions at 37°C. Time = 0 s represents the instance when leading edge of cell had just crossed the channel inlet. The time at which G" could be first recorded varied due to dissimilar entrance time for the different flow conditions. Value of G" for passive, round neutrophils at 37°C (Table 3) serves as control. Data are expressed as means ± SE. n = number of cells; N = number of granules; *P<0.05 and **P<0.01 when compared to control; †P<0.05 and ††P<0.01 when compared to data at t = 15s.

Using values obtained for passive, round neutrophils (Table 3) as controls, the data show that mechanical deformation causes a significant drop ($p<0.05$) in G' and G". For all the flow conditions, the

mean value of G' was reduced by approximately 50-60% from its pre-deformation value of 242 dyn/cm^2. Similarly the mean value of G"was reduced by approximately 35-50% after deformation. Interestingly, although mechanical deformation resulted in a softer and less viscous cytoplasm, the drop in magnitude of G' and G" was quantitatively similar and was independent of the degree of deformation. For the flow conditions of [D_L, 1 mm H_2O, 37 deg], [D_L, 10 mm H_2O, 37 deg] and [D_S, 50 mm H_2O, 37 deg], the cell maintained the softer, lower viscosity properties until pseudopod projections appeared. However, for the flow condition of [D_S, 10 mm H_2O, 37 deg], after the initial drop, G' and G" was seen to recover to roughly its pre-deformation value before pseudopod projection. This flow condition corresponded to the case of lowest rate of deformation in Fig. 27.

Although quantitative particle-tracking was not possible once the neutrophils begin to crawl, observation of random granule motion of the neutrophils showed periodic cycling of enhanced and reduced motion paralleling the cyclic projection of pseudopods during cell locomotion. The granules at the pseudopod leading edge were seen to have increased activity when a new wave of granules first flowed into the pseudopod, however, the granule activity soon diminished and remained low even during the next cycle of pseudopod projection. Only after the new pseudopod had fully extended would granular motion increase again when the next wave of granules entered the newly formed pseudopod. These observations are consistent with those seen in neutrophils locomoting on a flat substrate (108).

2.4 Discussion

This study provides direct evidence that mechanical force of a magnitude comparable to that encountered by a neutrophil during transit through the microcirculation exerts a strong and fundamental effect on cell structure and function. The consequences of mechanical stimulation are immediate, occurring within seconds of stimulation, and substantial. A drop in shear modulus by more than 60% is observed within seconds of entering a constriction, independent of magnitude of the stimulus. In contrast, pathways leading to migratory behavior are excited in a strain rate-dependent manner, suggesting that

these two phenomena may be independently controlled. Taken together, these results suggest an important role for mechanical stimulation of neutrophils, influencing both their rheology and their migratory tendencies.

The combination of microfabrication and particle tracking microrheology allowed us to simultaneously visualize and quantify the response of neutrophils. Previous studies of neutrophil deformation have been conducted using in-vitro filtration (21; 55; 80) or micropipette aspiration (18; 77). In the former, large cell numbers enabled studies of changes in deformabilities and biochemical analysis of the changes in F-actin content and free $[Ca^{2+}]_i$ for example, but direct rheological measurements were not possible. Micropipette experiments provide data on cell rheology, determined from entrance times, but provide limited data on time-dependent changes in viscoleastic properties or changes in specific cell constituents. Analysis of the thermal motions of endogenous granules would be difficult in this situation due to the requirement of high resolution optics. In particular, methods used previously to infer rheological properties from micropipette aspiration times assume that the rheological parameters are constant in time and unaffected by the mechanical forces imposed during manipulation of the cell. Our results suggest that this may not be a valid assumption.

The microfluidic device was coupled to a macrofluidic system consisting of a set of reservoirs. Pressure difference was imposed across the microchannel by varying the height of water in the reservoirs. The threshold pressure, ΔP_{thr}, for D_L and D_S in the experiment was compared with the theoretical expression, $\Delta P_{thr} = 4\gamma\left(\frac{1}{D_{pipet}} - \frac{1}{D_{cell}}\right)$, where the cell cortical tension, $\gamma = 35\text{pN} / \mu\text{m}$ has been measured previously (111). Due to the rectangular cross-section used in the present experiments, we can make only an approximate comparison by substituting D_{eff} for D_{pipet}. Doing so, we find that the experimentally measured values of ΔP_{thr} (0.4 and 2.0 mm H_2O for the large and small channels, respectively) are somewhat lower than the theoretically predicted values of 1.9 and 2.7 mm, H_2O but this difference could be attributable to the different cross-sectional shape or entrance geometry. In contrast, entrance times

observed in the present experiments were approximately 40 times smaller than those reported in the literature for micropipette aspiration under similar driving pressures and diameters. Cross-sectional shape might also influence entrance times, but the entrance geometry also likely contributes. Previous numerical simulations have shown that entrance times depend strongly upon the axial radius of curvature of the entrance (8). This would be consistent with the observation that the entrance to our microchannels tends to be somewhat more rounded than that of a micropipette. However, aside from a slight lowering of the threshold pressure and shorter entrance times, the effects of driving pressure, channel cross-sectional area and temperature (Fig. 25) are generally consistent with previously published results (25).

Mechanical deformation of neutrophils into the pulmonary capillaries induced pseudopod formation for all experimental conditions at 37°C but only at the higher values of ΔP for experiments at 23°C (Fig. 26). Comparing similar experimental conditions, it took considerably longer for pseudopod projection at the lower temperature (10-30 s at 37°C, and ~100s at 23°C). Furthermore, the results indicate that for a given temperature, the time to pseudopod projection is inversely correlated to the rate of deformation of the neutrophil (Fig. 27), which we use here as a measure of the stimulus magnitude. These results are consistent with observations of activation reported in a previous micropipette aspiration study (25) that reported a transition from passive to active motile state, with activation time varying between 0 and 120 s at 37°C and between 60-120 s at 23°C. Hence, our results confirm that mechanical deformation is not a passive event; that rather, it leads to neutrophil activation with pseudopod formation if the stimulus is sufficiently large. Above the threshold stimulus, it appears that the time required for activation is dependent upon the rate of deformation experienced by the cell, implying the existence of a mechanosensing or signal transduction mechanism in the cell that is able to modulate the response according to the magnitude of the mechanical stimulus. In contrast, we found that neutrophil entrance time behaved in a manner more consistent with a passive cell in that it was determined primarily by the initial value of the shear modulus, which was only slightly dependent upon temperature. (Fig. 25).

Our measurements of viscoelastic moduli of adherent, spread neutrophils obtained using the particle tracking system (Table 3) can be compared with published results of Yanai et al., who reported

mean values of G'~ 10 dyn/cm^2 and $\eta \sim 4.0$ dyn-s/cm^2 for the body and trailing region of the neutrophil using an optical trap to excite the granules at frequencies between 0.3 and 3 Hz. Our measurements for η matched closely with the previously published results while the value for G' was about 4 times higher. One potential explanation for this difference is that the optical trap technique was capable of measuring only those granules that were freely moving, while other particles were too stiff to be oscillated at maximum laser power.

Table 3 also shows the ratio of G"/G' for the measurements carried out on adherent, spread neutrophils and those for passive, round cells at 37°C and 23°C. Our value of G"/G' of 0.32 for adherent, spread neutrophils matches the value of ~0.3 obtained at 0.75 Hz using magnetic twisting cytometry (27). However, there are no similar figures reported in the literature for passive, round cells. Nevertheless, the values of G"/G' of ~2.0 for passive, round cells is within the limits of the values (0.25 to 20) reported for other cell types using various experimental techniques (27; 98; 107).

In order to gain further insight into the effects of mechanical deformation on the cytoskeletal structure of the neutrophil, the granules of the neutrophils were tracked to monitor the change in rheology of the cell before and after deformation. Mechanical deformation results in a reduction in elastic moduli by 50-60%, within 10-15 s after the initial stimulus, from its value as a passive, round cell before deformation (Figs. 28 and 29). Similarly, the loss moduli drop by 35-50% from the cells' unactivated values. These data demonstrate that mechanical deformation causes either disruption or remodeling of the neutrophil cytoskeleton. In view of the decrease in viscoelastic properties of the cell, this might be due either to a sudden depolymerization of filamentous actin or rupture of cross-links bridging between actin filaments. The lack of a significant temperature effect on entrance time, in combination with the short time scale of the modulus changes (~10s), leads us to favor the theory that the rapid deformation ruptures actin cross-links. In contrast, Kitagawa and co-workers (55), observed an immediate but short-lived increase in F-actin, leading them to conclude that mechanical deformation resulted in increase in

actin cross-linking events rather than actin polymerization. Further experiments are required to reconcile these seemingly contradictory results.

Another interesting observation is that the magnitude of drop in the values of G' and G'' after deformation was found to be independent of the degree of deformation. This is in contrast with the time to pseudopod formation which correlates with the rate of deformation. Also, neutrophils subjected to low deformation rates were observed to recover much of their modulus reduction within ~30 s and return nearly to their initial mechanical state. These data suggest that the extent of depolymerization or loss of actin-cross linking is similar regardless of the magnitude or rate of deformation, at least within the range of these experiments, but the initiation of actin polymerization to form pseudopods is dependent on the magnitude of force transduced. One scenario consistent with these observations is that the large strain deformations effectively shear and rupture many of the actin cross-links, leaving them attached to one filament but displaced relative to their initial cross-linking site. Once the deformation stops, these cross-links can reform, but do so in the new, deformed state, returning the cell to its initial mechanical state but in a new, deformed geometry. Thus, it appears that the molecular mechanism controlling the depolymerization/actin crosslink breakdown is separate from the mechanism governing pseudopod formation and viscoelastic recovery, however further experiments would be needed to confirm this.

This evidence of viscoelastic recovery could help explain results from neutrophil recovery experiments after deformation into micropipettes (93). In that study, neutrophils were aspirated fully into a micropipette and held for a various periods of time before being expelled. Cells held in the micropipette for a short time (< 5s) exhibited a rapid elastic rebound immediately after being expelled from the pipette. In contrast, neutrophils held for longer times (> 5s) displayed a smoother recovery, and took much longer to recover to their spherical shape (~75 s to reach 90% of its full recovery compared to ~55s for the short holding time). These observations can be explained on the basis of the rapid fall and slower recover of modulus following deformation observed in the present experiments. Cells ejected immediately after being aspirated, would have a low internal modulus and few cross-links, thus their surface tension could rapidly return the cell to a spherical shape. Cells held for a longer period, would remodel due to

reformation of actin cross-links; upon ejection the cell would need to remodel once again, but this time under the action of a much smaller restoring force, that due to surface tension alone.

We recognize that the multiple particle tracking technique used in this investigation has limitations especially when compared to the recently developed method of two-particle microrheology (15; 30). In multiple particle tracking, granule size must be estimated, introducing error (approximately a factor of 2) into the viscoelastic modulus obtained. In two-particle microrheology, the cross-correlated motion of pairs of particles is independent of particle size and shape and is unaffected by the coupling between the particles and the medium. Unfortunately, measurement by the two-particle technique requires data collection over a much longer period of time than the multiple particle tracking method, hence preventing us from monitoring temporal changes in the cell. The two particle microrheology technique is more suitable for measurements where the behavior of the cells is relatively unchanged over the period of data collection (59). Thus, we resort to the multiple particle tracking method in the present study, and in the application of this technique, we maximized the accuracy of the results by eliminating granules that are not circular and also selecting granules of almost equal size. Since active motion can only cause an apparent reduction in modulus (greater granular motion), however, these results represent a lower bound on modulus.

In summary, this study shows that mechanical deformation of neutrophils into pulmonary capillaries results in activation of the cell by inducing cytoskeletal remodeling, leading to changes in viscoelastic properties and pseudopod projection. Hence, mechanical deformations are capable of activating a neutrophil, providing a migratory stimulus and thereby enhancing their tendency to transmigrate across the endothelium.

Chapter 3

Cytoskeletal Remodeling and Cellular Activation during Deformation of Neutrophils into Narrow Channels

3.1 Introduction

As neutrophils travel from the arterial to the venous side of the pulmonary microcirculation, they must traverse 50-100 capillary segments (31; 38; 39), ranging in diameter from 2 to 15 μm (17). When neutrophils encounter a capillary segment narrower than their size (6-8 μm), they will have to deform in order to pass through.

Early studies on the behavior of neutrophils during deformation into narrow capillaries assumed that the cell remained passive throughout the process (26; 68; 93; 94) and that the induced stresses had no effect on cell behavior. However, recent studies have begun to address the dynamic response of leukocytes as a result of mechanical stimulation. In particular, mechanical deformation was shown to upregulate adhesion molecules, reorganize and stabilize the cell cytoskeleton and increase free $[Ca^{2+}]_i$ (55). Neutrophils have also been shown to respond to fluid shear stress by reducing their internal stiffness, altering their adhesion to substrates, as well as generating pseudopod projections (13; 56; 66). In our recent study (110), we designed an in-vitro microchannel and associated flow system to study the response of neutrophils to mechanical deformation, mimicking the physiological conditions experienced during passage through pulmonary microvessels. Results from rheological studies showed an immediate reduction in the complex shear modulus, with subsequent recovery within one minute, suggesting that the neutrophil rapidly remodeled its cytoskeleton when subjected to mechanical deformation. Above a threshold stimulus, mechanical stimulation resulted in cell activation evidenced by projection of

pseudopods. In the present work, we investigate the mechanism(s) governing this cytoskeletal remodeling process that takes place when the cell undergoes mechanical deformation.

3.2 Materials and Methods

3.2.1 Preparation of Human Neutrophils

Human neutrophils were isolated from healthy adult volunteers by Histopaque centrifugation, dextran sedimentation, followed by hypotonic lysis of contaminating erythrocytes, as described previously (110). The isolated neutrophils were suspended in medium (Hanks' balanced salt solution without Ca^{2+} or Mg^{2+} supplemented with 2% autologous plasma). The cells were counted, and the concentration was adjusted to 5.0×10^5 cells/ml. Subsequently, the neutrophils were kept either at room temperature or incubated in a 37°C water bath according to the required experimental conditions.

3.2.2 Constant-Pressure In-Vitro Filtration System

The constant-pressure filtration system consisted of a small reservoir connected to a filter holder on the downstream end, and to a large reservoir on the upstream side (Fig. 30). Both the small reservoir and the filter holder were enclosed in water jackets and maintained at constant temperature (either 23°C or 37°C). Two different polycarbonate filters were used (GE Osmonics, Inc., Minnetonka, MN) : one with a pore diameter of 3 μm , pore length of 9 μm , and pore density of 2.0×10^6 /cm^2; and another with a pore diameter of 5 μm , pore length of 10 μm , and pore density of 4.0×10^5 /cm^2. In order to minimize adhesion of neutrophils (47), before the start of experiments, the polycarbonate filters were immersed in a 1% Pluronic F108 solution (PEO/PPO/PEO triblock copolymers, BASF Corp, Mount Olive, NJ) in water for 2 hrs, and subsequently flushed with medium for 15 minutes.

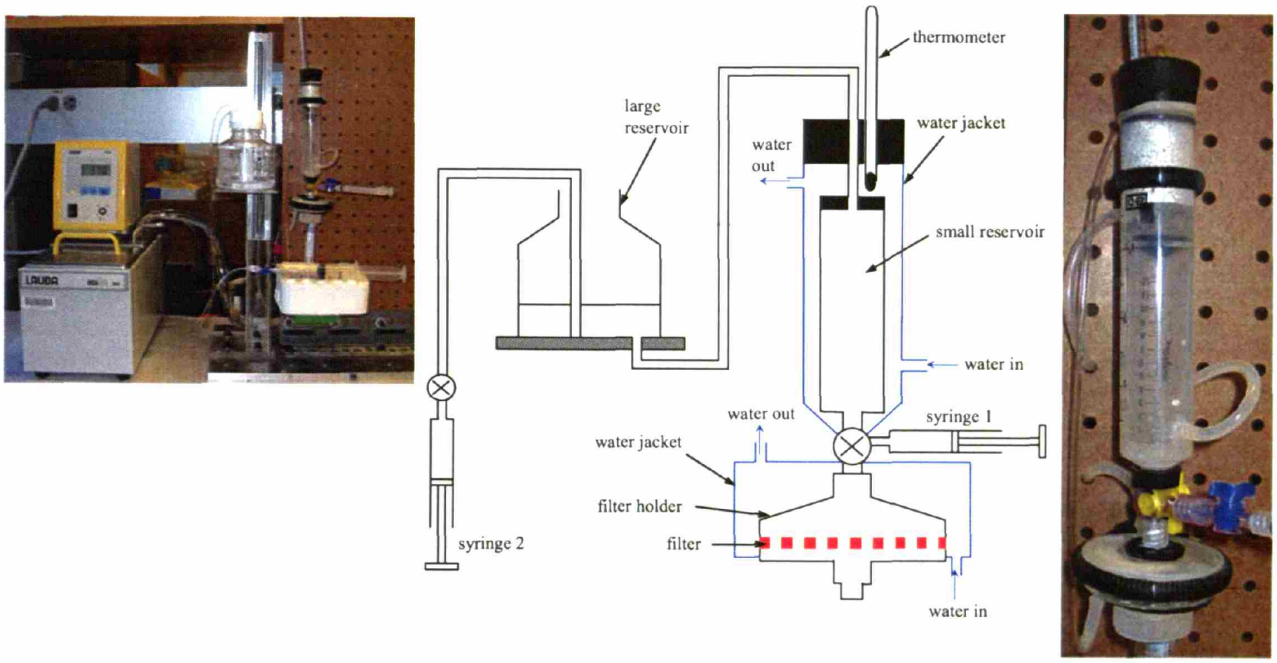

Fig. 30 Schematic showing design of the constant-pressure in-vitro filtration setup. Neutrophils were passed through the filters at upstream pressures determined by the height of the large reservoir. The post-filtered cells were subsequently collected and fixed in paraformaldehyde.

Medium was first introduced throughout the system with syringes 1 and 2 (Fig. 30) after equilibrating with the constant temperature water jackets for at least 10 minutes. Neutrophils were then introduced via syringe 1 into the small reservoir, ready for the filtration process. Pressure upstream of the filter could be changed by adjusting the height of the reservoir relative to the height of the filter with a linear vertical slide (Rapid Advance Unislides, Velmex, Inc., Bloomfield, NY). Finally, the valve was set to allow the neutrophils to flow directly into the filter holder. With the use of the large reservoir (to ensure that the level of fluid in the reservoir remained nearly constant during the experiment), neutrophils were passed through the filter holder at a constant pressure difference, which for this study was either 5 cm H_2O or 19.5 cm H_2O. The average volume flow rate of filtration was obtained by dividing the filtrate volume by the collection time .

3.2.3 Constant-Flow-Rate In-Vitro Filtration System

The system for constant-flow-rate filtration is designed after one used previously (55; 60). Neutrophils at concentration of 5.0×10^5 cells/ml were loaded into a 12 ml polypropylene syringe (Monoject®, Sherwood Davis & Geck, St. Louis, MO) which was mounted onto a syringe pump (pump 22, Harvard Apparatus, Holliston, MA), capable of delivering the sample fluid at a constant flow rate. Neutrophils were filtered through polycarbonate filters at 3 different flow rates, 1.0, 3.0 and 6.0 ml/min, at room temperature ($\sim 23°C$). The filter used has a pore diameter of $3\ \mu m$, with pore length and density as specified above. As before, the filters were also treated with 1% Pluronic F108 solution prior to use. Pressure upstream of the filter was continuously monitored with a pressure transducer (Validyne Engineering, Northridge, CA).

3.2.4 Quantitation of Neutrophil Morphology

Neutrophils filtered through the polycarbonate filters were fixed immediately in paraformaldehyde (4% vol/vol) for 20 min at room temperature, and washed twice in HBSS. For each preparation (n=3), 50 neutrophils were chosen randomly, and the cells were observed by light microscopy (Eclipse TE300, $60\times$, Melville, NY). Images were analyzed to determine cell circularity using the image analysis software ImageJ v.1.33 (National Institute of Health, Bethesda, MD). Circularity ($4\pi \times \text{area} / \text{perimeter}^2$) of the cell approaches 1.0 for a perfect circle; lower values reflect a progressively elongated ellipse.

3.2.5 Quantification of F-actin Content

As above, resting neutrophils or neutrophils filtered through the polycarbonate filters were fixed immediately in paraformaldehyde (4% vol/vol) for 20 min at room temperature, and washed twice in HBSS. Cells were then incubated in a final concentration of $2\ \mu M$ lysophosphatidylcholine (Sigma-Aldrich, St. Louis, MO) and $0.165\ \mu M$ TRITC-conjugated phalloidin (Sigma-Aldrich, St. Louis, MO) for

30 min in the dark at 37°C for permeabilization and staining, then washed and resuspended in HBSS. Stained cells were filtered (35 μm mesh nylon filter), and the F-actin content was analyzed using a flow cytometer (Cytomics FC500, Beckman Coulter, Inc., Fullerton, CA) within 1 hr of staining. A total of 20,000 cells were analyzed for each preparation (n=3). In all cases, the fluorescence histogram was a normal distribution from which the fluorescence mean was determined. The relative F-actin content of filtered neutrophils is the ratio of the mean intensity of the filtered samples to the mean intensity of resting neutrophils at the corresponding temperature (23°C or 37°C). As a positive control, neutrophils were stimulated with 10^{-7} M fMLP (Sigma-Aldrich, St. Louis, MO) for 10 s. In the case of neutrophil filtration through 3 μm filters at 37°C , the neutrophils were also fixed at 15, 30, 60 and 120s post-filtration and the corresponding F-actin content were quantified.

3.2.6 Visualization of F-Actin Reorganization and Analysis of Polarization in Neutrophils

Neutrophils prepared as described above for flow cytometry analysis was visualized under a fluorescent microscope (Eclipse TE300, 60×, Melville, NY) to determine the distribution of F-actin. For each preparation (n=3), 50 cells were chosen randomly, and neutrophils showing asymmetrical distribution of F-actin were scored as morphologically polarized. The percentage of polarized neutrophils was computed for each experimental condition.

3.2.7 Statistical Analysis

All results are expressed as the means ± SE. Data comparisons for circularity and F-actin content were carried out using the student t-test, while comparisons of results for polarity was analyzed using χ^2. Findings that showed either $p<0.05$ or $p<0.01$ were considered significant.

3.3 Results

Neutrophils were passed through polycarbonate filters using two different filtration setups: the constant-pressure and constant-flow-rate. For the constant-pressure system, measurements of the average volume flow-rates are shown in Table 4. Upstream pressures attained a nearly steady state after 1 min of filtration for the constant-flow-rate system, the values of which are reported in Table 4.

Table 4. Pressures and the corresponding flow rates for the in-vitro filtration systems

Experimental conditions	23°C		37°C	
	3 μm filtration	5 μm filtration	3 μm filtration	5 μm filtration
Constant-pressure system				
19.5 cm H_2O	3.5 ± 0.6 ml/min	64 ± 4.0 ml/min	5.4 ± 0.9 ml/min	74 ± 9.0 ml/min
5 cm H_2O	0.5 ± 0.1 ml/min	4.9 ± 0.3 ml/min	0.7 ± 0.1 ml/min	5.3 ± 0.5 ml/min
Constant-flow-rate system				
6ml/min	28.4 ± 4.8 cm H_2O			
3ml/min	20.6 ± 3.0 cm H_2O			
1ml/min	6.2 ± 0.9 cm H_2O			

3.3.1 Shape of Neutrophils that Undergo Large-scale Deformations is Affected by the Driving Force

Cells that had deformed through the polycarbonate filters were fixed immediately, and the shape departure from circular was quantified. Fig. 31a shows the circularity index of neutrophils deformed under constant-pressure. In 3 μm -filtered cells, an increase in filtration pressure from 5 cm H_2O to 19.5 cm H_2O resulted in a significant increase ($p<0.01$) in elongation of the neutrophils, at both temperatures of 23°C and 37°C . In contrast, comparison between 5 μm -filtered cells showed that filtration pressure has no effect on the circularity index. The circularity index for neutrophils deformed under constant-flow-rate is depicted in Fig. 31b. Comparison of results for 3 μm -filtered cells at 23°C showed a significant elongation ($p<0.01$) between cells filtered at 1 ml/min and 6 ml/min, and between cells filtered at 3 ml/min and 6 ml/min. However, the increase in filtration flow-rate from 1 ml/min to 3 ml/min did not change the neutrophil circularity index. These findings suggest that neutrophil shape is affected by

driving pressure for cells experiencing large-scale (3 μm pores) but not small-scale (5 μm pores) deformations.

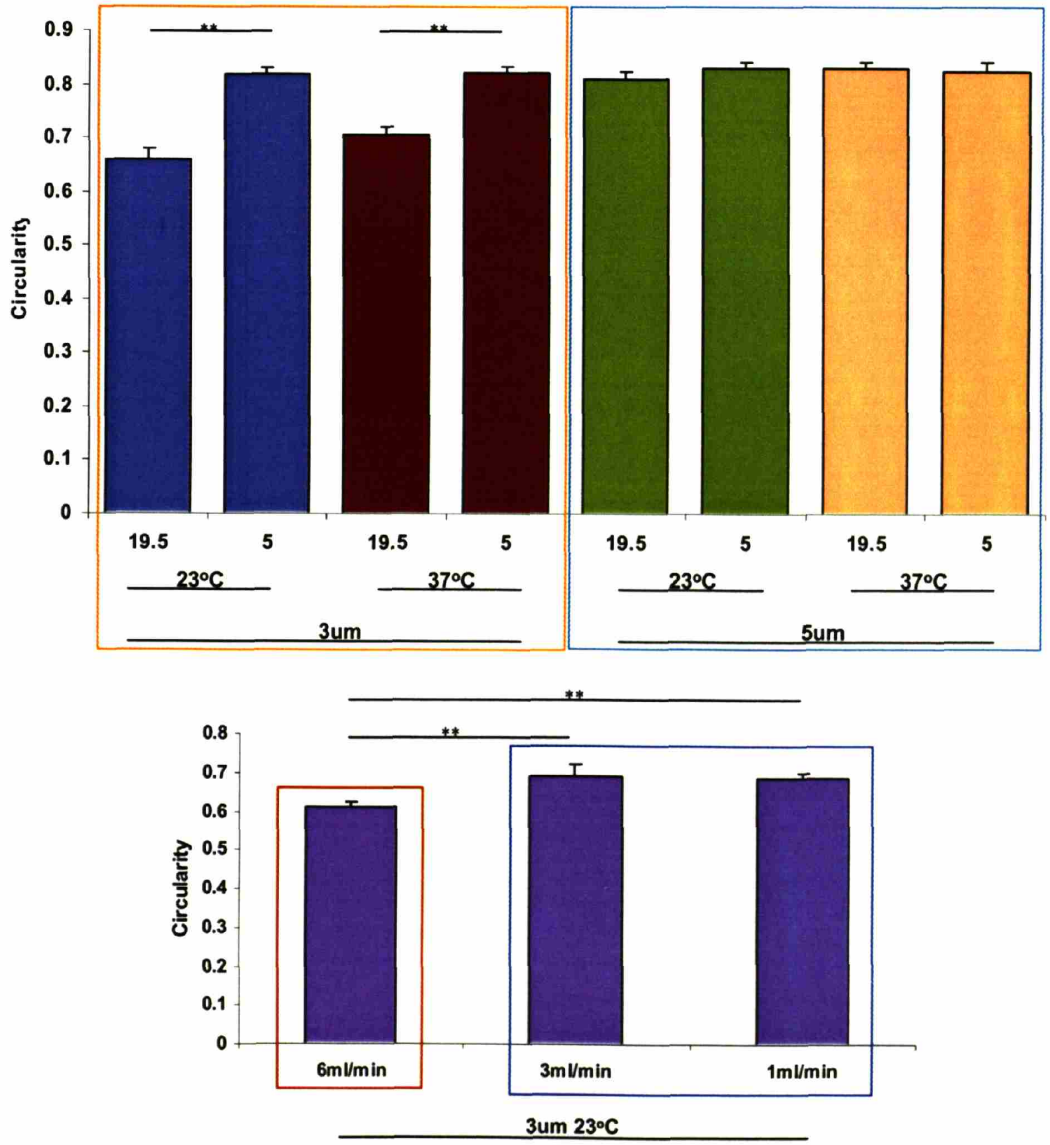

Fig. 31 (a) Circularity index of neutrophils deformed under constant-pressure. The horizontal axis represents the different filtration pressures (in units of cm H_2O), temperatures and filter pore sizes. (b) Circularity index of neutrophils deformed under constant-flow-rate. The horizontal axis represents the different filtration flow rates, temperatures and filter pore sizes; All values are expressed as means ± SE (n=3); **$p<0.01$.

3.3.2 Neutrophils Exhibit a Rapid Fall and Recovery in F-actin Content and Distribution after Large-scale Deformation

Measurements of F-actin content for neutrophils deformed under constant-pressure and constant-flow-rate, respectively, and fixed immediately after filtration, are shown in Figs. 32a and 32b.

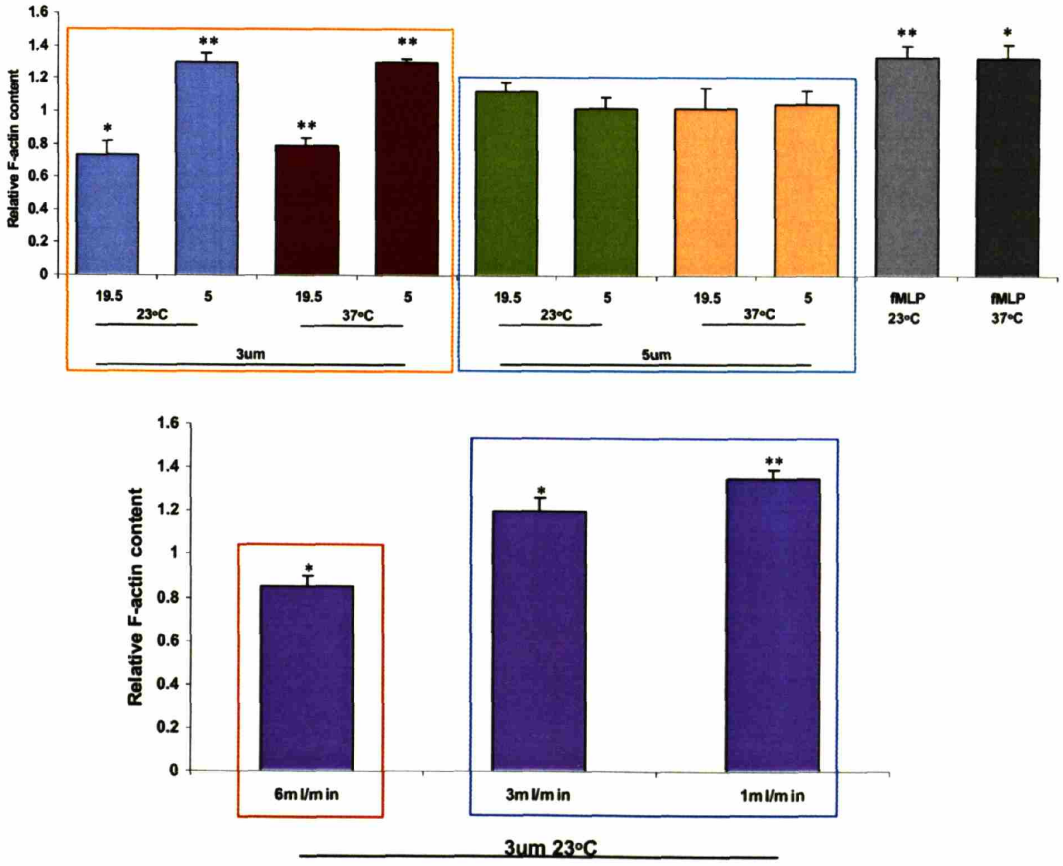

Fig. 32 (a) Relative F-actin content of neutrophils deformed under constant-pressure. The horizontal axis represents the different filtration pressures (in units of cm H_2O), temperatures and filter pore sizes. (b) Relative F-actin content of neutrophils deformed under constant-flow-rate. The horizontal axis represents the different filtration flow rates, temperatures and filter pore sizes; fMLP stimulated cells served as positive control; All values are expressed as means ± SE (n=3) and expressed as fraction of F-actin content in resting neutrophils ; *$p<0.05$ and **$p<0.01$.

Neutrophils passing through 3 μm filters under a constant-pressure of 19.5 cm H_2O showed a significant decrease in their F-actin content (Fig. 32a). In contrast, when the cells were filtered at 5 cm H_2O, they displayed a significant increase in F-actin content. Cells deformed through 5 μm filters under both pressures did not show any changes in their fluorescence intensity when compared to resting values. Stimulation with 10^{-7} M fMLP for 10 s resulted in increased fluorescence intensity. This observation holds true for experiments conducted at 23°C and 37°C. For the constant-flow-rate system (Fig. 32b), experiments carried out for 3 μm -filtered cells at 23°C showed a decrease in F-actin content for neutrophils filtered at 6 ml/min. However, cells filtered at 1 ml/min and 3 ml/min showed an increase in fluorescence intensity when compared to resting cells. The pattern of changes in F-actin content are therefore quite complex, with no change occurring under small-scale deformation (5 μm pores), while those undergoing large-scale deformation (3 μm pores) exhibit either a decrease or increase in F-actin, for high and low driving pressures, respectively.

Fluorescence microscopy revealed a diffuse distribution of F-actin for resting neutrophils at both 23°C and 37°C (Figs. 33a & 33b). Filtration through 3 μm filters under a constant-pressure of 19.5 cm H_2O resulted in a redistribution of F-actin, forming a discontinuous border around the cell edges (Fig. 33c). In contrast, neutrophils deformed through 3 μm filters under a lower constant-pressure of 5 cm H_2O showed increased ruffling of the plasma membrane and formation of pseudopods, which were also sites of F-actin localization (Fig. 33d). However, filtration through 5 μm filters under high or low constant-pressure did not result in F-actin reorganization (Fig. 33e). In the constant-flow-rate system, neutrophils passed through 3 μm filters under a high flow-rate of 6 ml/min exhibited F-actin localized discontinuously along the cell periphery (Fig. 33f). In contrast, cells filtered at flow-rates of 1 ml/min or 3 ml/min showed a more uniform distribution of F-actin within the cellular interior (Fig. 33g), with occasional cells forming pseudopods (Fig. 33h).

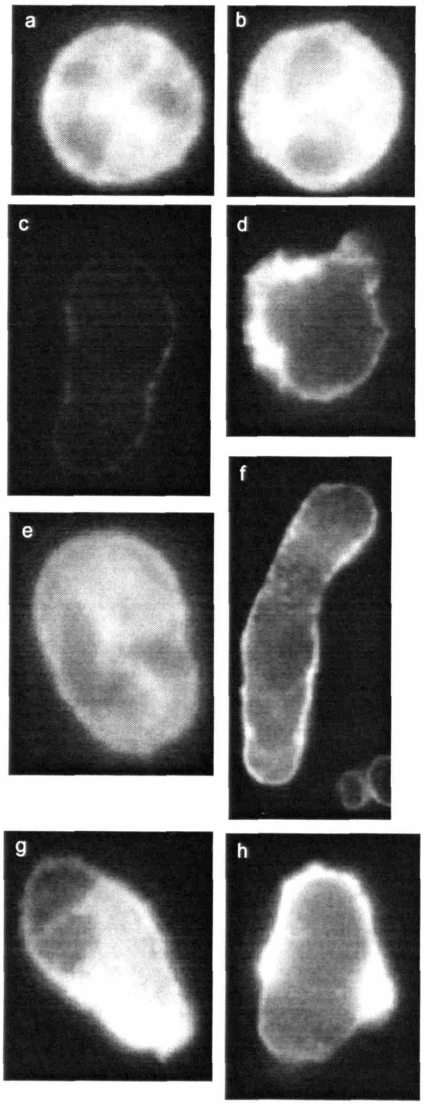

Fig. 33 Representative images showing distribution of F-actin and morphological changes in cells stained with TRITC-phalloidin in (a) resting neutrophils at 23°C (b) resting neutrophils at 37°C (c) neutrophils filtered through 3 μm pores under constant pressure of 19.5 cm H_2O (d) neutrophils filtered through 3 μm pores under constant pressure of 5 cm H_2O (e) neutrophils filtered through 5 μm pores under constant pressure of 19.5 cm H_2O (similar F-actin distribution for 5 cm H_2O filtration) (f) neutrophils filtered through 3 μm pores under constant flow rate of 6 ml/min (g and h) neutrophils filtered through 3 μm pores under constant flow rate of 1 ml/min (similar F-actin distribution for 3 ml/min filtration)

3.3.3 A Combination of Small Pore Dimension and Low Driving Force leads to Neutrophil Activation

Cells filtered through 3 μm filters under constant-pressure showed significantly increased polarization ($p<0.01$) when the pressure was reduced from 19.5 to 5 cm H_2O (Table 5). This observation holds true at both 23°C and 37°C. In contrast, none of the neutrophils filtered through 5 μm filters either at low or high pressures were polarized. Neutrophils deformed through 3 μm filters under constant-flow-rate also showed a significant increase in polarization when the flow-rate was decreased from 6 ml/min to 1 ml/min. No significant change in polarization was observed when comparing results for 6 ml/min and 3 ml/min or from comparison of the data for 3 ml/min and 1 ml/min.

Table 5 Percentage of polarized cells after filtration; *P<0.05 and **P<0.01

Experimental conditions	23°C		37°C	
	3 μm filtration	5 μm filtration	3 μm filtration	5 μm filtration
Constant-pressure system				
19.5 cm H_2O	19]†	0	9]†	0
5 cm H_2O	69]	0	67]	0
Constant-flow-rate system				
6ml/min	11]			
3ml/min	18]*			
1ml/min	25]			

3.3.4 Neutrophil allowed to Recover after High Driving Pressure and Large-scale Deformation exhibit Recovery in F-actin Content and Distribution

Neutrophils passed through 3 μm filters under a constant-pressure of 19.5 cm H_2O at 37°C, and subsequently fixed at different time points, showed a recovery of F-actin content to within 95% of baseline resting values (Fig. 34). The distributions of F-actin at different time points post-filtration are shown in Fig. 35. Neutrophils fixed 15s after filtration still showed F-actin localization around the periphery of the cell. Compared to cells fixed at earlier time points, however, neutrophils fixed at 30s and thereafter showed a recovery of F-actin in the cell interior.

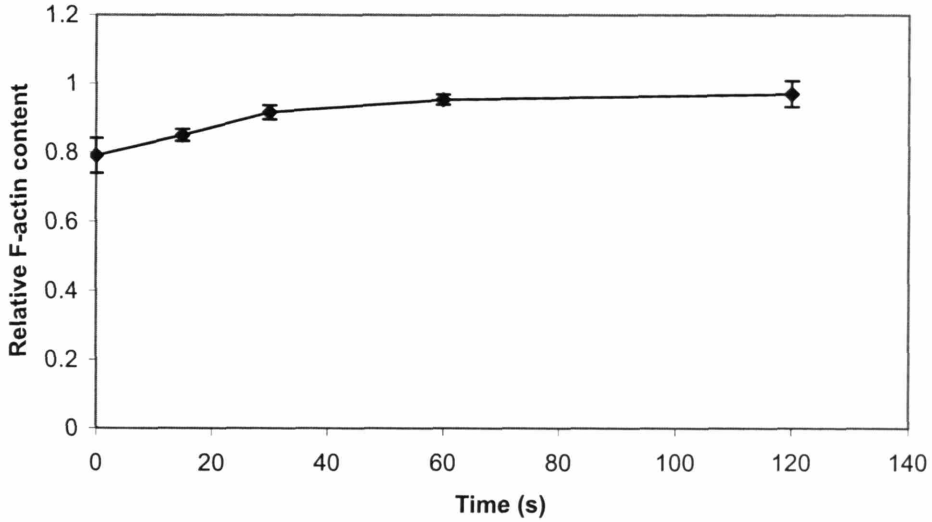

Fig. 34 Time course of F-actin content for neutrophils passed through 3 μm filters under a constant-pressure of 19.5 cm H_2O at 37°C

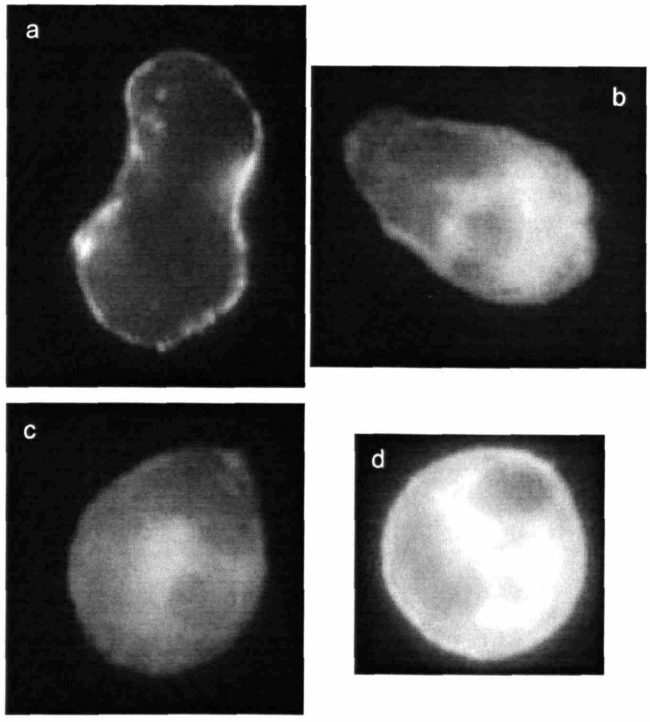

Fig. 35 Representative images showing distribution of F-actin in cells stained with TRITC-phalloidin and fixed at (a) 15s (b) 30s (c) 60s and (d) 120s post-filtration. The image of cell fixed immediately after filtration (time = 0s) is shown in Fig. 33c.

3.4 Discussion

Neutrophils often encounter narrow capillary segments during their passage through the pulmonary microcirculation, and as the cells deform to pass through these narrower segments, they are subjected to mechanical stimulation. In a previous work, we examined changes in the rheological behavior of neutrophils subjected to these mechanical forces (110). Our new results show that mechanical stimulus has the ability to remodel the neutrophil cytoskeleton as well as induce cell activation. Below a threshold pore size, mechanical deformation results in actin depolymerization, and is followed later by cellular activation.

A constant-pressure filtration setup was designed to mimic the deformation of neutrophils in pulmonary capillaries, similar to that used in previous studies (3; 4; 24; 28; 69). In this system, the driving pressure across the filter was maintained constant over time by a pressure reservoir. Two different filter pore sizes were chosen, 3 μm and 5 μm diameters, which are typical diameters of the narrower pulmonary capillary segments. Neutrophils, which have average diameters of 6-8 μm (17) consequently must deform when passing through the polycarbonate filters. This setup allowed the neutrophils to be fixed and stained post-filtration, hence, permitting visualization of the actin cytoskeleton of the cells. Our previous study (110) had utilized a microfluidic device, which was designed for single live cell imaging allowing the determination of changes in shear modulus but was not amenable to cell fixation and post-fixation staining. In this new system, we employed a constant-pressure filtration system as opposed to a constant-flow-rate system as used previously (22; 55; 80; 104), because studies (36; 42) have shown that this is a better representation of the physiological condition experienced by neutrophils in the pulmonary microcirculation.

Using the constant-pressure system during neutrophil filtration, an increase in filtration pressure resulted in a corresponding increase in flow-rate of the filtrate, as expected, all other conditions (temperature and pore size) being equal (Table 4). Similarly, a larger pore size increased the flow-rate of filtrate for a fixed filtration pressure and temperature. The effect of raising the experimental temperature

from 23°C to 37°C was to increase the filtrate flow-rate, indicative of a more easily deformable cell at a higher temperature, as has been reported by others (25; 26; 45).

Increasing the driving pressure for 3 μm filtration from 5 cm H_2O to 19.5 cm H_2O produced a more elongated cell (Fig. 31a). In contrast, driving pressure had no observable effect on cells filtered through 5 μm pores. These results may be explained if we consider the time delay between deformation and fixation, which we term t_F. Due to the collection procedure, at low filtration flow-rates, the elongated neutrophils post-filtration have the opportunity to partially recover their initial shape before encountering fixative. Conversely, high filtration flow-rates lead to rapid fixation, i.e. t_F is very short. Hence, in 3 μm filtration, due to the low flow-rate (Table 4) at 5 cm H_2O filtration pressure, neutrophils were less elongated at the time of fixation compared with cells that experienced the 19.5 cm H_2O filtration pressure. However, the larger pores of 5 μm filters allowed high enough flows at both 5 cm H_2O and 19.5 cm H_2O, that no differences were observed in the shape of the fixed cells.

In our previous study (110), we demonstrated that neutrophils subjected to mechanical deformation experienced an immediate decrease in both the storage and loss shear moduli. Within a minute after stimulation, the shear moduli recovered to near initial values. Mechanical force also activated the neutrophils as evidenced by the formation of pseudopods within one or two minutes of stimulation. In our current experiments, the neutrophils could be collected downstream after deformation, fixed, and their cytoskeleton revealed with appropriate staining. Hence, to understand the transient changes in neutrophil cytoskeleton as a result of mechanical deformation, the F-actin content of neutrophils was compared with resting cells. Cells filtered through 3 μm pores under a constant-pressure of 19.5 cm H_2O showed a decrease in F-actin content as measured by flow cytometry (Fig. 32a). In contrast, at a lower filtration pressure of 5 cm H_2O, the F-actin content was increased. This apparently anomalous behavior could be explained if we relate the present observations to results reported in (110). At higher filtration pressures, neutrophils were likely fixed at the initial stage of the remodeling process, at a time when the shear moduli of the cells were reduced, due to a combination of a short

entrance/residence time in the filter under the high driving pressure. In contrast, at lower driving pressures, the neutrophils required more time to deform into the pores, so the cells had ample opportunity to form pseudopods prior to fixation. Previous studies have shown that neutrophils require approximately 2 s at 20 cm H_2O aspiration pressure to enter a 3 μm pore, increasing to 15 s at 5 cm H_2O (36). Given that pseudopod formation occurs as early as 10 s after the onset of mechanical deformation (110), the neutrophils likely had ample time to form pseudopods for the 5 cm H_2O filtration while deforming into the pores. Experiments carried out previously in which neutrophils were deformed into microchannels under low pressure drop (close to threshold entrance pressure) (110) showed that neutrophils formed pseudopods in the microchannels while undergoing deformation (Fig. 36).

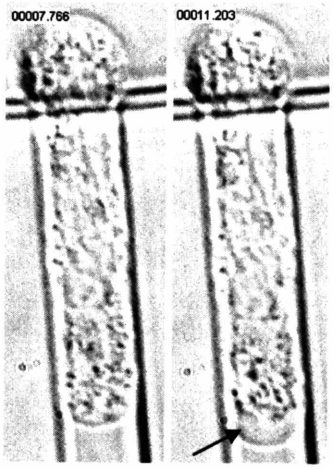

Fig. 36 Pseudopod formation (arrow) while the neutrophil was still deforming into the microchannel under very low pressure.

The high F-actin content of pseudopods, therefore may account for the increased F-actin content observed for filtration at lower driving force. This is also reflected in the results showing the percentage of polarized cells for each experimental condition (Table 5). Here, decreasing the filtration driving force clearly results in an increase in polarization of the neutrophil caused by formation of pseudopods. Pseudopod formation for the low driving pressure conditions can also be seen from F-actin stained images of the cells (Figs. 33d). In summary, it appears that neutrophils subjected to mechanical stimulus first

undergo F-actin depolymerization, followed by recovery and a subsequent increase in F-actin content attributable to the formation of pseudopods.

To investigate the contribution of t_F to cell activation, neutrophils filtered through 3 μm pores at high driving pressure were fixed at different time points after filtration. Figs. 34 and 35 show that the F-actin content of the cells recover to their baseline resting value without causing cell activation as reflected by pseudopod projection. Similar observations were noted in neutrophils flowing through the microchannel setup in (110). Neutrophils that were allowed to pass through the microchannels without trapping the cell, recover to their original resting spherical shape without any evidence of pseudopod projection (Fig. 37). These results show that t_F has no effect on neutrophil activation.

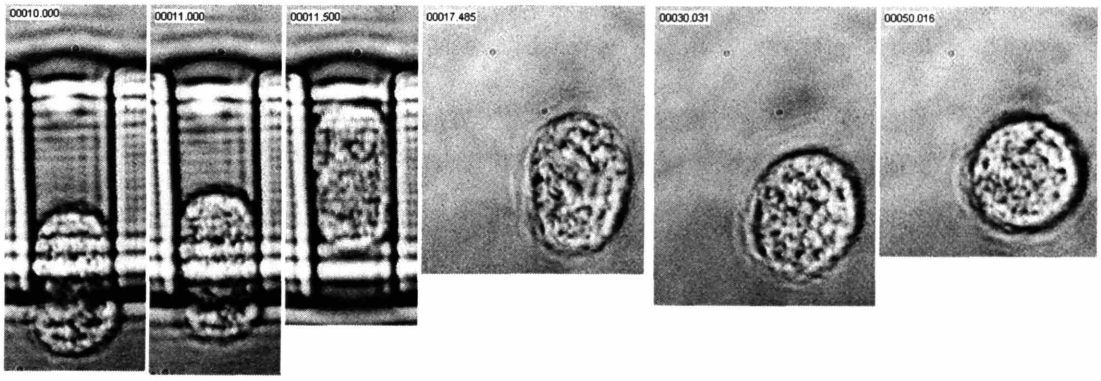

Fig. 37 Neutrophils passing through the micrchannel without being trapped recover back to its spherical shape after deformation.

However, the results strongly suggest that in addition to subjecting the neutrophils to mechanical stimulus through deformation into a narrower channel, the neutrophils must be retained in their deformed/elongated state for pseudopod to form. This implies that physiologically, there are at least two ways in which neutrophils can form pseudopods in the pulmonary circulation: either if the entrance time of the cell exceeds the time to pseudopod projection (as mentioned above) or if the neutrophils become

trapped in the capillaries, either due to the combined effects of low driving pressure and small capillary dimension or to active adhesion to the capillary endothelium.

A central question pertinent to cytoskeletal remodeling in neutrophils is the molecular mechanism governing the breakdown of the cytoskeleton due to mechanical deformation. Two hypotheses were presented in (110): sudden depolymerization of F-actin or rupture of actin cross-links between the filaments. The present experiments show that the initial rapid reduction in moduli is at least partially caused by depolymerization of F-actin. Further evidence of actin depolymerization during the early remodeling stage is provided by comparison of images of the cells before and after filtration. Neutrophils in the undeformed resting state exhibited a uniform distribution of F-actin over the entire cytoplasm (Figs 33a and 33b). However, after filtration under high driving force, F-actin was concentrated around the periphery of the cells (Figs. 33c) indicative of an absence of F-actin in the central region of the cells due to depolymerization. However, we cannot rule out the possibility that the rupture of actin cross-links could also play a role in assisting this depolymerization process. In-vitro results of Wirtz et.al. (97) demonstrate that F-actin networks abruptly soften under high deformation at low concentrations of actin cross-linking proteins (filamin in this case), pointing to the role of actin-binding proteins in modulating cytoskeletal stiffness when subjected to mechanical deformation. In the case of neutrophils subjected to mechanical stimulus, both mechanisms, actin depolymerization and actin cross-link rupture, might occur simultaneously, a possibility being that the unbinding of the cross-links or even rupture of actin filaments themselves might initiate the depolymerization process (52).

Constant-pressure filtration of neutrophils through 5 μm filters had no observable effect on the F-actin content of the cells (Fig 32a). Post-filtered neutrophils also showed no evidence of polarization (Table 5) nor reorganization of F-actin (Fig. 33e). Hence, these results suggest the existence of a threshold pore size below which the neutrophils sense the mechanical stimulus, remodel their cytoskeleton and induce activation.

Although the constant-pressure setup is perhaps a better physiological model, the in-vitro study of neutrophil deformation in pulmonary capillaries had previously been carried out under constant-flow-rate

using a syringe pump to deliver the neutrophil solution through polycarbonate filters. Kitagawa et.al. (55) investigated the role of mechanical deformation on the behavior of neutrophils under constant-flow-rate, and here, we repeated and extended some aspects of their experiments in order to confirm our results and compare observations from the two systems. Using flow-rates of 1 ml/min and 3 ml/min for 3 μm filtration as in (55), we were able to reproduce their results and similarly showed that post-filtered neutrophils at these flow-rates attain comparable circularity index (Fig. 31b) as well as display an increase in F-actin content after filtration (Fig. 32b). However, as we did not observe the reduction in F-actin content of neutrophils, we suspected that at these low flow-rates the cells were not fixed until reaching a latter stage of the remodeling process. This suspicion was confirmed by experiments repeated at a higher flow-rate of 6 ml/min, showing a significant reduction in the circularity index compared with 1 ml/min and 3 ml/min, indicative of a shorter t_F as discussed above (Fig. 31b). More importantly, there was indeed a reduction in F-actin content of the neutrophils (Fig. 32b) and depolymerization could also be observed from images of the cells (Fig. 33f). This confirmed our observation that neutrophils undergo an immediate but transient depolymerization of F-actin when subjected to mechanical deformation, which subsequently leads to formation of pseudopods. Nevertheless, although both the constant-pressure and constant-flow-rate system gave consistent results in this respect, there were discrepancies in other observations. From a comparison across the two setups (Table 4) it can be seen that the experimental conditions of 5 cm H_2O in the constant-pressure system is comparable to the 1 ml/min flow condition for the constant-flow-rate system and a similar matching occurs between the 19.5 cm H_2O constant-pressure system and the 3 ml/min constant-flow-rate system. However, although we see a distinct difference in the response of neutrophils at 5 cm H_2O when compared with that at 19.5 cm H_2O, there was little difference in the behavior of the cells filtered at 1 ml/min and 3 ml/min. Only when the flow-rate was stepped up to 6 ml/min, did the neutrophils display responses similar to the higher filtration pressure of 19.5 cm H_2O. Furthermore, as shown in Table 5, neutrophils filtered under constant-flow-rate display less activation as a whole compared to constant-pressure filtration. Further tests are needed to reconcile the discrepancies observed in these two setups.

The scenario that emerges is one in which all cells subjected to a minimum level of elongation exhibit an initial drop in F-actin content due to depolymerization, followed by a recovery to initial values over a time scale of 30-60 s. This pattern accounts, at least in part, for the immediate reduction in shear moduli, with recovery over a time scale similar to that seen in previous experiments (110). Those cells that experience a prolonged period of deformation, however, as occurs in the combination of low driving pressures and small pore diameters, become activated. This activation is reflected in an eventual increase in F-actin content, over initial baseline values, accompanied by polarization and pseudopod formation.

These findings have important implications with respect to neutrophil transmigration in the pulmonary capillaries. Due to the highly interconnected nature of the alveolar microvascular bed (84) , neutrophils will experience both a range of driving pressures and a range of capillary diameters, causing them to stop and undergo deformation in order to pass through. If the deformation is sufficiently large (capillary diameters ~ 3 μm) and the delay sufficiently long, the cells will become activated to migrate. This would presumably be accompanied by increased expression of adhesion receptors (6; 55), and potentially lead to migration out of the capillary and into the extracellular matrix of the lung.

Future Developments

The present work sets out to understand the effects of mechanical deformation on the structure and function of neutrophils during their passage through the pulmonary microcirculation. The results indicate that neutrophils are able to sense mechanical forces and respond accordingly, altering their cytoskeletal structure and migrational capabilities. The outcome of this work points to the need to adopt a new paradigm, one in which neutrophils have the ability to actively respond to mechanical stimulus; and consequently, to move away from the traditional passive neutrophil model. Aside from deformation into pulmonary capillaries, other physiologically relevant situations in which neutrophils experience mechanical deformation include neutrophil transmigration through endothelial junctions into surrounding tissues, and the release of the cells from the bone marrow into the circulation. This thesis serves as a starting point to explore the exciting, new field of mechanotransduction of neutrophils, and leukocytes in general. In particular, much interesting and relevant work could potentially be carried out to further elucidate the effects of mechanical deformation of neutrophils in the pulmonary circulation. From the knowledge and experience garnered from the current work, here are some suggestions pertaining to future directions that could be explored.

The observation of cytoskeletal remodeling immediately after the neutrophils were subjected to mechanical deformation suggests that the cells are capable of sensing this mechanical stimulus, and subsequently transmit the 'message' downstream, resulting in the breakdown of the cytoskeleton and reduction in cell stiffness. The signal transduction pathway responsible for this effect is completely unknown, as is the molecular structure/protein responsible for sensing the stimuli, but several promising leads can be identified from previous studies. Working out the signal transduction mechanism not only allows understanding of the behavior of the neutrophils in health and disease; but also points to the potential for modulation and control of these cells for purposes of therapy. At present, the only known effect of mechanical deformation pertaining to signal transduction is a spike in the level of intracellular calcium about 30s after the onset of mechanical deformation (55). Whether this increase in calcium

content is correlated with the remodeling process of the neutrophil (which occurs on similar time scale) is currently unknown. This thesis also demonstrated evidence of F-actin depolymerization, which likely contributes to the drop in modulus of the cell when measured rheologically. Earlier studies conducted on the link between calcium (9; 20) and F-actin suggest that calcium is in fact responsible for F-actin depolymerization. These results taken together suggest that calcium is a strong modulator of the cell stiffness when neutrophils are subjected to mechanical stimulation, leading to remodeling of the cytoskeleton; however, further experiments would be needed to prove this hypothesis.

As mentioned in Chapter 3, although the present work directly implicates F-actin depolymerization to the reduction in modulus of the neutrophils when subjected to mechanical deformation, studies done by others suggest that the breakdown in cell cytoskeleton could be partially attributed to dissociation of actin-binding proteins. The likely scenario would be that both mechanisms are involved. One could imagine that mechanical force breaks the links between the actin filaments, and in that process, exposes the linkage sites to actin severing proteins such as gelsolin, which bind on to the F-actin filaments and subsequently initiate actin depolymerization. However, this hypothesis could only be tested if a method could be developed to distinguish experimentally, either through direct visualization or quantitative measurement, the events taking place during each of these processes. This could then provide insights into the relative contributions of both processes to the reduction in viscoelasticity of the neutrophil immediately after deformation. Neutrophils were also seen to recover their initial rheological properties within one minute after deformation, indicating that the F-actin depolymerization process is reversed. The mechanism involved in this recovery process is also not understood and worthy of further investigation.

Mechanical deformation is not the only stimulus that neutrophils encounter while traversing the microcirculation. Concurrently, the cells could also be exposed to biochemical stimuli, notably chemoattractants such as fMLP. Although multiple studies have been carried out to study the effects of fMLP, particularly on the migrational behavior of neutrophils, no work has yet been done to understand the combined effects of both mechanical and chemical stimulants. Physiologically, when the host is

infected with pathogens, neutrophils will be exposed uniformly to chemoattractants in the bloodstream or via a chemoattractant gradient set up across the endothelial-tissue interface. The results of experiments subjecting neutrophils to mechanical and chemical stimuli will provide insights into the relationship between both stimulus, (if any), such as spatial and temporal dependence.

The current experimental setup, in particular, the microfabricated channel design, could be improved and made to recapitulate better the 'in-vivo' microenvironment, by lining the channels with endothelial cells, and subsequently, allowing neutrophils to deform into these endothelial-lined channels. This setup would permit investigation of neutrophil-endothelial interaction during neutrophil deformation into the microchannels; in particular, to determine if adhesion between neutrophil and endothelial cells is upregulated as suggested by (55). Also, it would be interesting to investigate any other cross talk between neutrophils and endothelial cells as a result of mechanical stimuli, for example, one which would affect the transmigration rate of the neutrophils through endothelial cell junctions.

Finally, results from the present work clearly showed that neutrophils are not passive cells when subjected to mechanical deformation, instead the cells are capable of remodeling their cytoskeleton and in response alter their rheology. Hence, this clearly demonstrated the inadequacy of current mathematical models of neutrophils, which assumed that the neutrophils have viscoelastic properties that remained constant with time. Efforts should be made to incorporate this dynamic behavior of the neutrophils either into present models or to formulate new models. These dynamic models would serve well to mimic better the actual behavior of these neutrophils and enable us to predict the behavior of the cells when they are traversing the pulmonary microcirculation or for that fact, in other physiological settings.

Bibliography

1. http://mems.egr.duke.edu/Faculty/rhochmuth.html. 2002.

2. http://www.mc.vanderbilt.edu/histo/blood/neutrophils/html. 2002.

3. **Acquaye C, Walker EC and Schechter AN**. The Development of A Filtration System for Evaluating Flow Characteristics of Erythrocytes. *Microvascular Research* 33: 1-14, 1987.

4. **Adams RA, Evans SA and Jones JG**. Characterization of Leukocytes by Filtration of Diluted Blood. *Biorheology* 31: 603-615, 1994.

5. **Anderson DC, Wible LJ, Hughes BJ, Smith CW and Brinkley BR**. Cytoplasmic Microtubules in Polymorphonuclear Leukocytes - Effects of Chemotactic Stimulation and Colchicine. *Cell* 31: 719-729, 1982.

6. **Anderson GJ, Roswit WT, Holtzman MJ, Hogg JC and Van Eeden SF**. Effect of mechanical deformation of neutrophils on their CD18/ICAM-1-dependent adhesion. *Journal of Applied Physiology* 91: 1084-1090, 2001.

7. **Anderson JR, Chiu DT, Jackman RJ, Cherniavskaya O, McDonald JC, Wu HK, Whitesides SH and Whitesides GM**. Fabrication of topologically complex three-dimensional microfluidic systems in PDMS by rapid prototyping. *Analytical Chemistry* 72: 3158-3164, 2000.

8. **Bathe M, Shirai A, Doerschuk CM and Kamm RD**. Neutrophil transit times through pulmonary capillaries: The effects of capillary geometry and fMLP-stimulation. *Biophysical Journal* 83: 1917-1933, 2002.

9. **Bengtsson T, Jaconi MEE, Gustafson M, Magnusson KE, Theler JM, Lew DP and Stendahl O**. Actin Dynamics in Human Neutrophils During Adhesion and Phagocytosis Is Controlled by Changes in Intracellular Free Calcium. *European Journal of Cell Biology* 62: 49-58, 1993.

10. **Caille N, Tardy Y and Meister JJ**. Assessment of strain field in endothelial cells subjected to uniaxial deformation of their substrate. *Annals of Biomedical Engineering* 26: 409-416, 1998.

11. **Chien S and Sung KLP**. Effect of Colchicine on Viscoelastic Properties of Neutrophils. *Biophysical Journal* 46: 383-386, 1984.

12. **Cokelet GR, Soave R, Pugh G and Rathbun L**. Fabrication of In-Vitro Microvascular Blood-Flow Systems by Photolithography. *Microvascular Research* 46: 394-400, 1993.

13. **Coughlin MF and Schmid-Schonbein GW**. Pseudopod projection and cell spreading of passive leukocytes in response to fluid shear stress. *Biophysical Journal* 87: 2035-2042, 2004.

14. **Crocker JC and Grier DG**. Methods of digital video microscopy for colloidal studies. *Journal of Colloid and Interface Science* 179: 298-310, 1996.

15. **Crocker JC, Valentine MT, Weeks ER, Gisler T, Kaplan PD, Yodh AG and Weitz DA**. Two-point microrheology of inhomogeneous soft materials. *Physical Review Letters* 85: 888-891, 2000.

16. **Doerschuk CM**. Mechanisms of leukocyte sequestration in inflamed lungs. *Microcirculation* 8: 71-88, 2001.

17. **Doerschuk CM, Beyers N, Coxson HO, Wiggs B and Hogg JC**. Comparison of Neutrophil and Capillary Diameters and Their Relation to Neutrophil Sequestration in the Lung. *Journal of Applied Physiology* 74: 3040-3045, 1993.

18. **Dong C, Skalak R and Sung KLP**. Cytoplasmic Rheology of Passive Neutrophils. *Biorheology* 28: 557-567, 1991.

19. **Dong C, Skalak R, Sung KLP, Schmidschonbein GW and Chien S**. Passive Deformation Analysis of Human-Leukocytes. *Journal of Biomechanical Engineering-Transactions of the Asme* 110: 27-36, 1988.

20. **Downey GP, Chan CK, Trudel S and Grinstein S**. Actin Assembly in Electropermeabilized Neutrophils - Role of Intracellular Calcium. *Journal of Cell Biology* 110: 1975-1982, 1990.

21. **Downey GP, Doherty DE, Schwab B, Elson EL, Henson PM and Worthen GS**. Retention of Leukocytes in Capillaries - Role of Cell-Size and Deformability. *Journal of Applied Physiology* 69: 1767-1778, 1990.

22. **Downey GP and Worthen GS**. Neutrophil Retention in Model Capillaries - Deformability, Geometry, and Hydrodynamic-Forces. *Journal of Applied Physiology* 65: 1861-1871, 1988.

23. **Drury JL and Dembo M**. Aspiration of human neutrophils: Effects of shear thinning and cortical dissipation. *Biophysical Journal* 81: 3166-3177, 2001.

24. **Engstrom KG**. A New Red Blood-Cell Filtration Device with Improved Time Resolution and Its Application to the Impaired Rbc Deformability in the Diabetic Ob/Ob Mouse. *Biorheology* 26: 711-721, 1989.

25. **Evans E and Kukan B**. Passive Material Behavior of Granulocytes Based on Large Deformation and Recovery After Deformation Tests. *Blood* 64: 1028-1035, 1984.

26. **Evans E and Yeung A**. Apparent Viscosity and Cortical Tension of Blood Granulocytes Determined by Micropipet Aspiration. *Biophysical Journal* 56: 151-160, 1989.

27. **Fabry B, Maksym GN, Butler JP, Glogauer M, Navajas D and Fredberg JJ**. Scaling the microrheology of living cells. *Physical Review Letters* 8714: art-148102, 2001.

28. **Frank RS and Hochmuth RM**. An Investigation of Particle Flow Through Capillary Models with the Resistive Pulse Technique. *Journal of Biomechanical Engineering-Transactions of the Asme* 109: 103-109, 1987.

29. **Gardel ML, Crocker JC, Valentine MT, Bausch AR and Weitz DA**. One- and two-particle microrheology of F-actin. *Biophysical Journal* 84: 437A, 2003.

30. **Gardel ML, Valentine MT, Crocker JC, Bausch AR and Weitz DA**. Microrheology of entangled F-actin solutions. *Physical Review Letters* 91: 2003.

31. **Gebb SA, Graham JA, Hanger CC, Godbey PS, Capen RL, Doerschuk CM and Wagner WW**. Sites of Leukocyte Sequestration in the Pulmonary Microcirculation. *Journal of Applied Physiology* 79: 493-497, 1995.

32. **Gilbert CS and Parmley RT**. Morphology of human neutrophils: A comparison of cryofixation, routine gluteraldehyde fixation, and the effects of dimethyl sulfoxide. *Anatomical Record* 252: 254-263, 1998.

33. **Hellewell PG and Williams TJ**. The neutrophil. In: Immunopharmacology of Neutrophils, edited by Hellewell PG, Williams and T.J. London ; San Diego: Academic Press, 1994, p. 1-4.

34. **Helmke BP, Goldman RD and Davies PF**. Rapid displacement of vimentin intermediate filaments in living endothelial cells exposed to flow. *Circulation Research* 86: 745-752, 2000.

35. **Helmke BP, Thakker DB, Goldman RD and Davies PF**. Spatiotemporal analysis of flow-induced intermediate filament displacement in living endothelial cells. *Biophysical Journal* 80: 184-194, 2001.

36. **Hochmuth RM and Needham D**. The Viscosity of Neutrophils and Their Transit Times Through Small Pores. *Biorheology* 27: 817-828, 1990.

37. **Hochmuth RM, Tingbeall HP, Beaty BB, Needham D and Transontay R**. Viscosity of Passive Human Neutrophils Undergoing Small Deformations. *Biophysical Journal* 64: 1596-1601, 1993.

38. **Hogg JC**. Neutrophil Kinetics and Lung Injury. *Physiological Reviews* 67: 1249-1295, 1987.

39. **Hogg JC, Coxson HO, Brumwell ML, Beyers N, Doerschuk CM, Macnee W and Wiggs BR**. Erythrocyte and Polymorphonuclear Cell Transit-Time and Concentration in Human Pulmonary Capillaries. *Journal of Applied Physiology* 77: 1795-1800, 1994.

40. **Huang H, Dong CY, Kwon HS, Sutin JD, Kamm RD and So PTC**. Three-dimensional cellular deformation analysis with a two-photon magnetic manipulator workstation. *Biophysical Journal* 82: 2211-2223, 2002.

41. **Huang HD, Kamm RD and Lee RT**. Cell mechanics and mechanotransduction: pathways, probes, and physiology. *American Journal of Physiology-Cell Physiology* 287: C1-C11, 2004.

42. **Huang YQ, Doerschuk CM and Kamm RD**. Computational modeling of RBC and neutrophil transit through the pulmonary capillaries. *Journal of Applied Physiology* 90: 545-564, 2001.

43. **Ingber DE**. Mechanobiology and diseases of mechanotransduction. *Annals of Medicine* 35: 564-577, 2003.

44. **Janeway CA, Travers P, Walport M and Shlomchik M**. *Immunobiology 5 : the immune system in health and disease*. New York: Garland Science Publishing, 2001.

45. **Jetha KA, Egginton S and Nash GB**. Increased resistance of neutrophils to deformation upon cooling and rate of recovery on rewarming. *Biorheology* 40: 567-576, 2003.

46. **Jo BH, Van Lerberghe LM, Motsegood KM and Beebe DJ**. Three-dimensional micro-channel fabrication in polydimethylsiloxane (PDMS) elastomer. *Journal of Microelectromechanical Systems* 9: 76-81, 2000.

47. **Jo S and Park K**. Surface modification using silanated poly(ethylene glycol)s. *Biomaterials* 21: 605-616, 2000.

48. **Juncker D, Schmid H, Bernard A, Caelen I, Michel B, de Rooij N and Delamarche E**. Soft and rigid two-level microfluidic networks for patterning surfaces. *Journal of Micromechanics and Microengineering* 11: 532-541, 2001.

49. **Kamm RD**. Cellular fluid mechanics. *Annual Review of Fluid Mechanics* 34: 211-232, 2002.

50. **Kan HC, Shyy M, Udaykumar HS, Vigneron P and Tran-Son-Tay R**. Effects of nucleus on leukocyte recovery. *Annals of Biomedical Engineering* 27: 648-655, 1999.

51. **Kan HC, Udaykumar HS, Shyy W and Tran-Son-Tay R**. Hydrodynamics of a compound drop with application to leukocyte modeling. *Physics of Fluids* 10: 760-774, 1998.

52. **Khan S and Sheetz MP**. Force effects on biochemical kinetics. *Annual Review of Biochemistry* 66: 785-805, 1997.

53. **Kikuchi Y**. Effect of Leukocytes and Platelets on Blood-Flow Through A Parallel Array of Microchannels - Microflow and Macroflow Relation and Rheological Measures of Leukocyte and Platelet Activities. *Microvascular Research* 50: 288-300, 1995.

54. **Kikuchi Y, Sato K and Mizuguchi Y**. Modified Cell-Flow Microchannels in A Single-Crystal Silicon Substrate and Flow Behavior of Blood-Cells. *Microvascular Research* 47: 126-139, 1994.

55. **Kitagawa Y, VanEeden SF, Redenbach DM, Daya M, Walker BAM, Klut ME, Wiggs BR and Hogg JC**. Effect of mechanical deformation on structure and function of polymorphonuclear leukocytes. *Journal of Applied Physiology* 82: 1397-1405, 1997.

56. **Kitayama J, Hidemura A, Saito H and Nagawa H**. Shear stress affects migration behavior of polymorphonuclear cells arrested on endothelium. *Cellular Immunology* 203: 39-46, 2000.

57. **Kole TP, Tseng Y, Huang L, Katz JL and Wirtz D**. Rho kinase regulates the intracellular micromechanical response of adherent cells to rho activation. *Mol Biol Cell* 15: 3475-3484, 2004.

58. **Kole TP, Tseng Y, Jiang I, Katz JL and Wirtz D**. Intracellular Mechanics of Migrating Fibroblasts. *Mol Biol Cell* 2004.

59. **Lau AWC, Hoffman BD, Davies A, Crocker JC and Lubensky TC**. Microrheology, stress fluctuations, and active behavior of living cells. *Physical Review Letters* 91: 2003.

60. **Lennie SE, Lowe GDO, Barbenel JC, Forbes CD and Foulds WS**. Filterability of White Blood-Cell Subpopulations, Separated by An Improved Method. *Clinical Hemorheology* 7: 811-816, 1987.

61. **Lien DC, Wagner WW, Capen RL, Haslett C, Hanson WL, Hofmeister SE, Henson PM and Worthen GS**. Physiological Neutrophil Sequestration in the Lung - Visual Evidence for Localization in Capillaries. *Journal of Applied Physiology* 62: 1236-1243, 1987.

62. **Lodish HF, Berk A, Zipursky SL, Matsudaira P, Baltimore D and Darnell J**. *Molecular Cell Biology*. New York: W.H.Freeman and Company, 1999.

63. **MacKintosh FC and Schmidt CF**. Microrheology. *Current Opinion in Colloid & Interface Science* 4: 300-307, 1999.

64. **Mason TG, Ganesan K, vanZanten JH, Wirtz D and Kuo SC**. Particle tracking microrheology of complex fluids. *Physical Review Letters* 79: 3282-3285, 1997.

65. **McDonald JC, Duffy DC, Anderson JR, Chiu DT, Wu HK, Schueller OJA and Whitesides GM**. Fabrication of microfluidic systems in poly(dimethylsiloxane). *Electrophoresis* 21: 27-40, 2000.

66. **Moazzam F, Delano FA, Zweifach BW and Schmidschonbein GW**. The leukocyte response to fluid stress. *Proceedings of the National Academy of Sciences of the United States of America* 94: 5338-5343, 1997.

67. **Mukhopadhyay A and Granick S**. Micro- and nanorheology. *Current Opinion in Colloid & Interface Science* 6: 423-429, 2001.

68. **Needham D and Hochmuth RM**. Rapid Flow of Passive Neutrophils Into A 4 Mu-M Pipette and Measurement of Cytoplasmic Viscosity. *Journal of Biomechanical Engineering-Transactions of the Asme* 112: 269-276, 1990.

69. **Nossal R**. Cell transit analysis of ligand-induced stiffening of polymorphonuclear leukocytes. *Biophysical Journal* 75: 1541-1552, 1998.

70. **Pryzwansky KB**. Human-Leukocytes As Viewed by Stereo High-Voltage Electron-Microscopy. *Blood Cells* 12: 505-530, 1987.

71. **Pryzwansky KB and Bretongorius J**. Identification of A Subpopulation of Primary Granules in Human-Neutrophils Based Upon Maturation and Distribution - Study by Transmission Electron-Microscopy Cyto-Chemistry and High-Voltage Electron-Microscopy of Whole Cell Preparations. *Laboratory Investigation* 53: 664-671, 1985.

72. **Puig-de-Morales M, Grabulosa M, Alcaraz J, Mullol J, Maksym GN, Fredberg JJ and Navajas D**. Measurement of cell microrheology by magnetic twisting cytometry with frequency domain demodulation. *Journal of Applied Physiology* 91: 1152-1159, 2001.

73. **Saito H, Lai J, Rogers R and Doerschuk CM**. Mechanical properties of rat bone marrow and circulating neutrophils and their responses to inflammatory mediators. *Blood* 99: 2207-2213, 2002.

74. **Sato Y, Sato S, Yamamoto T, Ishikawa S, Onizuka M and Sakakibara Y**. Phosphodiesterase type 4 inhibitor reduces the retention of polymorphonuclear leukocytes in the lung. *American Journal of Physiology-Lung Cellular and Molecular Physiology* 282: L1376-L1381, 2002.

75. **Schmid-Schonbein GW**. Rheology of leukocytes. In: Handbook of Biomedical Engineering, New York: McGraw Hill, 1987.

76. **Schmid-Schonbein GW**. Biomechanics of microcirculatory blood perfusion. *Annual Review of Biomedical Engineering* 1: 73-102, 1999.

77. **Schmid-Schonbein GW, Sung KLP, Tozeren H, Skalak R and Chien S**. Passive Mechanical-Properties of Human-Leukocytes. *Biophysical Journal* 36: 243-256, 1981.

78. **Schmidschonbein GW, Shih YY and Chien S**. Morphometry of Human-Leukocytes. *Blood* 56: 866-875, 1980.

79. **Schmidschonbein GW, Sung KLP, Tozeren H, Skalak R and Chien S**. Passive Mechanical-Properties of Human-Leukocytes. *Biophysical Journal* 36: 243-256, 1981.

80. **Selby C, Drost E, Wraith PK and Macnee W**. Invivo Neutrophil Sequestration Within Lungs of Humans Is Determined by Invitro Filterability. *Journal of Applied Physiology* 71: 1996-2003, 1991.

81. **Shevkoplyas SS, Gifford SC, Yoshida T and Bitensky MW**. Prototype of an in vitro model of the microcirculation. *Microvascular Research* 65: 132-136, 2003.

82. **Simon SI and Schmidschonbein GW**. Cytoplasmic Strains and Strain Rates in Motile Polymorphonuclear Leukocytes. *Biophysical Journal* 58: 319-332, 1990.

83. **Simon SI and Schmidschonbein GW**. Kinematics of Cytoplasmic Deformation in Neutrophils During Active Motion. *Journal of Biomechanical Engineering-Transactions of the Asme* 112: 303-310, 1990.

84. **Staub N and Schultz E**. Pulmonary capillary length in dog, cat and rabbit. *Respiratory Physiology* 5: 371-378, 1968.

85. **Sung KLP, Dong C, Schmidschonbein GW, Chien S and Skalak R**. Leukocyte Relaxation Properties. *Biophysical Journal* 54: 331-336, 1988.

86. **Sutton N, Tracey MC, Johnston ID, Greenaway RS and Rampling MW**. A novel instrument for studying the flow behaviour of erythrocytes through microchannels simulating human blood capillaries. *Microvascular Research* 53: 272-281, 1997.

87. **Takubo T and Tatsumi N**. Dual image of myosin and actin in human neutrophils during movement by fluorescence microscopy. *Haematologia* 28: 247-253, 1997.

88. **Tingbeall HP, Lee AS and Hochmuth RM**. Effect of Cytochalasin-D on the Mechanical-Properties and Morphology of Passive Human Neutrophils. *Annals of Biomedical Engineering* 23: 666-671, 1995.

89. **Tingbeall HP, Needham D and Hochmuth RM**. Volume and Osmotic Properties of Human Neutrophils. *Blood* 81: 2774-2780, 1993.

90. **Torres M and Coates TD**. Function of the cytoskeleton in human neutrophils and methods for evaluation. *Journal of Immunological Methods* 232: 89-109, 1999.

91. **Tracey MC, Greenaway RS, Das A, Kaye PH and Barnes AJ**. A Silicon Micromachined Device for Use in Blood-Cell Deformability Studies. *Ieee Transactions on Biomedical Engineering* 42: 751-761, 1995.

92. **Tran-Son-Tay R, Kan HC, Udaykumar HS, Damay E and Shyy W**. Rheological modelling of leukocytes. *Medical & Biological Engineering & Computing* 36: 246-250, 1998.

93. **Transontay R, Needham D, Yeung A and Hochmuth RM**. Time-Dependent Recovery of Passive Neutrophils After Large Deformation. *Biophysical Journal* 60: 856-866, 1991.

94. **Tsai MA, Frank RS and Waugh RE**. Passive Mechanical-Behavior of Human Neutrophils - Power-Law Fluid. *Biophysical Journal* 65: 2078-2088, 1993.

95. **Tsai MA, Frank RS and Waugh RE**. Passive Mechanical-Behavior of Human Neutrophils - Effect of Cytochalasin-B. *Biophysical Journal* 66: 2166-2172, 1994.

96. **Tsai MA, Waugh RE and Keng PC**. Passive mechanical behavior of human neutrophils: Effects of colchicine and paclitaxel. *Biophysical Journal* 74: 3282-3291, 1998.

97. **Tseng Y, An KM, Esue O and Wirtz D**. The bimodal role of filamin in controlling the architecture and mechanics of F-actin networks. *Journal of Biological Chemistry* 279: 1819-1826, 2004.

98. **Tseng Y and Wirtz D**. Mechanics and multiple-particle tracking microheterogeneity of alpha-actinin-cross-linked actin filament networks. *Biophysical Journal* 81: 1643-1656, 2001.

99. **Tsukada K, Sekizuka E, Oshio C and Minamitani H**. Direct measurement of erythrocyte deformability in diabetes mellitus with a transparent microchannel capillary model and high-speed video camera system. *Microvascular Research* 61: 231-239, 2001.

100. **Urbanik E and Ware BR**. Actin Filament Capping and Cleaving Activity of Cytochalasin-B, Cytochalasin-D, Cytochalasin-E, and Cytochalasin-H. *Archives of Biochemistry and Biophysics* 269: 181-187, 1989.

101. **Voldman J, Gray ML and Schmidt MA**. Microfabrication in biology and medicine. *Annual Review of Biomedical Engineering* 1: 401-425, 1999.

102. **Wang N, Butler JP and Ingber DE**. Mechanotransduction Across the Cell-Surface and Through the Cytoskeleton. *Science* 260: 1124-1127, 1993.

103. **Whitesides GM, Ostuni E, Takayama S, Jiang XY and Ingber DE**. Soft lithography in biology and biochemistry. *Annual Review of Biomedical Engineering* 3: 335-373, 2001.

104. **Worthen GS, Schwab B, Elson EL and Downey GP**. Mechanics of Stimulated Neutrophils - Cell Stiffening Induces Retention in Capillaries. *Science* 245: 183-186, 1989.

105. **Xia YN, Rogers JA, Paul KE and Whitesides GM**. Unconventional methods for fabricating and patterning nanostructures. *Chemical Reviews* 99: 1823-1848, 1999.

106. **Xia YN and Whitesides GM**. Soft lithography. *Angewandte Chemie-International Edition* 37: 551-575, 1998.

107. **Yamada S, Wirtz D and Kuo SC**. Mechanics of living cells measured by laser tracking microrheology. *Biophysical Journal* 78: 1736-1747, 2000.

108. **Yanai M, Butler JP, Suzuki T, Kanda A, Kurachi M, Tashiro H and Sasaki H**. Intracellular elasticity and viscosity in the body, leading, and trailing regions of locomoting neutrophils. *American Journal of Physiology-Cell Physiology* 277: C432-C440, 1999.

109. **Yanai M, Butler JP, Suzuki T, Sasaki H and Higuchi H**. Regional rheological differences in locomoting neutrophils. *American Journal of Physiology-Cell Physiology* 287: C603-C611, 2004.

110. **Yap B and Kamm RD**. Mechanical deformation of neutrophils into narrow channels induces pseudopod projection and changes in biomechanical properties. *J Appl Physiol* 98: 1930-1939, 2005.

111. **Yeung A and Evans E**. Cortical Shell-Liquid Core Model for Passive Flow of Liquid-Like Spherical Cells Into Micropipets. *Biophysical Journal* 56: 139-149, 1989.

112. **Zahalak GI, Mcconnaughey WB and Elson EL**. Determination of Cellular Mechanical-Properties by Cell Poking, with An Application to Leukocytes. *Journal of Biomechanical Engineering-Transactions of the Asme* 112: 283-294, 1990.

113. **Zhao XM, Xia YN and Whitesides GM**. Soft lithographic methods for nano-fabrication. *Journal of Materials Chemistry* 7: 1069-1074, 1997.

APPENDIX

A.1 IDL Commands for First Frame

The commands used in the tracking of particles is shown below together with a brief description of the utility of each command (in blue). Part of the command lines are highlighted in red; which indicates the parameters that could be varied for each command.

Particle Identification

window,0,xsize=740,ysize=252
Creates an image window number 0, with horizontal pixel size of 740 and vertical pixel size of 252.

wset,0
Sets image window 0 as the current active window.

a=read_nih('c:\RSI\IDL60\reslice1\frame0000.tif')
Reads in a single NIH image from file named 'frame0000.tif' in the c:\RSI\IDL60\reslice1 directory.

tvscl,a
Displays the image file that has been read in the active window.

temp=255b-a
Inverts the image color (i.e. white becomes black and vice-versa).

b=bpass(temp,1,9)
bpass is the spatial bandpass filter which smooths the image and substracts the background off. The two numbers are the spatial wavelength cutoffs in pixels. The first one is almost always '1'. The second number is set to be approximately the size of the granules in pixels.

f=feature(b,9)
Finds the coordinates of the particles. The parameter (9) is again the diameter of the granules in pixels, similar to that used in the bpass upper cutoff above.

fo=fover2d(a,f)
Plots dots where each particle was found.

plot,f(2,*),f(3,*),psym=6
Plots the graph of radius of gyration (vertical axis) vs. brightness (horizontal axis). The brightness helps to distinguish the dots that represent the granules, which are brighter, from the dimmer dots that are due to random noise in the starting image.

f=feature(b,9,masscut=5000)
Isolates the coordinates of granules by setting the 'masscut', which is the minimum brightness value above which the dots are regarded as granules. The parameter (9) is again the diameter of the granules in pixels.

plot_hist,f(0,*) mod 1
Plots histogram to test for pixel-biasing. The histogram obtained should look flat if the length scale in **feature** (diameter of granules in pixels) is large enough. If the histogram has a deep dip in the middle, the length scale in **feature** should be increased.

More details on the tracking macros can be found on the website,
http://www.physics.emory.edu/~weeks/idl/tracking.html.

A.2 IDL Commands for All Frames

The commands used in the tracking of particles is shown below together with a brief description of the utility of each command (in blue). Part of the command lines are highlighted in red; which indicates the parameters that could be varied for each command.

Particle Tracking

jpretrackmod,'c:\RSI\IDL60\reslice1\',[1,9,9,5000],740,252, invert=1
Applies the various parameters from the previous particle identification step to all images in the stack. The argument has a 4-component vector: the first two components are the two bpass parameters, the third is the feature size parameter, and the fourth is the masscut parameter.
The goal of this command is to create one file of coordinates 'xys.result'.

pt=read_gdf('xys.result')
Reads in the xys.result file that contains the pre-tracked data.

pta=eclip(pt,[0,0,297],[1,0,100])
Crops any section of the image of interest for particle tracking. The first bracket crops the x-pixels while the second bracket crops the y-pixels (in this case, the section of the image cropped is between 0 and 297 for x-pixels and between 0 and 100 for y-pixels).

plot_hist,pta(0,*) mod 1
Plots histogram to test for pixel-biasing again.

t=track(pta,5,goodenough=30)
Connects the particles identified in the stack of images to form trajectories of particles. The first number represents displacement, i.e. the maximum distance in pixels that the particle is expected to move between frames.
"Goodenough" specifies the minimum duration for the particle trajectory (in no. of frames) for it to be accepted as a valid trajectory.

write_gdf,t,'track.result'
Creates a file of coordinates 'track.result' that contains the individual trajectories.

write_textmod,t,'result.txt'
Writes the 'track.result' file in text format so that it can be opened in Excel.

plottr,t,goodenough=1
Plots all the trajectories that are tracked for at the least the duration specified in "goodenough".

info=monitor_mod(t)
Rearranges and extracts information out from the track.results file for part_find_mod1 command below.

write_gdf,info,'info.result'
Creates a file of coordinates 'info.result' from the monitor_mod command above.

write_textmod,info,'info.txt'
Writes the 'info.result' file in text format so that it can be opened in Excel.

part_find_mod1,info,30,797,297,100
Animates each granule trajectory separately. Each granule is given a unique particle identification (ID) number. Observation of the individual trajectory animation ensures that the granules do not exhibit directed motion and that

the trajectory of each granule is not mistaken for that of neighboring granules that might cross its path. The first number represents the "goodenough" value;
The second number specifies the number of frames in the stack of images tracked; while the third and fourth number denotes the number of x-pixels and y-pixels in the images respectively.

particle_IDs=part_input(62)
After verifying and selecting the granules that satisfies all requirements for tracking, the ID nos of these granules are noted down and input back into the program with this command. The number (in this case 62) represents the total number of granule IDs that has been chosen. After execution of the command, the program returns a commad asking the user to input the ID nos of this particles one after another until all (62 in this case) IDs nos have been keyed in.

write_gdf,particle_IDs,'particle_IDs.result'
Creates a file of coordinates 'particle_IDs.result' which contain the particle ID nos that was input in the step above.

region_time_blocks_front,t,info,particle_Ids,100,0,297,0,252,1,797,150
This command generates the MSD for each granule selected in the steps above. The first number represents the "goodenough" value, the second and third numbers specify the cropped x-pixel values, the fourth and fifth numbers denote the cropped y-pixel values, the fifth and sixth numbers specify the start and end frames for the MSD calculation, and the last number indicates the interval (in no of frames) for each MSD blocks. After execution, the command will return the MSD values at each time interval specified (in this case, 150 frames, i.e. 5 s)

A.3 IDL Codes

The following section lists the codes used in the various IDL commands in section A.1 and A.2. Most of the codes were either newly written or modified from their original form to suit the particle tracking requirements for the present study.

A.3.1 bpass

```
; ********** start of bpass.pro
;
; see http://www.physics.emory.edu/~weeks/idl
;  for further documentation
;
;+
; NAME:
;                   bpass
; PURPOSE:
;                   Implements a real-space bandpass filter which suppress
;                   pixel noise and slow-scale image variations while
;                   retaining information of a characteristic size.
;
; CATEGORY:
;                   Image Processing
; CALLING SEQUENCE:
;                   res = dgfilter( image, lnoise, lobject )
; INPUTS:
;                   image:  The two-dimensional array to be filtered.
;                   lnoise: Characteristic lengthscale of noise in pixels.
;                           Additive noise averaged over this length should
;                           vanish. MAy assume any positive floating value.
;                   lobject: A length in pixels somewhat larger than a typical
;                           object. Must be an odd valued integer.
; OUTPUTS:
;                   res:    filtered image.
; PROCEDURE:
;                   simple 'wavelet' convolution yields spatial bandpass filtering.
; NOTES:
; MODIFICATION HISTORY:
;                   Written by David G. Grier, The University of Chicago, 2/93.
;                   Greatly revised version DGG 5/95.
;                   Added /field keyword JCC 12/95.
;                   Revised & added 'stack','voxel' capability JCC 5/97.
;
;         This code 'bpass.pro' is copyright 1997, John C. Crocker and
;         David G. Grier.  It should be considered 'freeware'- and may be
;         distributed freely in its original form when properly attributed.
;-
function bpass, image, lnoise, lobject, field = field, noclip=noclip

nf = n_elements(image(0,0,*))

;on_error, 2                                ; go to caller on error
```

```
b = float( lnoise )
w = round( lobject > (2. * b) )
N = 2*w + 1

r = (findgen( N ) - w)/(2. * b)
xpt = exp( -r^2 )
xpt = xpt / total(xpt)
factor = ( total(xpt^2) - 1/N )

gx = xpt
gy = transpose(gx)

bx = fltarr(N) - 1./N
by = transpose(bx)

if keyword_set( field ) then begin
        if N mod 4 eq 1 then indx = 2*indgen(w+1)$
                        else indx = 1+ (2*indgen(w))
        gy = gy(indx)
        gy = gy/total(gy)

        nn = n_elements(indx)
        by = fltarr(nn) - 1./nn
endif

res = float(image)
; do x and y convolutions
for i = 0,nf-1 do begin
        g = convol( float(image(*,*,i)), gx )
        g = convol( g, gy )

        b = convol( float(image(*,*,i)), bx )
        b = convol( b, by )

        res(*,*,i) = g-b
endfor

if keyword_set( noclip ) then $
        return,res/factor $
else $
        return,res/factor > 0

end

;********** end of bpass.pro
```

A.3.2 eclip

```
; eclip                    Eric Weeks, 9-22-98
; see http://glinda.lrsm.upenn.edu/~weeks/idl/

function eclip,data,f1,f2,f3,f4,f5,f6,invert=invert
; data in form (*,*)
;
; datanew=eclip(data,[A,B,C])
;   w=where(data(A,*) ge B and data(A,*) le C)
;   datanew=data(*,w)
;


if (keyword_set(invert)) then flag=lindgen(n_elements(data(0,*)))


s=size(f1)
if (s(1) gt 1) then begin
        w=where((data(f1(0),*) ge f1(1)) and (data(f1(0),*)) le f1(2),nw)
        if (nw gt 0) then begin
                result=data(*,w)
                if keyword_set(invert) then flag=flag(w)
        endif
endif
s=size(f2)
if (s(1) gt 1) then begin
        w=where((result(f2(0),*) ge f2(1)) and (result(f2(0),*)) le f2(2),nw)
        if (nw gt 0) then begin
                result=result(*,w)
                if keyword_set(invert) then flag=flag(w)
        endif
endif
s=size(f3)
if (s(1) gt 1) then begin
        w=where((result(f3(0),*) ge f3(1)) and (result(f3(0),*)) le f3(2),nw)
        result=result(*,w)
        if keyword_set(invert) then flag=flag(w)
        s=size(f4)
        if (s(1) gt 1) then begin
                w=where((result(f4(0),*) ge f4(1)) and (result(f4(0),*)) le f4(2),nw)
                if (nw gt 0) then begin
                        result=result(*,w)
                        if keyword_set(invert) then flag=flag(w)
                endif
        endif
        s=size(f5)
        if (s(1) gt 1) then begin
                w=where((result(f5(0),*) ge f5(1)) and (result(f5(0),*)) le f5(2),nw)
                if (nw gt 0) then begin
                        result=result(*,w)
                        if keyword_set(invert) then flag=flag(w)
                endif
        endif
        s=size(f6)
        if (s(1) gt 1) then begin
```

```
                w=where((result(f6(0),*) ge f6(1)) and (result(f6(0),*)) le f6(2),nw)
                if (nw gt 0) then begin
                        result=result(*,w)
                        if keyword_set(invert) then flag=flag(w)
                endif
        endif
endif

if (keyword_set(invert)) then begin
        flag2=lindgen(n_elements(data(0,*)))
        flag2(flag) = -1
        w=where(flag2 ge 0)
        result=data(*,w)
endif

return,result
end
```

A.3.3 feature

```
;+
;
; see http://www.physics.emory.edu/~weeks/idl
;   for more information
;
; NAME:
;                 Feature
; PURPOSE:
;                 Finds and measures roughly circular 'features' within
;                 an image.
; CATEGORY:
;                 Image Processing
; CALLING SEQUENCE:
;                 f = feature( image, diameter [, separation, masscut = masscut,
;                         min = min, iterate = iterate, /field, /quiet ] )
; INPUTS:
;                 image:  (nx,ny) array which presumably contains some
;                         features worth finding
;                 diameter: a parameter which should be a little greater than
;                         the diameter of the largest features in the image.
;                         Diameter MUST BE ODD valued.
;                 separation: an optional parameter which specifies the
;                         minimum allowable separation between feature
;                         centers. The default value is diameter+1.
;                 masscut:Setting this parameter saves runtime by reducing the
;                         runtime wasted on low mass 'noise' features.
;                 min:    Set this optional parameter to the minimum allowed
;                         value for the peak brightness of a feature. Useful
;                         for limiting the number of spurious features in
;                         noisy images.
;                 field:  Set this keyword if image is actually just one field
;                         of an interlaced (e.g. video) image. All the masks
;                         will then be constructed with a 2:1 aspect ratio.
;                 quiet:  Supress printing of informational messages.
;                 iterate: if the refined centroid position is too far from
;                         the initial estimate, iteratively recalc. the centroid
;                         using the last cetroid to position the mask.  This
;                         can be useful for really noisy data, or data with
;                         flat (e.g. saturated) peaks.  Use with caution- it
;                         may 'climb' hills and give you multiple hits.
; OUTPUTS:
;                 f(0,*):   this contains the x centroid positions, in pixels.
;                 f(1,*): this contains the y centroid positions, in pixels.
;                 f(2,*): this contains the integrated brightness of the
;                         features.
;                 f(3,*): this contains the square of the radius of gyration
;                         of the features.
;                 f(4,*): this contains the eccentricity, which should be
;                         zero for circularly symmetric features and order
;                         one for very elongated images.
; SIDE EFFECTS:
;                 Displays the number of features found on the screen.
; RESTRICTIONS:
;                 To work properly, the image must consist of bright,
```

```
;                circularly symmetric regions on a roughly zero-valued
;                background. To find dark features, the image should be
;                inverted and the background subtracted. If the image
;                contains a large amount of high spatial frequency noise,
;                performance will be improved by first filtering the image.
;                BPASS will remove high spatial frequency noise, and
;                subtract the image background and thus provides a good
;                complement to using this program. Individual features
;                should NOT overlap.
; PROCEDURE:
;                First, identify the positions of all the local maxima in
;                the image ( defined in a circular neighborhood with diameter
;                equal to 'diameter' ). Around each of these maxima, place a
;                circular mask, of diameter 'diameter', and calculate the x & y
;                centroids, the total of all the pixel values, and the radius
;                of gyration and the 'eccentricity' of the pixel values within
;                that mask. If the initial local maximum is found to be more
;                than 0.5 pixels from the centroid and iterate is set, the mask
;                is moved and the data are re-calculated. This is useful for
;                noisy data. If the restrictions above are adhered to, and the
;                features are more than about 5 pixels across, the resulting x
;                and y values will have errors of order 0.1 pixels for
;                reasonably noise free images.
;
; *********            READ THE FOLLOWING IMPORTANT CAVEAT!        **********
;                'feature' is capable of finding image features with sub-pixel
;                accuracy, but only if used correctly- that is, if the
;                background is subtracted off properly and the centroid mask
;                is larger than the feature, so that clipping does not occur.
;                It is an EXCELLENT idea when working with new data to plot
;                a histogram of the x-positions mod 1, that is, of the
;                fractional part of x in pixels.  If the resulting histogram
;                is flat, then you're ok, if its strongly peaked, then you're
;                doing something wrong- but probably still getting 'nearest
;                pixel' accuracy.
;
;                For a more quantitative treatment of sub-pixel position
;                resolution see:
;                J.C. Crocker and D.G. Grier, J. Colloid Interface Sci.
;                *179*, 298 (1996).
;
; MODIFICATION HISTORY:
;                This code is inspired by feature_stats2 written by
;                        David G. Grier, U of Chicago,                  1992.
;                Written by John C. Crocker, U of Chicago, optimizing
;                        runtime and measurement error,                         10/93.
;                Added field keyword,                                   4/94.
;                Added eccentricity parameter,                          5/95.
;                Added quiet keyword                                    12/95.
;                Added iteration, fixed up the radius/diameter fiasco and
;                did some debugging which improves non-centroid data.   4/96.
;
;        This code 'feature.pro' is copyright 1997, John C. Crocker and
;        David G. Grier.  It should be considered 'freeware'- and may be
;        distributed freely in its original form when properly attributed.
;-
```

```
;
;       produce a parabolic mask
;
function rsqd,w,h

if n_params() eq 1 then h = w
r2 = fltarr(w,h,/nozero)
xc = float(w-1) / 2.
yc = float(h-1) / 2.
x = (findgen(w) - xc)
x = x^2
y = (findgen(h)- yc)
y = y^2

for j = 0, h-1 do begin
        r2(*,j) = x + y(j)
endfor

return,r2
end
;
;       produce a 'theta' mask
;
function thetarr,w

theta = fltarr(w,w,/nozero)
xc = float(w-1) / 2.
yc = float(w-1) / 2.

x = (findgen(w) - xc)
x(xc) = 1e-5
y = (findgen(w) - yc)

for j = 0, w-1 do begin
        theta(*,j) = atan( y(j),x )
endfor

return,theta
end
;
;       This routine returns the even or odd field of an image
;
function fieldof,array,odd=odd,even=even

sz = size(array)
if sz(0) ne 2 then message,"Argument must be a two-dimensional array!"
if keyword_set(odd) then f=1 else f=0

ny2 = fix( (sz(2)+(1-f))/2 )
rows = indgen(ny2)*2 + f
return,array(*,rows)

end
;
;       barrel "shifts" a floating point arr by a fractional pixel amount,
;               by using a 'lego' interpolation technique.
```

```
;
function fracshift,im,shiftx,shifty

ipx = fix( shiftx )
ipy = fix( shifty )
fpx = shiftx - ipx
fpy = shifty - ipy
if fpx lt 0 then begin
        fpx=fpx+1 & ipx=ipx-1
endif
if fpy lt 0 then begin
        fpy=fpy+1 & ipy=ipy-1
endif

image = im

imagex  = shift( image,ipx+1,ipy   )
imagey  = shift( image,ipx  ,ipy+1 )
imagexy = shift( image,ipx+1,ipy+1 )
image   = shift( image,ipx  ,ipy   )

res   = ( (1. - fpx) * (1. - fpy) * image   ) + $
        ( (     fpx) * (1. - fpy) * imagex  ) + $
        ( (1. - fpx) * (     fpy) * imagey  ) + $
        ( (     fpx) * (     fpy) * imagexy )

return,res
end
;
;       John's version of local_max2, which supports the field keyword
;       and is otherwise identical.
;
function lmx, image, sep, min = min, field = field

range = fix(sep/2)
a = bytscl(image)
w = round( 2 * range + 1 )          ; width of sample region
s = rsqd( w )                       ; sample region is circular
good = where( s le range^2 )
mask = bytarr( w, w )
mask(good) = 1b
yrange = range
if keyword_set( field ) then begin
        mask = fieldof( mask, /even )
        yrange = fix(range/2.) +1
endif

b = dilate( a, mask, /gray )        ; find local maxima in given range

                                    ; but don't include pixels from the
                                    ; background which will be too dim
if not keyword_set( min ) then begin
        h = histogram( a )
        for i = 1, n_elements(h) - 1 do $
                h(i) = h(i) + h(i-1)
        h = float( h ) / max( h )
```

```
        min = 0
        while h(min) lt 0.64 do $
                min = min + 1
        min = min + 1
        endif

r = where( a eq b and a ge min )

                                        ; Discard maxima within range of the edge
sz = size( a )
nx = sz(1) & ny = sz(2)
x = r mod nx & y = r / nx
x0 = x - range & x1 = x + range
y0 = y - yrange & y1 = y + yrange
good = where( x0 ge 0 and x1 lt nx and y0 ge 0 and y1 lt ny,ngood )
if ngood lt 1 then $
        return,[-1]
r = r(good)
x = x(good) & y = y(good)
x0 = x0(good) & x1 = x1(good)
y0 = y0(good) & y1 = y1(good)
                                        ; There may be some features which get
                                        ; found twice or which have flat peaks
                                        ; and thus produce multiple hits.  Find
                                        ; and clear such spurious points.
c = 0b * a
c(r) = a(r)
center = w * yrange + range
for i = 0D, n_elements(r) - 1D do begin
        b = c(x0(i):x1(i),y0(i):y1(i))

        b =  b * mask               ; look only in circular region
        m = max( b, location )
        if location ne center then $
                c(x(i),y(i)) = 0b
        endfor
                                        ; Ideally, the above routine would shrink
                                        ; clusters of points down to their center.
                                        ; As written, this will leave the lower
                                        ; right (?) pixel of a cluster.

r = where( c ne 0 )                     ; What's left are valid maxima.

return,r                    ; return their locations

end
;
;       John's version of DGG's feature_stats2.
;       which: a) avoids some unnecessary computation (convolutions)
;              b) uses fractional shift techniques to reduce pixel bias in m and Rg
;              c) has the field keyword
;
function feature, image, extent, sep,  min=min, masscut = masscut, field = field,$
        quiet = quiet,iterate = iterate

extent = fix(extent)
```

```
if (extent mod 2) eq 0 then begin
        message,'Requires an odd extent.  Adding 1...',/inf
        extent = extent + 1
        endif

sz = size( image )
nx = sz(1)
ny = sz(2)
if n_params() eq 2 then sep = extent+1

;       Put a border around the image to prevent mask out-of-bounds
a = fltarr( nx + extent, ny + extent )
a(extent/2:(extent/2)+nx-1,extent/2:(extent/2)+ny-1) = float( image )
nx = nx + extent

;       Finding local maxima
if keyword_set( field ) then $
        if not keyword_set( min ) then loc = lmx(a,sep,/field) else $
                loc=lmx(a,sep,min=min,/field) $
else $
        if not keyword_set( min ) then loc = lmx(a,sep) else $
                loc=lmx(a,sep,min=min)

if loc(0) eq -1 then return,-1
x  = float( loc mod nx )
y  = float( loc / nx )

nmax=n_elements(loc)
xl = x - fix(extent/2)
xh = xl + extent -1
m  = fltarr(nmax)

;       Set up some masks
rsq = rsqd( extent )
t = thetarr( extent )
mask = rsq le (float(extent)/2.)^2
mask2 = make_array( extent , extent , /float, /index ) mod (extent ) + 1.
mask2 = mask2 * mask
mask3= (rsq * mask) + (1./6.)
cen = float(extent-1)/2.
cmask = cos(2*t) * mask
smask = sin(2*t) * mask
cmask(cen,cen) = 0.
smask(cen,cen) = 0.

;       Extract fields of the masks, if necessary
if keyword_set( field ) then begin
        suba = fltarr(extent , fix(extent/2) , nmax)
        mask = fieldof(mask,/odd)
        xmask = fieldof(mask2,/odd)
        ymask = fieldof(transpose(mask2),/odd)
        mask3 = fieldof(mask3,/odd)
        cmask = fieldof(cmask,/odd)
        smask = fieldof(smask,/odd)

        halfext = fix( extent /2 )
```

```
        yl = y - fix(halfext/2)
        yh = yl + halfext -1
        yscale = 2
        ycen = cen/2

endif else begin
        suba = fltarr(extent, extent, nmax)
        xmask = mask2
        ymask = transpose( mask2 )

        yl = y - fix(extent/2)
        yh = yl + extent -1
        yscale = 1
        ycen = cen
endelse

;       Estimate the mass
for i=0,nmax-1 do m(i) = total( a(xl(i):xh(i),yl(i):yh(i)) * mask )

if keyword_set( masscut ) then begin
        w = where( m gt masscut, nmax )
        if nmax eq 0 then begin
                message,'No features found!',/inf
                return,-1
        endif
        xl = xl(w)
        xh = xh(w)
        yl = yl(w)
        yh = yh(w)
        x = x(w)
        y = y(w)
        m = m(w)
endif

if not keyword_set(quiet) then message, strcompress( nmax ) + ' features found.',/inf

;       Setup some result arrays
xc = fltarr(nmax)
yc = fltarr(nmax)
rg = fltarr(nmax)
e  = fltarr(nmax)

;       Calculate feature centers
for i=0,nmax-1 do begin
        xc(i) = total( a(xl(i):xh(i),yl(i):yh(i)) * xmask )
        yc(i) = total( a(xl(i):xh(i),yl(i):yh(i)) * ymask )
endfor

;       Correct for the 'offset' of the centroid masks
xc = xc / m - ((float(extent)+1.)/2.)
yc = (yc / m - ((float(extent)+1.)/2.)) / yscale

;       Iterate any bad initial estimate.
if keyword_set( iterate ) then begin
counter = 0
repeat begin
```

```
        counter = counter + 1

        w = where( abs(xc) gt 0.6, nbadx )
        if nbadx gt 0 then begin
                dx = round( xc(w) )
                xl(w) = xl(w) + dx
                xh(w) = xh(w) + dx
                x(w) = x(w) + dx
        endif
        w = where( abs(yc) gt 0.6, nbady )
        if nbady gt 0 then begin
                dy = round( yc(w) )
                yl(w) = yl(w) + dy
                yh(w) = yh(w) + dy
                y(w) = y(w) + dy
        endif

        w = where( (abs(xc) gt 0.6) or (abs(yc) gt 0.6), nbad )
        if nbad gt 0 then begin    ; recalculate the centroids for the guys we're iterating

                for i=0,nbad-1 do m(w(i)) = total( a(xl(w(i)):xh(w(i)),$
                        yl(w(i)):yh(w(i))) * mask )
                for i=0,nbad-1 do begin
                        xc(w(i)) = total( a(xl(w(i)):xh(w(i)),yl(w(i)):yh(w(i))) * xmask )
                        yc(w(i)) = total( a(xl(w(i)):xh(w(i)),yl(w(i)):yh(w(i))) * ymask )
                endfor

                xc(w) = xc(w) / m(w) - ((float(extent)+1.)/2.)
                yc(w) = ( yc(w) / m(w) - ((float(extent)+1.)/2.) ) / yscale

        endif
endrep until (nbad eq 0) or (counter eq 10)
endif

;       Update the positions and correct for the width of the 'border'
x = x + xc - extent/2
y = ( y + yc - extent/2 ) * yscale

;       Construct the subarray
for i=0,nmax-1 do suba(*,*,i) = fracshift( a(xl(i):xh(i),yl(i):yh(i)), -xc(i) , -yc(i) )

;       Calculate the 'mass'
for i=0,nmax-1 do m(i) = total( suba(*,*,i) * mask )

;       Calculate radii of gyration squared
for i=0,nmax-1 do rg(i) = total( suba(*,*,i) * mask3 ) / m(i)

;       Calculate the 'eccentricity'
for i=0,nmax-1 do e(i) = sqrt(( total( suba(*,*,i) * cmask )^2 ) +$
        ( total( suba(*,*,i) * smask )^2 )) / (m(i)-suba(cen,ycen,i)+1e-6)

params = [transpose(x),transpose(y),transpose(m),transpose(rg),transpose(e)]
return,params
end
```

A.3.4 fover2d

```
;function fover2d,image,points,radius=radius,big=big,nodot=nodot,circle=circle
;
; see http://www.physics.emory.edu/~weeks/idl
;   for more information and software updates
;+
; NAME:
;                   fover2d
; PURPOSE:
;                   Overlay points onto a 2d image.
; CALLING SEQUENCE:
;                   newimage=foverlay,image,points
; INPUTS:
;                   image:  2D data set onto which the points should be overlaid
;                   points: (2,npoints) array of overlay points
; OUTPUTS:
;                   returns an image ready for 'tv'.  The color palette
;                   is adjusted to be the foverlay palette.  Redraws screen.
; KEYWORDS:
;                   radius sets size of circles
;     /big doubles the picture in size in each direction
;     /nodot turns off the black dot at the center of each circle
;     /circle draws a circle around each point, rather than a disk
; PROCEDURE:
;                   Rescale the image to leave some color table indices free.
;                   Make the rest of the color table into a grey ramp and
;                   turn the 3 highest indices into 3 new colors.  Plot a
;     disk at each particle position.
; MODIFICATION HISTORY:
;     Lookup table code taken from David G. Grier's f_overlay
;     routine.  Mostly written by Eric Weeks in summer '98.
;     Ability to handle movies added 2-20-99.
;-

;First a utility function....

; circarray.pro,  started 6-22-98 by ERW
;   shortened into fo_circ 2-20-99 by ERW
;
function fo_circ,array,radius=radius,center=center,circle=circle
; returns an array, size equal to "array" variable, with value 1
; everywhere within a circle of diameter of the array size.  Circle
; is at center of array.
;
; 'radius' sets a radius different from the default radius (half the array size)
; 'center' overrides the default center of the circle

s=size(array)
result=array*0

sx=s(1) & sy=s(2)
minsize = (sx < sy)
cx=(sx-1)*0.5 & cy=(sy-1)*0.5
if keyword_set(center) then begin
        cx=center(0)
```

```
        cy=center(1)
endif
if keyword_set(radius) then begin
        irad=radius
endif else begin
        irad=minsize/2
endelse
jrad=(irad-1.2)*(irad-1.2)
irad = irad*irad
if (keyword_set(circle)) then begin
        for j=0,sy-1 do begin
                rad2 = (cy-j)*(cy-j)
                for k=0,sx-1 do begin
                        rad3 = rad2 + (cx-k)*(cx-k)
                        result(k,j) = ((rad3 le irad) and (rad3 ge jrad))
                endfor
        endfor
endif else begin
        for j=0,sy-1 do begin
                rad2 = (cy-j)*(cy-j)
                for k=0,sx-1 do begin
                        rad3 = rad2 + (cx-k)*(cx-k)
                        result(k,j) = (rad3 le irad)
                endfor
        endfor
endelse

return,result
end



function fover2d,image,points,radius=radius,big=big,nodot=nodot,circle=circle
if not keyword_set(radius) then radius=5
if (not keyword_set(nodot)) then nodot=0
if not keyword_set(circle) then begin
        circle=0
endif else begin
        nodot=1
endelse

nc = !d.table_size
if nc eq 0 then message,'Device has static color tables: cannot adjust'
red = byte(indgen(nc))
green = red
blue = red
green(nc-1) = 0b
;blue(nc-1)=128b
tvlct,red,green,blue

output = byte ( ((image*0.98) mod (nc-5)) + floor(image / (nc-5))*256 )
x=reform(points(0,*))
y=reform(points(1,*))
s = size(output)
if (s(0) eq 3) then begin
        ; 3-D array
```

```
        nel=n_elements(points(*,0))
        t = reform(points(nel-1,*))
        tmax=max(t,min=tmin)
endif
if (keyword_set(big)) then begin
        if (s(0) eq 2) then begin
                output=rebin(output,s(1)*2,s(2)*2);       2-D array
        endif else begin
                output=rebin(output,s(1)*2,s(2)*2,s(3));  3-D array
        endelse
        x = x * 2 & y = y * 2
endif
x2=n_elements(output(*,0,0));              3rd array index just for safety
y2=n_elements(output(0,*,0))
w=where((x ge 0) and (x lt x2))
x=x(w) & y=y(w)
w=where((y ge 0) and (y lt y2))
x=x(w) & y=y(w)

for i = 0,n_elements(x)-1 do begin
        minx = long((x(i)-radius) > 0)
        miny = long((y(i)-radius) > 0)
        maxx = long((x(i)+radius) < (x2-1))
        maxy = long((y(i)+radius) < (y2-1))
        foo=[x(i)-minx,y(i)-miny]
        blob=fo_circ(output[minx:maxx,miny:maxy],  $
                        center=foo,radius=radius,circle=circle)
        blob = (blob < 1) * (nc - 1b)
        if (s(0) eq 2) then begin
                ; 2-D image
                output(minx:maxx,miny:maxy) =                    $
                        output(minx:maxx,miny:maxy) > blob
                if (nodot eq 0) then begin
                        if (x(i) gt 1) and (x(i) lt (x2-1)) then $
                                output(x(i)-1:x(i)+1,y(i))=0b
                        if (y(i) gt 1) and (y(i) lt (y2-1)) then $
                                output(x(i),y(i)-1:y(i)+1)=0b
                endif
        endif else begin
                ; 3-D image
                tnow=t(i)-tmin
                output(minx:maxx,miny:maxy,tnow) =                    $
                        output(minx:maxx,miny:maxy,tnow) > blob
                if (nodot eq 0) then begin
                        if (x(i) gt 1) and (x(i) lt (x2-1)) then $
                                output(x(i)-1:x(i)+1,y(i),tnow)=0b
                        if (y(i) gt 1) and (y(i) lt (y2-1)) then $
                                output(x(i),y(i)-1:y(i)+1,tnow)=0b
                endif
        endelse
endfor

tv,output
return, output
end
```

A.3.5 jpretrackmod

```
;
;
; see http://www.physics.emory.edu/~weeks/idl
;   for more information
;
; dead simple routine to analyse 2+1d 'stacks' into trackable files
; whammy = [lnoise,extent1,extent2,masscut]
;
;  ppretrack -- Peter's version (begun 7/8/97)
;  jpretrack -- John's version (begun 7/8/98)
;
pro jpretrackmod,name,whammy,horpix,verpix,invert=invert,field=field,first=first,fskip=fskip,$
   gdf=gdf

if n_elements(whammy) ne 4 then $
   message,'usage: pretrack,fname,[lnoise,extent1,extent2,masscut],invert=invert,field=field'

lnoise = whammy(0)
extent1 = whammy(1)
extent2 = whammy(2)
masscut = whammy(3)

filetotal = findfile(name +'*.tif')
if filetotal(0) eq '' then message,"No file '"+name+"' found"
ns = n_elements(filetotal)

filen=strarr(ns)

if (ns gt 1000) then begin
   for k=1000,ns-1 do begin
      l=string(k)
      m=strcompress(l,/remove_all)
      filen(k)=findfile(name +'frame'+ m + '.tif')
   endfor
   for k=100,999 do begin
      l=string(k)
      m=strcompress(l,/remove_all)
      filen(k)=findfile(name +'frame0'+ m + '.tif')
   endfor
   for k=10,99 do begin
      l=string(k)
      m=strcompress(l,/remove_all)
      filen(k)=findfile(name +'frame00'+ m + '.tif')
   endfor
   for k=0,9 do begin
      l=string(k)
      m=strcompress(l,/remove_all)
      filen(k)=findfile(name +'frame000'+ m + '.tif')
   endfor
endif else begin
   if (ns gt 100) then begin
     for k=100,ns-1 do begin
        l=string(k)
        m=strcompress(l,/remove_all)
```

```
        filen(k)=findfile(name +'frame0'+ m + '.tif')
      endfor
      for k=10,99 do begin
          l=string(k)
          m=strcompress(l,/remove_all)
          filen(k)=findfile(name +'frame00'+ m + '.tif')

      endfor
      for k=0,9 do begin
          l=string(k)
          m=strcompress(l,/remove_all)
          filen(k)=findfile(name +'frame000'+ m + '.tif')
      endfor
   endif else begin
       for k=10,ns-1 do begin
           l=string(k)
           m=strcompress(l,/remove_all)
           filen(k)=findfile(name +'frame00'+ m + '.tif')
       endfor
       for k=0,9 do begin
            l=string(k)
            m=strcompress(l,/remove_all)
            filen(k)=findfile(name +'frame000'+ m + '.tif')
         endfor
   endelse
endelse


;  fskip is the frame/field # increment during time lapse video
if not keyword_set(fskip) then fskip=1

stk=bytarr(horpix,verpix,ns)

for j=0,ns-1 do begin

   print,'reading image stack: '+filen(j)
   if keyword_set(gdf) then stk = read_gdf(filen(j)) else $
     frame = read_nih(filen(j))

   if keyword_set(invert) then frame = 255b-frame

   stk(*,*,j)=frame

   ns = n_elements(stk(0,0,*))

endfor

   ss=size(stk(*,*,0))
   sx = ss(1)

   if keyword_set(first) then ns = 1  ;handy for a quick looksee...

   res = fltarr(6)
   if keyword_set(field) then begin
     for i = 0,ns-1 do begin
     print,'processing fields of frame'+strcompress(i)+' out of'+$
```

```
      strcompress(ns)+'....'
    im = bpass(fieldof(stk(*,*,i)),lnoise,extent1,/field)
    f = feature(im(2*extent1:sx-2*extent1,*),extent2,masscut = masscut,/field)
    if f(0) ne -1 then begin
      f(0,*,*) = f(0,*,*)+2*extent1
      nf = n_elements(f(0,*))
      res = [[res],[f,fltarr(1,nf)+2*i*fskip]]
    endif
    im = bpass(fieldof(stk(*,*,i)),lnoise,extent1,/field)
    f = feature(im(2*extent1:sx-2*extent1,*),extent2,masscut = masscut,/field)
    if f(0) ne -1 then begin
      f(0,*,*) = f(0,*,*)+2*extent1
      f(1,*) = f(1,*)+1
      nf = n_elements(f(0,*))
      res = [[res],[f,fltarr(1,nf)+2*i*fskip+1]]
    endif
    endfor
  endif else begin
    for i = 0,ns-1 do begin
    print,'processing frame'+strcompress(i)+' out of'+$
      strcompress(ns)+'....'
    im = bpass(stk(*,*,i),lnoise,extent1)
    f = feature(im,extent2,masscut = masscut)
    nf = n_elements(f(0,*))
    if (f(0) ne -1) then res = [[res],[f,fltarr(1,nf)+i*fskip]]
    endfor
  endelse

  wname = 'xys.result'
  print,'writing output file to:' + wname
  write_gdf,res(*,1:*),wname


end
```

A.3.6 monitor_mod

```
function monitor_mod,t

sz=size(t)

n_rows=sz(2,0)

extract=extrac(t,6,0,1,n_rows)

max_track=max(extract)

max_track_int=uint(max_track)

info=fltarr(7,max_track_int+1)

for i=0,max_track_int do begin
   w=where(t(6,*) eq i)
   nf=n_elements(w)
   first_frame=w(0)
   info(0,i)=t(0,first_frame)
   info(1,i)=t(1,first_frame)
   info(2,i)=t(4,first_frame)
   info(3,i)=nf
   info(4,i)=t(5,first_frame)+1
   info(5,i)=info(4,i)+nf-1
   info(6,i)=t(6,first_frame)
endfor

return,info


end
```

A.3.7 part_find_mod1

```
pro part_find_mod1,info,goodenough,total_frames,xpixel,ypixel

for i=1,total_frames-goodenough+1 do begin
   p=string(i)
   w=where (info(4,*) eq i)
   sz=size(w)
   type=sz(0,0)

   if type ne 0 then begin
   n=n_elements(w)
   for j=0,n-1 do begin
     print,'start frame = '+p
     particle_no=w(j)
     s=info(4,particle_no)-1
     frame_no=long(s)

     if (frame_no lt 10) then begin
        l=string(frame_no)
        m=strcompress(l,/remove_all)
        no='000'+m
        a=read_nih('c:\RSI\IDL60\reslice1\frame'+no+'.tif')
        tvscl,a
     endif

     if (frame_no ge 10) and (frame_no lt 100) then begin
        l=string(frame_no)
        m=strcompress(l,/remove_all)
        no='00'+m
        a=read_nih('c:\RSI\IDL60\reslice1\frame'+no+'.tif')
        tvscl,a
     endif

     if (frame_no ge 100) and (frame_no lt 1000) then begin
        l=string(frame_no)
        m=strcompress(l,/remove_all)
        no='0'+m
        a=read_nih('c:\RSI\IDL60\reslice1\frame'+no+'.tif')
        tvscl,a
     endif

     if (frame_no ge 1000) then begin
        l=string(frame_no)
        m=strcompress(l,/remove_all)
        no=m
        a=read_nih('c:\RSI\IDL60\reslice1\frame'+no+'.tif')
        tvscl,a
     endif

     fo=fover2d(a,info(*,particle_no),/circle,rad=7)
     d=long(info(5,particle_no))
     end_frame=string(d)
     particle_info=string(particle_no)
     print,'end frame= '+end_frame
     print,'particle no= '+particle_info
```

```
      no_frames=info(3,particle_no)

      if no_frames ge 230 then no_frames=230

      base = WIDGET_BASE(TITLE = 'Animation Widget')
      animate = CW_ANIMATE(base, xpixel, ypixel, no_frames,/track)
      WIDGET_CONTROL, /REALIZE, base

      for k=0,no_frames-1 do begin
      if (frame_no lt 10) then begin
         l=string(frame_no)
         m=strcompress(l,/remove_all)
         no='000'+m
         a=read_nih('c:\RSI\IDL60\reslice1\frame'+no+'.tif')
        CW_ANIMATE_LOAD, animate, FRAME=k, IMAGE=a
      endif

      if (frame_no ge 10) and (frame_no lt 100) then begin
         l=string(frame_no)
         m=strcompress(l,/remove_all)
         no='00'+m
         a=read_nih('c:\RSI\IDL60\reslice1\frame'+no+'.tif')
         CW_ANIMATE_LOAD, animate, FRAME=k, IMAGE=a
      endif

      if (frame_no ge 100) and (frame_no lt 1000) then begin
         l=string(frame_no)
         m=strcompress(l,/remove_all)
         no='0'+m
         a=read_nih('c:\RSI\IDL60\reslice1\frame'+no+'.tif')
        CW_ANIMATE_LOAD, animate, FRAME=k, IMAGE=a
      endif

      if (frame_no ge 1000) then begin
         l=string(frame_no)
         m=strcompress(l,/remove_all)
         no=m
         a=read_nih('c:\RSI\IDL60\reslice1\frame'+no+'.tif')
         CW_ANIMATE_LOAD, animate, FRAME=k, IMAGE=a
      endif

      frame_no=frame_no+1

       endfor

    CW_ANIMATE_RUN, animate,40
     XMANAGER, 'CW_ANIMATE Demo', base, EVENT_HANDLER = 'EHANDLER'

    prom=''
    read, prom

    endfor
    endif
endfor
end
```

A.3.8 part_input

```
function part_input,no_particle

particles=intarr(no_particle)
for i=1,no_particle do begin
   read,a
   particles(i-1)=a
endfor

return,particles

end
```

A.3.9 plot_hist

```
; plot_hist
;
; see http://www.physics.emory.edu/~weeks/idl
;   for more information and software updates
;
;       A user-friendly way to plot roughly normal distributed histograms
;               easily with optional gaussian fits.
;       The relevant data can be returned with the optional parameter 'data'
;       and coff.  set number of terms in fit (must be 3 or more) using nterms
;
; original version by John C. Crocker
; slightly revised, Feb '99, Eric R. Weeks; /log added 2-23-99
;
pro plot_hist,d,data,coff,nterms=nterms,fit=fit,xrange=xrange,binsize=binsize,$
        noplot=noplot,oplot=oplot,jitter = jitter,center=center,log=log

if keyword_set(fit) then center=1;       ERW 2-22-99
if not keyword_set(jitter) then jitter = 0
if keyword_set(nterms) then begin
        if (nterms lt 3 or nterms gt 6) then begin
                print,'Resetting nterms to 6.  nterms must be 3, 4, 5, or 6!  See gaussfit.'
                nterms = 6
        endif
endif
if not keyword_set(nterms) then nterms = 3

; don't know why, just gotta do it
data = float(d)

; get a little info about the distribution
n=n_elements(data)
logn=alog10(n)
min = min(data,max=max)
stdev = stdev(data,mean)
min = min([min,mean-(6*stdev)])
max = max([max,mean+(4*stdev)])
if keyword_set(xrange) then begin
        min = xrange(0)
        max = xrange(1)
        w=where(data ge min and data le max,ndata)
        logn = alog10(ndata)
        stdev=stdev(data(w))
endif

; calculate a nice binsize if the user doesn't give us one
if not keyword_set(binsize) then begin
        binsize=stdev/logn
;       reduce the binsize slightly so that its either 1,2 or 5 times a power of ten
        logbin=alog10(binsize)
        fp = (logbin-fix(logbin))
        ip = fix(logbin)
        if (fp lt 0) then begin
                fp = fp+1 & ip = ip-1
        endif
```

```
        coeff = 10^(fp)
        if (coeff lt 2) then fp = 0
        if (coeff ge 2) AND (coeff lt 5) then fp = alog10(2)
        if (coeff ge 5)    then fp = alog10(5)
        binsize = 10^(float(ip + fp))
endif

; adjust the min value down so that 0 is at the center of a partition
minbin = long(min/binsize)
if minbin lt 0 then minbin = minbin-1
min = minbin * binsize
if (keyword_set(center) and (not keyword_set(xrange))) then xrange=[min,max]

; oh yeah, calculate the histogram
hist = histogram(data,binsize=binsize,min=min-(binsize*jitter),max=max+binsize*jitter)

; pad out the hist with a zero so the plot doesn't hang in the air!
hist=[hist,[0]]
np = n_elements(hist)

; make an 'x' vector for the plot and the fit
x = (findgen(np)*binsize) + min - (binsize*jitter)

if (not keyword_set(center)) then begin
        w=where(hist gt 0,nw)
        minw=w(0) > 1
        maxw=w(nw-1) < (n_elements(hist)-2)
        hist=hist(minw-1:maxw+1)
        x=x(minw-1:maxw+1)
endif
; plot the histogram
if not keyword_set(noplot) then begin
        if keyword_set(oplot) then begin
                oplot,x,hist,psym=10
        endif else begin
                w=where(hist gt 0)
                if (keyword_set(xrange)) then begin
                        if (keyword_set(log)) then begin
                                plot,x(w),hist(w),xrange=xrange,psym=4,/ylog
                        endif else begin
                                plot,x,hist,xrange=xrange,psym=10
                        endelse
                endif else begin
                        if (keyword_set(log)) then begin
                                plot,x(w),hist(w),psym=4,/ylog
                        endif else begin
                                plot,x,hist,psym=10
                        endelse
                endelse
        endelse
endif
data = [transpose(x),transpose(hist)]

; do the fit, if desired
if keyword_set(fit) then begin
        ft = gaussfit(x,hist,coff,nterms=nterms)
```

```
        data = [transpose(x),transpose(hist),transpose(ft)]
        if not keyword_set(noplot) then begin
                oplot,x,ft,linestyle=3
                dy = !y.crange(1)-!y.crange(0)
                dx = !x.crange(1)-!x.crange(0)
                yy = !y.crange(0)
                xx = !x.crange(0)
                if (keyword_set(log)) then begin
                        xyouts, xx + (dx*0.15), 10^(yy + (dy*.90)), "Height = "+$
                                strcompress(string(coff(0),format='(g9.4)')) ,alignment=0.5
                        xyouts, xx + (dx*0.15), 10^(yy + (dy*.85)), "Offset = "+$
                                strcompress(string(coff(1),format='(g9.4)')) ,alignment=0.5
                        xyouts, xx + (dx*0.15), 10^(yy + (dy*.80)), "Sigma = "+$
                                strcompress(string(coff(2),format='(g9.4)')) ,alignment=0.5
                endif else begin
                        xyouts, xx + (dx*0.15), yy + (dy*.90), "Height = "+$
                                strcompress(string(coff(0),format='(g9.4)')) ,alignment=0.5
                        xyouts, xx + (dx*0.15), yy + (dy*.85), "Offset = "+$
                                strcompress(string(coff(1),format='(g9.4)')) ,alignment=0.5
                        xyouts, xx + (dx*0.15), yy + (dy*.80), "Sigma = "+$
                                strcompress(string(coff(2),format='(g9.4)')) ,alignment=0.5
                endelse
                if (nterms gt 3) then begin
                        if (keyword_set(log)) then begin
                xyouts, xx + (dx*0.15), 10^(yy + (dy*.75)), "Polynomial:" ,alignment=0.5
                xyouts, xx + (dx*0.15), 10^(yy + (dy*.70)), $
                        strcompress(string(coff(3),format='(g10.4)')) ,alignment=0.5
                        endif else begin
                xyouts, xx + (dx*0.15), yy + (dy*.75), "Polynomial:" ,alignment=0.5
                xyouts, xx + (dx*0.15), yy + (dy*.70), $
                        strcompress(string(coff(3),format='(g10.4)')) ,alignment=0.5
                        endelse

                if (nterms gt 4) then begin
                        if (keyword_set(log)) then begin
                xyouts, xx + (dx*0.15), 10^(yy + (dy*.65)), "+ "+$
                        strcompress(string(coff(4),format='(g9.4)'))+" x" ,alignment=0.5
                        endif else begin
                xyouts, xx + (dx*0.15), yy + (dy*.65), "+ "+$
                        strcompress(string(coff(4),format='(g9.4)'))+" x" ,alignment=0.5
                        endelse
                if (nterms gt 5) then begin
                        if (keyword_set(log)) then begin
                xyouts, xx + (dx*0.15), 10^(yy + (dy*.60)), "+ "+$
                        strcompress(string(coff(5),format='(g10.4)'))+" x^2" ,alignment=0.5
                        endif else begin
                xyouts, xx + (dx*0.15), yy + (dy*.60), "+ "+$
                        strcompress(string(coff(5),format='(g10.4)'))+" x^2" ,alignment=0.5
                        endelse
                endif ; five
                endif ; four
                endif ; three
        endif
endif

end
```

A.3.10 plot_tr

```
;pro plottr,tarray,result,goodenough=goodenough,tv=tv,noconnect=noconnect, $
;  x=x,y=y,_extra=eee
;
; see http://www.physics.emory.edu/~weeks/idl
;    for more information and software updates
;
; plottr.pro  (formerly ericplot2.pro)
;
; started 6-15-98   Eric R. Weeks
; /tv added 8-13-98
; /noconnect added 8-13-98
; uberized 9-21-98
;
; duplicates somewhat "plot_tracks"
;

; lentrk                        Eric Weeks 9-22-98
;
; modified from JCC's len_trk.pro

function pt_lentrk,t
; works for either uber or normal tracked data
;
; returns (2,*) array:  (0,*) is the length, (1,*) is particle #

s=size(t)
if (s(0) eq 2) then begin
        ; UBER TRACKER
        ; get the indices of the unique id's
        ndat=n_elements(t(*,0))
        u = uniq(t(ndat-1,*))
        ntracks = n_elements(u)
        u = [-1,u]

        res = fltarr(2,ntracks)
        for i = 1L,ntracks do begin
                res(0,i-1) = t(ndat-2,u(i))-t(ndat-2,u(i-1)+1)
                res(1,i-1) = t(ndat-1,u(i))
        endfor
endif else begin
        ; OLD TRACKER
        ntracks=n_elements(t(0,*,0))
        res=fltarr(2,ntracks)
        for i=0,ntracks-1 do begin
                w=where(t(0,i,*) ge 0)
                res(0,i)=w(n_elements(w)-1)-w(0)+1
                res(1,i)=i
        endfor
endelse

return,res
end
```

```
; first a utility function:
; eline.pro    started 8-13-98 by Eric Weeks
;
; linearray=eline(pt1,pt2)
; pt1, pt2 are n-dimensional pofloors (integers)
; result is an array of pofloors connecting them
;
; vectorized 11-2-98
; turned into pt_eline 2-25-99

function pt_eline,pt1,pt2

ndim=n_elements(pt1)
ndim2=n_elements(pt1)
if (ndim ne ndim2) then message,"error! pts must be same dimension"
result=floor(pt1)

delta=pt2-pt1
max=max(abs(delta))
epsilon=float(delta)/float(max)
if (max le 0) then begin
        message,"warning! begin and end pts are identical",/inf
endif else begin
        pt0=float(pt1)
        temp=epsilon # findgen(max+1)
        n=n_elements(pt1)
        result=intarr(n,max+1)
        for i=0,n-1 do begin
                result(i,*)=floor(pt0(i)+temp(i,*))
        endfor
endelse

return,result
end

pro plottr,tarray,result,goodenough=goodenough,tv=tv,noconnect=noconnect, $
  x=x,y=y,_extra=eee
; tarray is an array of tracked data (2D for the moment)
; goodenough works like plot_tracks -- only tracks at least 'goodenough'
;    in duration will be plotted
; /tv uses tv mode to plot, rather than axes; use x and y to adjust size
; result gets picture from /tv
;
; WARNING: tracked data must be "uberize'd" before using! (if ubertracker)

s = size(tarray)
if (s(0) eq 2) then uber=1

if (not keyword_set(x)) then x=512
if (not keyword_set(y)) then y=480
if (not keyword_set(noconnect)) then connect=1

if (not keyword_set(uber)) then begin
        ; REGULAR TRACKER
        if not keyword_set(goodenough) then goodenough=s(3)
        ; default is number of frames
```

```
        ww=where( total(tarray(0,*,*) ge 0,3) ge goodenough )
        ; ww locates all valid data pts (not equal to -1)

        if (keyword_set(tv)) then begin
                ; added 8-13-98
                picture=bytarr(x,y)
                if (keyword_set(connect)) then begin
                        for i=0,s(2)-1 do begin
                                ; loop over each particle
                                w1=where(tarray(0,i,*) gt 0)
                                pt0=tarray(0:1,i,w1(0))
                                for j=1,n_elements(w1)-1 do begin
                                        ; loop over each valid frame
                                        pt1=tarray(0:1,i,w1(j))
                                        lineline=pt_eline(pt0,pt1)
                                        picture(lineline(0,*),lineline(1,*)) = 255
                                        pt0=pt1
                                endfor
                        endfor
                endif else begin
                        for i=0,s(3)-1 do begin
                                ; loop over each frame
                                if (ww(0) ge 0) then begin
                                        w = where(tarray(0,ww,i) gt 0)
                                        ptrs=ww(w)
                                        picture(tarray(0,ptrs,i),tarray(1,ptrs,i)) = 255
                                endif
                        endfor
                endelse
                tv,picture
                result=picture
        endif else begin
                ; original pre-August 1998 routine
                if (ww(0) ge 0) then begin
                        w = where(tarray(0,ww,0) gt 0)
                        ptrs=ww(w)
                        plot,tarray(0,ptrs,0),tarray(1,ptrs,0),/nodata, $
                                _extra=eee,/ynozero,/ysty,/xsty,/isotropic
                        ; loop over each frame
                        if (keyword_set(connect)) then begin
                                for i=0,s(3)-1 do begin
                                        w = where(tarray(0,ww,i) gt 0)
                                        ptrs=ww(w)
                                        oplot,tarray(0,ptrs,i),tarray(1,ptrs,i),psym=3
                                endfor
                        endif else begin
                                for i=0,s(3)-1 do begin
                                        w = where(tarray(0,ww,i) gt 0)
                                        ptrs=ww(w)
                                        oplot,tarray(0,ptrs,i),tarray(1,ptrs,i),psym=3
                                endfor
                        endelse
                endif
        endelse
endif else begin
        ; UBER-TRACKER
```

```
        ndat=n_elements(tarray(*,0))
        ntime=max(tarray(ndat-2,*))
        if not keyword_set(goodenough) then goodenough=ntime
        length=pt_lentrk(tarray)
        w=where(length(0,*) ge goodenough,nw)
        if (keyword_set(tv)) then begin
                picture=bytarr(x,y)
                u=uniq(tarray(ndat-1,*))
                ntracks=n_elements(u)
                u=[-1,u]
                if (keyword_set(connect)) then begin
                        for i=0L,nw-1L do begin
                                j=length(1,w(i))
                                traj=tarray(*,u(j)+1:u(j+1))
                                k=n_elements(traj(0,*))
                                pt0=traj(0:1,0)
                                for kk=1L,k-1L do begin
                                        pt1=traj(0:1,kk)
                                        lineline=pt_eline(pt0,pt1)
                                        picture(lineline(0,*),lineline(1,*)) = 255
                                        pt0=pt1
                                endfor
                        endfor
                endif else begin
                        for i=0L,nw-1L do begin
                                j=length(1,w(i))
                                traj=tarray(*,u(j)+1:u(j+1))
                                picture(traj(0,*),traj(1,*)) = 255b
                        endfor
                endelse
                tv,picture
                result=picture
        endif else begin
                plot,tarray(0,*),tarray(1,*),/nodata,/ynozero,_extra=eee,   $
                        /ysty,/xsty,/isotropic
                u=uniq(tarray(ndat-1,*))
                ntracks=n_elements(u)
                u=[-1,u]
                if (keyword_set(connect)) then begin
                        for i=0L,nw-1L do begin
                                j=length(1,w(i))
                                traj=tarray(*,u(j)+1:u(j+1))
                                oplot,traj(0,*),traj(1,*)
                        endfor
                endif else begin
                        for i=0L,nw-1L do begin
                                j=length(1,w(i))
                                traj=tarray(*,u(j)+1:u(j+1))
                                oplot,traj(0,*),traj(1,*),psym=3
                        endfor
                endelse
        endelse
endelse

end
; this ends the procedure
```

A.3.11 read_gdf

```
function read_gdf,filespec
;
; see http://www.physics.emory.edu/~weeks/idl
;   for more information
;
;+
; NAME:
;                   read_gdf
; PURPOSE:
;                   Read in data files created by WRITE_GDF.
; CATEGORY:
;                   General Purpose Utility
; CALLING SEQUENCE:
;                   data = read_gdf(file)
; INPUTS:
;                   file:     Complete pathname of the file to be read.
; OUTPUTS:
;                   data:     Data structure.  For example, if the original
;                             data was stored as an array of bytes, then
;                             DATA will be returned as an array of bytes also.
; RESTRICTIONS:
;                   Current implementation does not support structures or
;                   arrays of structures.
; PROCEDURE:
;                   Reasonably straightforward.
;                   Determines if the file is ASCII or binary, reads the size
;                   and dimension info from the header, and reads in the data
; MODIFICATION HISTORY:
;                   Written by David G. Grier, AT&T Bell Laboratories, 9/91
;          12/95 Figures out how to deal with data from different-endian
;                   machines DGG.
;-
on_error,2                          ; return to caller on error

MAGIC = 082991L
HEADER = 'GDF v. 1.0'
debug = keyword_set(debug)

file = findfile(filespec, count=nfiles)

if nfiles eq 0 then message,'No files matched specification '+filespec

d = -1
ascii = 0

openr,lun,file(0),/get_lun

mgc = 0L
readu,lun,mgc
doswap = swap_endian(mgc) eq MAGIC; Check for binary GDF file written on
                                    ; different-endian machine

                                    ; Check for ASCII GDF file
```

```
if (mgc ne MAGIC) and (not doswap) then begin
        point_lun,lun,0
        str = ''
        fmt = '(A'+strtrim(strlen(HEADER),2)+')'
        readf,lun,format=fmt,str
        if str eq HEADER then $
                ascii = 1 $
        else begin
                message,filespec+' is not a GDF file',/inf
                goto,done
                endelse
        endif
ndim = 0L

                                        ; Get number of data dimensions
if ascii then readf,lun,ndim else readu,lun,ndim
if doswap then ndim = swap_endian(ndim)
sz = lonarr(ndim+2,/nozero)
                                        ; Get data type description
if ascii then readf,lun,sz else readu,lun,sz
if doswap then sz = swap_endian(sz)
sz = [ndim,sz]

d = make_array(size=sz,/nozero)
if ascii then readf,lun,d else readu,lun,d
if doswap then d(*) = swap_endian(d(*))

done:
close,lun
free_lun,lun
return,d
end
```

A.3.12 read_nih

```
function read_nih,fname,first=first,last=last
;
; see http://www.physics.emory.edu/~weeks/idl
;   for more information
;
;
;   reads 2 and 3 dimensional 8-bit TIFF files as produced by
;   NIH Image.  It tries to detect and fix 'endian' problems.
;   Also allows user to read a subset of frames, which is useful
;   for really big files.
;
f = findfile(fname)          ; check to see if the file is actually *there*
if f(0) eq '' then message,'File: "'+fname+'" not found!'

cookie = intarr(1)
head = intarr(383)

; check for endian independent cookie
openr,1,fname
readu,1,cookie
if (cookie(0) ne 19789 and cookie(0) ne 18761) then begin
        close,1
        message,'"'+fname+'" is not a valid NIH Image tiff file!'
endif
readu,1,head

; fix endian
if head(2) eq 2048 then head = swap_endian(head)
; check endian
if head(2) ne 8 then begin
        close,1
        message,'"'+fname+'" is not a valid NIH Image tiff file!'
endif

tmp = FSTAT(1)

x = head(14) + 0L
y = head(20) + 0L
z = head(257) + 0L
if z eq 0 then z = 1L                        ; fix for 2d nih tiff images

; watch out for EOF errors- is the file big enough?
sz = (x*y*z) + 768L
if sz gt tmp.size then $
        message,'"'+fname+'" is not a valid NIH Image tiff file!'

; do Peter's browsing thing
s = 0
if keyword_set( first ) then begin
        if (first le z-1) and (first ge 0) then s=first $
                else begin
                        close,1
                        message,'invalid first position!!'
```

```
                endelse
endif
if keyword_set( last ) then begin
        if (last ge s) and (last le z-1) then z=last $
                else begin
                        close,1
                        message,'invalid last position!'
                endelse
endif

if (s gt 0) then begin
        z = z - s + 1
        offset = x * y * s + 768L
        point_lun,1,offset
endif

; read in the data
im = bytarr(x,y,z)
readu,1,im
close,1

; fix the data up for IDL conventions
for i = 0,z-1 do im(*,*,i) = 255b-rotate(im(*,*,i),7)

return,im

end
```

A.3.13 region_time_blocks_front

```
pro region_time_blocks_front,t,info,particle_IDs,goodenough,$
   xpixel_min,xpixel_max,$
   ypixel_lowerfrontproj,ypixel_upperfrontproj,$
   start_frame,end_frame,frame_duration


m=n_elements(particle_IDs)

sel_part_orig=fltarr(7,m)

for i=0,m-1 do begin
   sel_part_orig(*,i)=info(*,particle_IDs(i))
endfor

no_block=(end_frame-start_frame)/frame_duration

end_block=start_frame-1

for j=0,no_block-1 do begin
   n=0
   sel_part=sel_part_orig

   l=string(j+1)
   r=strcompress(l,/remove_all)

   start_block=end_block+1
   end_block=start_block+frame_duration-1

   for k=0,m-1 do begin
     if (sel_part(0,k) ge xpixel_min) and (sel_part(0,k) le xpixel_max) $
     and (sel_part(1,k) ge ypixel_lowerfrontproj) and (sel_part(1,k) le ypixel_upperfrontproj) $
     then begin
     if sel_part(4,k) lt end_block then begin
           if sel_part(4,k) lt start_block then begin
           sel_part(4,k)=start_block
           endif

         if sel_part(5,k) gt start_block then begin
          if sel_part(5,k) gt end_block then begin
            sel_part(5,k)=end_block
          endif
         endif

         if (sel_part(5,k)-sel_part(4,k)) ge goodenough then begin
         n=n+1
         endif
      endif
     endif
    endfor


   sel_part=sel_part_orig
   pt_info=fltarr(7,n)
```

```
   n=0

   for k=0,m-1 do begin
    if (sel_part(0,k) ge xpixel_min) and (sel_part(0,k) le xpixel_max) $
    and (sel_part(1,k) ge ypixel_lowerfrontproj) and (sel_part(1,k) le ypixel_upperfrontproj) $
    then begin
    if sel_part(4,k) lt end_block then begin
          if sel_part(4,k) lt start_block then begin
          sel_part(4,k)=start_block
          endif

         if sel_part(5,k) gt start_block then begin
          if sel_part(5,k) gt end_block then begin
            sel_part(5,k)=end_block
          endif
         endif

         if (sel_part(5,k)-sel_part(4,k)) ge goodenough then begin
       pt_info(*,n)=sel_part(*,k)
       write_gdf, pt_info, 'pt_info 3 quarter front projection block'+r+'.result'
         write_textmod,pt_info,'pt_info 3 quarter front projection block'+r+'.txt'
         n=n+1
         endif
      endif
     endif
    endfor


   h=MSD_header_mod1(t,pt_info)
   write_textmod,h,'particle track header 3 quarter front projection block'+r+'.txt'
   p=msd_mod3(t,pt_info)
   write_textmod,p,'particle track 3 quarter front projection block'+r+'.txt'
   average=ave_timelag(p)
   write_textmod,average,'average particle track 3 quarter front projection block'+r+'.txt'

 endfor

end
```

A.3.14 write_gdf

```
pro write_gdf, data, file, ascii=ascii
; see http://www.physics.emory.edu/~weeks/idl
;   for more information
;+
; NAME:
;                   write_gdf
; PURPOSE:
;                   Writes IDL-style data to disk in a format which can be
;                   easily read back in.
; CATEGORY:
;                   General Purpose Utility
; CALLING SEQUENCE:
;                   write_gdf,data,file
; INPUTS:
;                   data:    Data structure to be written to disk.
;                   file:    Complete pathname of the file to be written.
; KEYWORD:
;                   ascii:   Produce an ASCII file rather than the default
;                            binary file.
; SIDE EFFECTS:
;                   Creates a file.
; RESTRICTIONS:
;                   Current version does not support structures or arrays of
;                   structures.
; PROCEDURE:
;                   Writes a header consisting of a long MAGIC number followed
;                   by the long array produced by SIZE(DATA), followed by the
;                   data itself.
;                   If the file is ASCII, the header tag is an identifying
;                   statement, followed by all of the same information in
;                   ASCII format.
; MODIFICATION HISTORY:
;                   Written by David G. Grier, AT&T Bell Laboratories, 9/91
;-
on_error,2                          ; return to caller on error
MAGIC = 082991L
HEADER = 'GDF v. 1.0'
openw, lun, file, /get_lun
sz = size(data)
if keyword_set(ascii) then begin
        printf,lun,HEADER
        printf,lun,sz(0)
        printf,lun,sz(1:*)
        printf,lun,data
        endif $
else begin
        writeu,lun,MAGIC
        writeu,lun,sz
        writeu,lun,data
        endelse
close,lun
free_lun, lun
end
```

A.3.15 write_textmod

```
;  Written by John C. Crocker
;
;
;  Saves the data in an array as a tab delimited text file
;  which can be easily read in by a spread sheet program.
;  default delimiter is the tab
;
pro write_textmod,data,filename,comma=comma

sz = size(data)
if sz(0) ne 2 then message,'Array argument must be 2 dimensional'

if keyword_set( comma ) then num_delter = ',' else num_delter = string( 9B ) ; tab is ASCII 9

close,1
openw,1,filename

for i=0.0,sz(2)-1 do begin
   astring = ''
   for j=0.0,sz(1)-2 do begin
      astring = astring + strcompress( string( data(j,i) ), /remove_all ) + num_delter
   endfor
   astring = astring + strcompress( string( data(sz(1)-1,i) ), /remove_all )
   printf,1,astring
endfor

close,1

end
```